2002-09-10

Ultrasonic Measurement of Thin Condensing Fluid Films

Michael A. Shear
Worcester Polytechnic Institute

Ultrasonic Measurement of Thin Condensing Fluid Films

By

Michael A. Shear

A Thesis

Submitted to the Faculty

Of the

Worcester Polytechnic Institute

In partial Fulfillment of the Requirements for the

Degree of Master of Science

In

Electrical Engineering

April 18, 2002

APPROVED:

_____

Prof. Peder C. Pedersen, Advisor

_____

Prof. James C. Hermanson, Co-Advisor

_____

Prof. Fred J. Looft III, Committee Member

Abstract

The condensation of vapor onto a cooled surface is a phenomenon which can be difficult to quantify spatially and as a function of time; this thesis describes an ultrasonic system to measure this phenomenon. The theoretical basis for obtaining condensate film thickness measurements, which can be used to calculate growth rates and film surface features, from ultrasonic echoes will be discussed and the hardware and software will be described. The ultrasonic system utilizes a 5MHz planar piston transducer operated in pulse-echo mode to measure the thickness of a fluid film on a cooled copper block over the fluid thickness range of 50 microns to several centimeters; the signal processing algorithms and software developed to carry out this task are described in detail. The results of several experiments involving the measurement of both non-condensing and condensing films are given. In addition, numerical modeling of specific condensate film geometries was performed to support the experimental system; the results of modeling nonuniform fluid layers are discussed in the context of the effect of such layers on the measurement system.

Acknowledgements

The financial support of NASA and the National Center for Microgravity Research on Fluids and Combustion is gratefully appreciated, as is the assistance of Dr. Jeff Allen, NASA/GRC project liaison.

I would also like to thank Prof. Peder C. Pedersen, my thesis advisor, for his endless help and encouragement throughout the course of this project. His eternally optimistic and friendly attitude somehow managed to turn this project from something that I *had* to do into something that I *wanted* to do.

Prof. James C. Hermanson, the condensation project Principal Investigator and my thesis co-advisor, along with his post-doctoral fellow Dr. Zhenqian Chen, were extremely helpful in working with the physical experiments and in teaching me enough about fluids to understand *why* this project was important.

Finally, I would like to thank my family and friends, without whose support I would never have managed to complete this project.

Extended Abstract/Summary

The mechanics and behavior of condensation phenomena are poorly understood under even relatively commonplace conditions; in unusual conditions, such as reduced gravity as experienced in the course of space flight, the condensation process is expected to proceed differently and current theory may not adequately predict condensation behavior in such a case. As a result the National Aeronautics and Space Administration (NASA), through the Glenn Research Center in Cleveland, Ohio, has funded a project to develop a low-gravity experiment to empirically determine the condensation dynamics of assorted fluids in altered gravity conditions. The results of this research will be valuable in designing future spacecraft to minimize concerns about water condensation at unwanted locations and to enable better design of spacecraft thermal control systems. In existing spacecraft, condensate management has largely been an empirical art; this has for example resulted in modifications to the International Space Station while in orbit when certain radiators had to have insulation added to reduce unwanted – and unexpected – condensation problems. Additionally, many thermal control devices such as heat pipes depend on the high heat flux associated with the phase change occurring at condensation.

The goal of this thesis project is the development of a pulse-echo ultrasonic system to measure the thickness of a condensing film in real time, as well as being able to post-process the data to determine wave velocity and wavelength data for perturbations within the condensing film. This is done using several (as many as eight in the current version) ultrasound transducers on the outside surface of the condensation chamber. It is envisioned that in laboratory

experiments the ultrasound system will be used with an optical imaging system due to an optical system's much better spatial resolution for imaging perturbations in the film and the ultrasound system's ability to perform quantitative thickness measurements. In an actual low-gravity experiment, the optical system may prove to be impractical and thus may be eliminated if the laboratory experiments show the ultrasound system able to produce all needed data.

This research was conducted using a condensation test cell. The cell consists of a cylindrical shell constructed of relatively insulating plastic, with several fittings for introducing vapor into the test cell, and one end of the cell made of copper with cooling channels piped through it. The cell can be placed in either "plate-down" or "plate-up" orientation on the benchtop; in the former case, +1g conditions apply to the condensation and in the latter case a –1g effective gravity level is present. An instrumented version of the test cell is scheduled to be flown on NASA's KC-135 low-gravity parabolic trajectory aircraft, permitting experiments to be conducted in effective gravity levels ranging from 1g to 0.01g.

In operation, the end plate will be cooled by a refrigerant pumped through the cooling channels. When heated vapor is introduced to the test cell, the vapor will begin to condense onto the cooled plate. Monitoring the progress of this condensation is no simple task as no direct measurements (e.g. using a float gauge) can be made since they would disturb the condensation process. A simple optical technique can image perturbations in a fluid film, but it is a generally qualitative measurement. While the optical technique can determine the presence of perturbations and their lateral characteristics, it cannot easily determine film thickness or, for that matter, the depth of the perturbations on the film. The need for accurate determination of condensate film thickness, as a

function of time and at several locations, has motivated the development of the ultrasound-based measurement system.

Eight ultrasonic transducers are connected through a multiplexer to a pulser-receiver (P/R) unit; this P/R unit is then connected to a computer-based oscilloscope which both triggers the P/R unit and records its output. The oscilloscope hardware is entirely contained within a single Type II PCMCIA, or laptop computer expansion, card; this card is inserted into one of the two Type II PCMCIA expansion slots in the laptop and can then be treated as an integral part of the laptop itself. The oscilloscope is controlled through a control program written in the National Instruments Inc. LabVIEW language; this program performs all data processing as well as all control of the multiplexer as well as the oscilloscope. The data from the P/R unit is processed through several signal-processing steps, and the thickness estimate is extracted from this data. This process is repeated for each of the active transducers (from one to eight transducers can be used) and is continuously repeated to generate a thickness-vs-time record. The maximum sampling rate with multiple transducers is approximately 30 samples/second (i.e. 15 samples/second/transducer for two transducers, 10/second for three, etc.) or up to 60 samples/second with a single transducer since the delay introduced by switching channels in the multiplexer is removed. The multiplexer is also controlled by the LabVIEW program, and is connected to the laptop using a standard serial interface.

Condensate layers which are thin relative to the wavelength of the ultrasonic signal have the frequency response of a “comb filter”; in other words, the reflected energy due to a broadband ultrasound pulse falls in certain

narrowband frequency ranges. The center frequencies of the passbands of the comb filter fulfill the equation $(2n+1)f_o$ where n is an integer greater than or equal to zero and:

$$f_o = \frac{c}{4d} \tag{1}$$

or, equivalently,

$$d = \frac{c}{4f_o} \tag{2}$$

where *d* is the thickness of the fluid layer in meters and *c* is the speed of sound in the fluid in meters/second.

The f_0 value is extracted through Fourier analysis of the signals acquired by the system. If the fluid layer is of an appropriate thickness for this technique to work (approximately 50-2000 microns) the FFT will have clear peaks at odd multiples of f_0 (f_0, 3 f_0, 5 f_0, 7 f_0, etc.) and the locations of these peaks are extracted using a peak-detection algorithm which produces an estimated f_0 and thus through equation (2) the estimated layer thickness.

Due to the fact that the echo received by transducer from the copper/water interface is much larger than the “comb-filtered” signal of interest from the fluid layer, the signal must be normalized by subtracting the effect of the copper/water interface echo before this analysis can be done. This normalization is accomplished by subtracting the echo received from a fluid layer of sufficient thickness to approximate an infinite layer from the raw received signal prior to performing the FFT; this signal-processing step also eliminates effects from structures within the copper block itself.

For thicker layers, a more conventional echo-delay method is used. In this method, the interval between the arrival time of the echo from the copper-fluid interface and the arrival time of the echo from the fluid-vapor interface is measured directly and yields a thickness estimate through:

$$d = \frac{c \cdot t}{2} \tag{3}$$

This method works for layers which are at least one or two wavelengths thick. For the 5MHz center frequency transducers used, this means that this method becomes useful for fluid layers with a thickness of approximately 0.5mm or greater. Tests to this point have demonstrated its use at up to 4cm of thickness. Since the thin-film method becomes noisier above 750 microns and the thick-film measurement is accurate above 500 microns, the system uses the thick-film algorithm first, and if an invalid result or a result less than 750 microns is generated, the thin-film algorithm is then run with the same data.

Numerical modeling using the Wave2000 software package has also been performed; this software models the wave propagation in a 2-D object from a 2-D transducer (the third dimension is assumed infinite). The Wave2000 system is a finite time difference modeling system which models a 2-D object as a matrix of points; the pressure at each point at a given time is used to calculate the pressure at each adjoining point at the next time interval.

The simulation package was first used to model simple situations such as a flat film, which was used to verify that the model was in good agreement with the same experiment run in the lab. It was then used to investigate situations

which would be very difficult to create experimentally under controlled conditions, such as a thin film which varied in thickness or layers with droplet formation.

Experiments thus far have verified the validity of the results from the ultrasound system; this has been done using a level block with the transducers on the bottom surface and a fluid film on the top (i.e. a “+1g” environment). Both static and dynamic – i.e. excited by some external mechanical activity – fluid films have been used; the excitations have ranged from a slow, steady addition of fluid to a dropwise addition of fluid resulting in ripples to waves generated by a paddle.

In the initial set of experiments, static films of non-condensing fluid with different thicknesses were used. This verified the system’s ability to detect a fluid layer and accurately measure its thickness. The film thicknesses were measured correctly by the system as far as could be verified although verification by non-ultrasound means proved difficult for some of the thinner layers.

In the next set of experiments, the measurement began with an extremely thin fluid layer to which fluid was added at a constant rate. Since the fluid was added at a constant rate, the growth rate of the fluid was known to be constant. The constant growth rate was directly verifiable and indeed is what was measured by the system.

In the excited layer experiments, thickness-vs-time plots from multiple transducers were used to calculate the wave velocity and the wavelength for several different fluids at several layer thicknesses

Finally, a series of measurements of actual condensation have been conducted. These tests have shown that the ultrasonic system developed for this project can successfully monitor condensation in benchtop experiments.

Table Of Contents

Table Of Figures

Table Of Tables

Chapter 1: Introduction

A. Background for Condensation

This thesis deals with an ultrasound-based method for measuring the thickness of a thin film of condensing fluid. It is thus pertinent to begin with a brief description of condensation dynamics.

Under normal conditions, matter is found in one of three phases listed here in order of increasing internal energy: solid, in which molecules are rigidly attached to each other; liquid, in which molecules are loosely and fluidly bound together; and gaseous, in which very little intermolecular bonding is present. When a substance changes from one phase to another, internal energy (or "enthalpy") must be added or removed by an external source; for example, in order to boil water to create steam, heat must be added by a burner or other heat source. More pertinently, when water vapor condenses into liquid water, the heat released by the condensation phase change must be removed; in an everyday example, water vapor from the air condensing onto a glass of a cold beverage transmits the heat from the phase change through the glass into the cold beverage.

This process is, however, complex. In the example above of condensation onto a glass, the condensation dynamics are affected by many parameters. Some of these are: the partial pressure and temperature of the water vapor; the initial temperature, thermal conductivity, and thermal capacity of the glass; the temperature, thermal conductivity, and thermal capacity of the liquid in the glass; the orientation of the condensing surface; the velocity of airflow past the glass; and the viscosity and thermal conductivity of the condensate.

The ambient water vapor, being intermixed with the ambient air, circulates with that air and is cooled by the liquid water layer on the glass. When a molecule of water vapor has been sufficiently cooled, it experiences a phase change to liquid thus adding to the liquid water layer. The circulation of the ambient air, which brings the water vapor in contact with the liquid water layer, is in part due to the convection caused by the cooling effect of the glass. Convection, as will be discussed below, is a gravity-driven process.

When a water molecule condenses from the ambient water vapor to join the liquid water layer, the enthalpy of phase change (approximately 2.5×10^6 J/Kg for water) is released. This heat is deposited into the liquid water layer on the outside of the glass, from where it is removed by heat conduction through the liquid layer (assuming that the layer is thin enough to prevent convection). For fluids significantly thicker than usually found in terrestrial situations, convection would be expected to play a role in this process as well. The heat is then

transferred through the solid glass layer by the mechanism of conduction, which is independent of gravity.

Heat is transferred from the inner wall of the glass to the beverage through the mechanism of convection, which is often the predominant mechanism of heat transfer in liquids and gasses. Convection is a gravity-driven process in which the fluid circulates because of the different densities of cold and warm fluid. In most fluids, warming the fluid causes it to expand, and thus become less dense; having become less dense, the warmer fluid tends to rise and be replaced by colder and thus denser fluid. This mechanism distributes added heat throughout the body of the fluid, minimizing the amount of heat absorbed by any particular portion of the fluid. Convection also applies to heat loss, in that the fluid that has lost heat will become denser and thus sink and be replaced by warmer and less dense fluid.

Of the four regions discussed in the example of a glass filled with a cold beverage, two have behaviors which are dependent on gravity: the air/water vapor mixture and the beverage in the glass. However, if the condensate film were to grow thick enough, convection would be expected to play a part in that region as well. In an environment without gravity, convection will not occur. It is theorized that this will significantly slow heat transfer which normally occurs convectively, as it will now be limited to heat conduction instead which implies a much lower rate of heat transfer. This means that, for example, the air/water vapor mixture will not move past the surface due to natural convection;

implications of this could be a significant slowing of the condensation process due to less water vapor being present immediately adjacent to the condensing surface. Additionally, the fluid mechanics of all three non-solids in this example will be significantly altered by the absence of gravity.

While the condensation onto a glass of a cold beverage in a reduced gravity environment may not be very important, the reduced gravity behavior of cooling systems that exploit the same physical phenomena is critically important. As a result, the National Aeronautics and Space Administration (NASA), through the National Center for Microgravity Research on Fluids and Combustion at Glenn Research Center in Cleveland, Ohio, has funded research into condensation physics in reduced-gravity environments.

Condensation behavior is an important factor in the design of spacecraft systems such as air circulation and atmospheric water recovery systems based on condensation. Among other functions, these systems ensure that cabin air in spacecraft is at an appropriate humidity level for both crew and equipment. To do this, a device similar to a household dehumidifier condenses excess atmospheric water vapor to remove it from the air.

Additionally, condensation is a critical part of certain thermal control systems, which utilize the high heat flux from the phase change as an important part of their function. A phase change of water between liquid and gaseous, or vice versa, involves a heat flux of approximately 2.5×10^6 Joules per kilogram of water; the same kilogram of water would have to be heated or cooled several

hundreds of °C – assuming it could be kept liquid – to accommodate the same heat flux without a phase change. An example of such a component using this high heat flux would be “heat pipes”; these are passive heat transport devices which are commonly used in spacecraft. A heat pipe consists of a sealed metal tube, with a wick on the inner surface of the tube, containing a working fluid with a high enthalpy of vaporization (examples are water, methanol, and ammonia). Because of the physics of the phase change, thermal energy is absorbed by changing the working fluid from liquid to gas with no change in temperature since the phase change is an isothermal process; this means that the entire heat pipe will always be at the boiling point of the working fluid at the pressure in the tube. Energy released from the working fluid changing from gas to liquid is transmitted out of the heat pipe to a radiator or other heat sink, still at the same boiling point temperature. The name “heat pipe” refers to the phenomenon that the heat is transferred from one end to the other at a constant temperature.

When one end of the heat pipe is heated and the other cooled, for example by attaching one end to an electronics rack and the other to a radiator, heat energy at the hot end is used to change the phase of the working fluid from liquid to vapor at a constant temperature. The vapor travels down the tube, and upon reaching the cold end condenses onto the end plate releasing the enthalpy of vaporization that it absorbed at the hot end. The pressure differential created by vaporization at the hot end and condensation at the cold end acts as a passive pump for the vapor; the wick built into the tube passively transports the

liquid phase back from the cold end to the hot end. No active parts are required, and the passive components are extremely simple, and as a result these devices are very reliable; this is, of course, important for spacecraft applications.

However, in terrestrial applications the heat transfer occurring between the end plate and the fluid at both the hot end and the cold end is by the mechanism of convection; in a reduced gravity environment, it would take place solely by conduction. Heat pipes have been used extensively in spacecraft design, but the fundamental physics of their operation in reduced gravity is not well understood.

Various aspects of the fundamentals of condensation have been studied many times under terrestrial conditions. However, the terrestrial mechanism of condensation is highly complex; thus, the implications of a reduced gravity environment on the condensation phenomenon are poorly understood and cannot be inferred from current data. The reverse process from that of condensation is boiling, which has been studied extensively in microgravity conditions. However, the fundamental fluid physics of condensation in microgravity have not been investigated; although the two are inverse processes, the results from pool boiling experiments cannot be used to infer condensation behavior.

A series of condensation experiments is planned in order to explore the phenomenon of condensation in reduced gravity. However, the approach to measuring condensation as it progresses is not obvious. The subject of this

thesis is a monitoring system to measure the progress of condensation in this test cell, which is intended for use in reduced-gravity experiments.

B. Measurement of Condensation

Several methods of measurement of condensation experiments have been considered, and the ones used in the current project are briefly described here. A more thorough description is given in Chapter 2, which covers the condensation test cell and its instrumentation.

One technique for measuring condensation is in the form of an optical system which illuminates the condensate layer with a light source and projects the reflections off of the fluid layer onto a screen where it is recorded with a video camera. This system measures the topology of the fluid layer, but not its thickness or growth rate.

A second approach to condensation measurement utilizes heat flux measurements; if the temperature of the vapor is known, and the temperature of the block onto which the vapor is condensing is known, the amount of fluid condensing can be calculated from the total heat flux of the system. This measures the condensation rate, but provides no information about the topology of the fluid film nor about the film thickness at any given time.

The third measurement system used to monitor the progress of condensation in the current experiments is an ultrasonic system. This system is the subject of this thesis, and as such will be described in much greater detail in later chapters. The ultrasound system uses several transducers in pulse-echo mode to determine the thickness of the fluid film in discrete locations opposite each transducer. This can yield limited topographic information as well as thickness and growth rate information.

C. Development Stages of the Proposed Measurement System

The ultimate goal of this research will be the ability to perform meaningful study of condensation in reduced gravity. However, many aspects of the fluid physics of condensation take place over too long of a time frame to be studied in short periods (less than several minutes) of microgravity. These aspects of condensation can only be fully studied in a spaceflight experiment to be flown on the Space Shuttle or the International Space Station. It is hoped that the systems developed for the current project can be used in a modified form for such spaceflight experiments. However, the goals of the current project are more modest: a system will be developed to perform condensation research on NASA's KC-135 parabolic trajectory aircraft which provides a reduced-gravity environment in 20-25 second periods.

Before the KC-135 flights can take place, a condensation test cell and measurement systems to monitor condensation progress within the test cell must be developed. This was begun using a series of benchtop tests in the laboratory. These tests will be discussed in detail in a later section of this thesis, but in general consisted of using the ultrasound system to first measure non-condensing films of various fluids in both static fluid films and fluid films excited by external stimuli. These benchtop tests were designed to validate the optical and ultrasonic measurement systems.

Once these measurement systems were validated, benchtop condensation experiments were carried out. These were performed in two orientations: +1g (fluid condensing on the bottom of the test cell) and –1g (fluid condensing on the top of the test cell). These experiments have further validated the measurement systems, including the heat flux sensor system, and also provide a baseline data set for comparison to reduced-gravity trials.

After benchtop condensation experiments have been successfully accomplished, planning will begin for the KC-135 reduced-gravity flight experiments. These experiments are anticipated to occur in the summer of 2003.

D. Thesis Goals

The main goal for this thesis project is the development, construction, and performance evaluation of an ultrasonic system for the dynamic measurement of

condensation film thickness. As of the writing of this document, this system has been developed and is functional, and evaluation with actual condensation is ongoing. A secondary goal is to test this system, and verify its performance experimentally. The system has been tested with several different fluids, with both static and wavy fluid films, and with a wide range of fluid film thicknesses. Finally, numerical simulations of the ultrasound interactions with the fluid film have been carried out and used to verify the behavior of the system in situations not easily created experimentally, such as droplet formation. This goal was also fulfilled, as the system has been tested with simulations of nonuniform layers of different thicknesses and shapes.

E. Thesis Outline

This thesis is structured as follows:

In Chapter 1, a general introduction to the thesis project and the larger project of which it is a part is given. The motivation for both the overall condensation research project and the ultrasound thesis project itself is explained.

Chapter 2 describes the design of the condensation test cell, including the mechanical construction of the cell, the functionality of the cell, and the instrumentation installed in and on the test cell.

Chapter 3 explains basic ultrasonic theory pertaining to this project. Included are such topics as general ultrasonic wave propagation theory, descriptions of the ultrasound transducers used for the measurements and transducer theory, and characteristics of the materials used in the condensing block and fluid films.

Chapter 4 discusses all signal processing steps used in the course of the project. This includes data extraction from the raw signals, algorithms for generating a film thickness from the processed signal, and a flow chart of the ultrasonic measurement software.

The numerical modeling of the ultrasound wave propagation carried out for this project is discussed in Chapter 5. An overview of the modeling software used is given, followed by a detailed discussion of modeling parameters used and modeling techniques. Details of each modeled scenario are given, along with details of the modeling parameters used.

In Chapter 6, detailed descriptions of the ultrasound measurement system and experimental tests are provided. The chapter begins with an overall system explanation, which is then followed by a detailed explanation of each segment of

the system including both hardware and software. The experimental setup is then discussed, for each of several experimental scenarios.

The results of all experimentation along with all modeling results are given in Chapter 7. The results of each experimental and modeling scenario are given, along with a brief summary of the scenario conditions and parameters. The experimental results are compared to the modeling results as well as to results from other measurement systems (optical and heat transfer) furnished by the Mechanical Engineering team.

Finally, Chapter 8 is a conclusion that addresses the question of whether this thesis was successful in producing a satisfactory ultrasonic fluid layer measurement system and suggests areas for further research.

Chapter 2: Condensation Test Cell Construction and Instrumentation

A. Test Cell Mechanical Configuration

1. Structural Configuration

The basic structure of the condensation test cell is that of a cylinder with thermally insulating plastic walls. The end of the cylinder at which condensation occurs is made of copper and contains a cooling system and several types of instrumentation; the other end is simply an optically clear layer of glass. The test cell is shown schematically in Figure 2-1. A clamping mechanism, consisting of a round metal plate at each end of the system bolted together via four threaded rods, holds the system together; the center of each plate is milled out, making each a ring, to allow for the placement of ultrasound transducers on one end and light transmission on the other.

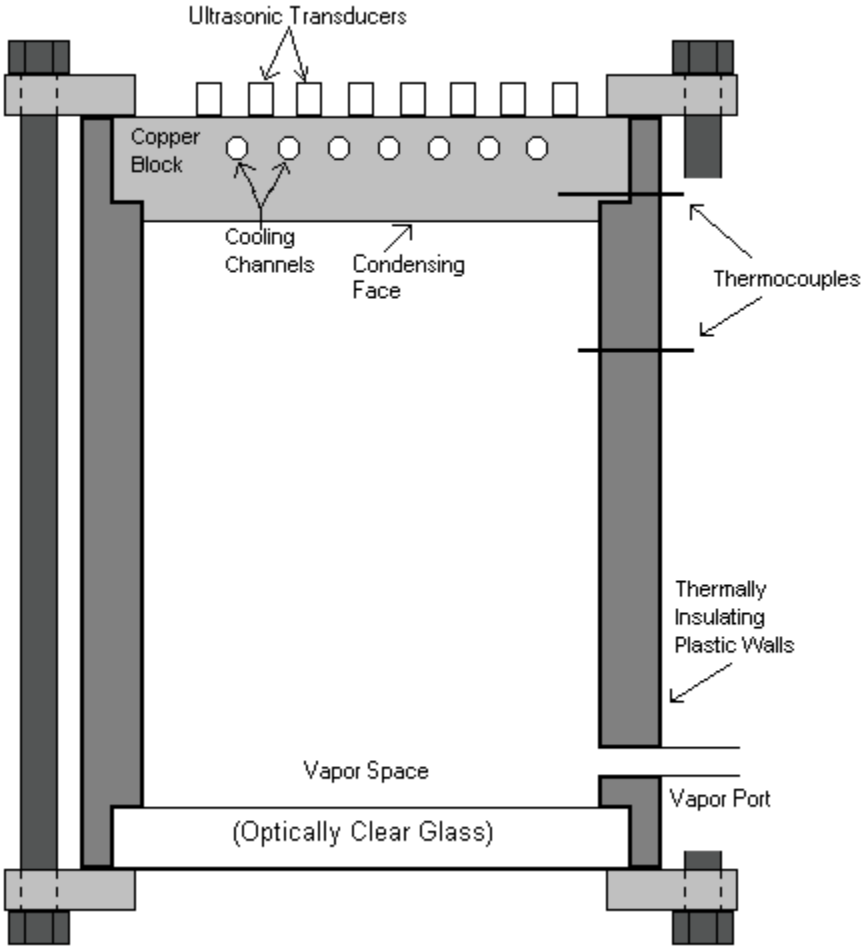

Figure 2-1: Schematic cross-sectional view of the condensation test cell. Note that for clarity, portions of the right threaded rod are not shown.

2. Cooling System

Several fluid channels are drilled through the copper block, as shown in Fig. 2-1. Chilled water is pumped from a Cole-Parmer "Polystat" chiller/pump unit through these channels to allow the block to be cooled to the desired temperature. The cooling channels are drilled with 1" (25.4mm) center to center

spacing and ½" (12.7mm) diameter, resulting in a ½" (12.7mm) space between each adjacent pair of channels.

3. Vapor Introduction System

A vapor generator (not shown in Fig. 2-1) has been constructed which allows the heating of the desired fluid to a controlled temperature to create a specified partial vapor pressure. The vapor generator consists of a glass cylinder which is sealed on the bottom and has a metal top containing instrumentation to measure pressure and temperature and a fitting to connect to the pipe which carries the vapor to the condensation cell. Electrical heating coils are wrapped around the outside of the glass cylinder, and a thermocouple to sense temperature is installed in the top to measure the temperature of the vapor generated. The output of this thermocouple is sent to a heater control unit which regulates the current through the heating coils so that a constant set vapor temperature is maintained. A pressure gauge is also attached to monitor pressure inside the vapor generator; when the desired pressure has been reached, a valve is opened allowing the vapor into an insulated ½" copper pipe leading to the condensation cell.

B. Non-Ultrasonic Instrumentation

1. Optical System

The optical monitoring system used in this project is the conceptually simplest method to observe the progress of condensation, which is to simply record a visual image of the fluid film as a movie. In practice, difficulties arise since in the "double-pass shadowgraph" system used one is observing a transparent fluid film at normal incidence. As shown in Fig. 2-2, the optical system consists of an arc lamp shining through a partially silvered mirror and reflecting off of a concave mirror onto the condensing surface which has been polished to a high degree of reflectivity. The light is then reflected back onto the concave mirror from where the light is directed towards the partially silvered mirror, which reflects it onto a screen where it is captured by a video camera. This method works well for recording perturbations in the fluid film, such as waves and droplets, but is not capable of determining the depth of the film. Because one of the main goals of this condensation research is to determine condensation rate, knowing the fluid film thickness is critical; thus, the optical method alone is an inadequate measurement methodology. However, the optical method is potentially a valuable adjunct to other methods since it can in principle detect disturbances in the fluid film and measure their size, shape, location, wavelength, and velocity with high precision despite being unable to determine

their amplitude. The optical system has not performed as well as hoped to date, and if the ultrasound system can acquire all needed topographic data the optical system would not be needed for the reduced gravity experiments.

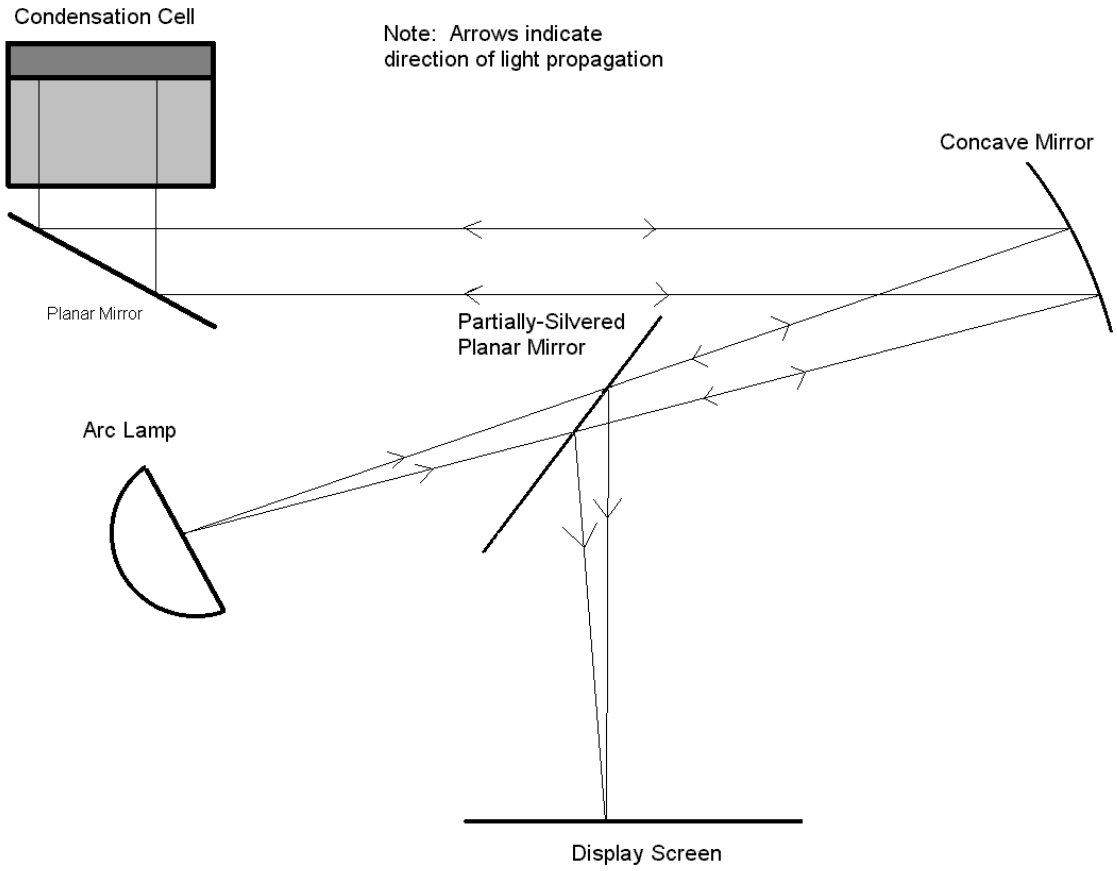

Figure 2-2: A schematic representation of the optical monitoring system.

The physics of how this system works optically are shown in Fig. 2-3. A thicker portion of the layer, such as a droplet, acts as a convex mirror and reflects light away from a direct reflection resulting in a dark area on the display screen. In contrast, a thinner portion, such as the trough of a wave, acts as a concave mirror which focuses light creating a bright area on the screen. In both Fig. 2-2 and Fig. 2-3, only two rays are shown in each figure to illustrate the

concept. The case shown in Fig. 2-3 is an ideal case, where the focal distance of the trough is exactly the distance to the screen resulting in a perfectly focused image. However, since waves vary in size and shape this is not usually the case.

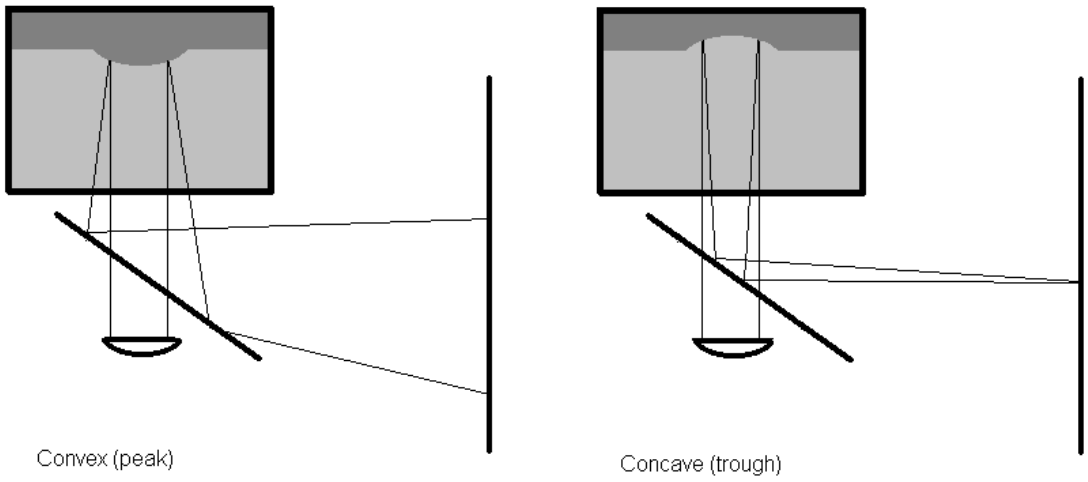

Figure 2-3: Optical System Physics. Left: convex wave (peak); Right: concave wave (trough).

2. Heat Flux Sensor

A second technique for monitoring the progress of condensation is to measure the heat flux through the condensing surface. The condensing surface is cooled by circulating a chilled fluid through cooling channels, and a heat flux sensor is placed between these cooling passages and the condensing surface. When condensation occurs, the heat released by the phase change travels from the condensing surface through the copper block with high thermal conductivity and through the heat flux sensor to the region of the block with the cooling channels. The heat is then removed by the chilled water which is circulating

through the channels. By measuring the heat flux, and knowing the specific heat of the condensing fluid as well as all temperatures involved, the mass of fluid condensing can be calculated. The heat flux sensor can thus measure the spatially averaged condensation rate potentially very accurately; however, it can not reveal any information about any other behavior, such as instabilities in the film or droplet formation. Used together with the optical system described above, both the condensation rate and the film perturbations can be sensed; however, only the average thickness of the fluid layer will be known – from integrating the heat flux – and the amplitude of any given perturbation cannot be determined. Note that the filler material surrounding the heat flux sensor itself to make up the layer across the entire metal block must have the same thermal resistance as the heat flux sensor; since the heat flux sensor is basically two thin Kapton sheets with a small amount of metal foil sandwiched between them, a double layer of similarly thick Kapton sheets are used as the filler material. The heat flux sensor is approximately 0.2mm thick, as is the filler material layer. The heat flux sensor and filler material are not used in the same condensing block as the ultrasonic system at present; the heat flux sensor requires a thick metal block with the heat sensor layer embedded, while the ultrasonic system requires a thin metal block.

3. Temperature Sensors

Thermocouples are placed at various locations in the test cell, to allow for monitoring of temperatures during the experimental runs. Knowledge of the

temperature differential between the copper block and the vapor allows theoretical calculations of condensation rates, and also allows for more accurate calculation of the conventional fluid dynamics found in drop formation and release.

C. Ultrasonic Instrumentation

The measurement system developed in this thesis project to monitor the progress of condensation is based on pulse-echo ultrasound measurements. Only a brief overview is presented here; this system will be described in much greater detail in chapters 4 and 6. The ultrasound system uses ultrasonic pulses from several transducers mounted on the non-wetted face of the copper block to probe the thickness of the fluid layer at a location approximately the size of the transducer face directly opposite each transducer (see Fig. 2-1). This holds true as long as the condensing film is in the near field of the transducer, where the effective lateral beam dimensions correspond very closely to the transducer dimensions. The near field for a ¼" 5MHz transducer, such as the ones used for this project, extends approximately 10mm in copper; this implies that for copper blocks less than 10mm thick the film will be in the near field and each transducer will measure an area of fluid roughly the same size as the transducer itself while for copper blocks greater than 10mm thick the film will be in the far-field of the transducers resulting in a larger beam area and significantly decreased SNR.

The system operates in pulse-echo mode, meaning that the piezoelectric transducer which produced the transmitted pulse also receives the echoes from the emitted pulse and converts them to a voltage output, allowing for a single transducer to be used for each point where layer thickness is measured. The great advantage of the ultrasonic system over the optical and heat transfer measurement methodologies is that the fluid layer thickness can be measured directly. The main advantage of the optical system is that it can image the entire surface of the fluid film while thickness can only be measured ultrasonically at discrete points. However, since the data from the ultrasound system is in digital form it is easily stored; the optical data must be recorded using a video camera which severely limits the performance of the optical system.

Chapter 3: Acoustic Theory

A. Pertinent Aspects of Ultrasonic Wave Theory

1. Ultrasonic Wave Propagation Theory

a. Propagation In a Homogeneous Material

An ultrasonic wave field emitted by a planar piston transducer, such as those used in this project, presents a complex analytical situation due mostly to diffraction effects. To greatly simplify the mathematical treatment of the wave field, it will be analyzed based on a single plane wave assumption; this means that the actual wave field is approximated as an infinite plane moving in a direction normal to the plane. All signals which will be discussed in this chapter will be treated as plane waves.

The representation of an ultrasonic wave in this chapter will be an equation describing the acoustic pressure as a function of axial location and time. The equation for the initial pulse emitted by the transducer is given as (3-1), where the actual form of the pulse is not specified but is expressed as the time-varying pressure at a given location x=0.

$$p(t,0) = p(t,x)\,|_{x=0} \tag{3-1}$$

The coordinate system can be selected such that the plane of the wave is the *yz* plane, and thus since the plane wave moves in a direction normal to the plane of the wavefront all motion of the wave is along the *x*-axis. The origin is chosen such that *x=0* at the face of the transducer. Since the wave is a plane wave traveling along the x-axis with velocity *c*, no amplitude or waveform changes will occur if attenuation is neglected and *p(t,x)* can be represented by a time shifted version of (3-1), given here as (3-2):

$$p(t,x) = p\left(t - \frac{x}{c}, 0\right) \tag{3-2}$$

which can be written as:

$$p(t,x) = p(t,0) \cdot \delta\left(t - \frac{x}{c}\right) \tag{3-3}$$

The wave described in (3-3) moves with a velocity c in the +*x* direction, with waveform *p(t,0).*

Thus far, all discussion has been in the time domain. It is, however, pertinent to set the framework for a frequency-domain analysis since the thin-film resonant layer system is analyzed in the frequency domain. Additionally, attenuation is a frequency-dependent phenomenon which can be most accurately addressed in the frequency domain. The frequency domain

representation $P(\omega,t)$ is defined as the Fourier transform of the time domain pulse $p(x,t)$ as in (3-4):

$$P(\omega,x)=\Im\{p(t,x)\} \tag{3-4}$$

where

$$P(\omega,0)=\Im\{p(t,0)\} \tag{3-5}$$

Referring to (3-2), (3-4) can be rewritten as (3-6):

$$P(\omega,x)=\Im\left\{p(t,0)\cdot\delta\left(t-\frac{x}{c}\right)\right\} \tag{3-6}$$

which can be evaluated to (3-7):

$$P(\omega,x)=P(\omega,0)\cdot e^{-j\cdot\omega\cdot\frac{x}{c}} \tag{3-7}$$

Noting that the wave number k is defined by $k=\omega/c$, (3-7) can be rewritten as (3-8):

$$P(\omega,x)=P(\omega,0)\cdot e^{-j\cdot k\cdot x} \tag{3-8}$$

In the ideal case, (3-8) would accurately describe the propagation of an ultrasonic signal through a medium. However, there are two major non-ideal conditions seen in the situations analyzed for this project. The first condition is that the assumption of lossless media is invalid for any real medium; since both the condensate fluid and copper are real and thus attenuating media the assumption of lossless media is not technically valid. Water and the other fluids used have very low attenuation and thus can be approximated as lossless for the frequencies and thicknesses encountered in this project. Copper, however, has significant attenuation which must be taken into account. The second condition is that in addition to attenuation through the classical mechanisms of shear viscosity and thermal conductivity, copper exhibits a grain scattering effect. The former effect can be calculated and incorporated in theoretical analysis; the latter exhibits macroscopic effects which are unpredictable. These effects can be modeled once measured, but are different for each possible transducer placement on a given block and of course differ from block to block as well. However, the signal processing discussed in Chapter 4 will essentially eliminate the effects of grain scattering so its absence from the theoretical discussion will not be significant.

The standard attenuation equation used to account for the classical attenuation in a homogeneous medium with constant attenuation is given as (3-

9) where α is the attenuation coefficient as a function of the angular frequency ω, and *d* is the path length traveled through the attenuating medium:

$$\widetilde{P} = P_0 \cdot e^{-\alpha(\omega)\cdot d} \tag{3-9}$$

In this equation, α is a function of frequency. When only classical attenuation is considered, α is proportional to the square of the frequency; (3-9) can thus be restated as (3-10):

$$\widetilde{P} = P_0 \cdot e^{-\alpha_0 \cdot \omega^2 \cdot d} \tag{3-10}$$

While this does not account for non-classical losses such as molecular relaxation, it will be shown in Chapter 4 that the signal processing used makes the calculation of the exact losses unimportant since they are normalized out.

Combining (3-10) with (3-8), the pulse corrected for attenuation can be expressed as (3-11):

$$P(\omega, x) = P(\omega, 0) \cdot e^{-j\cdot k\cdot x} \cdot e^{-\alpha_0 \cdot \omega^2 \cdot d} \tag{3-11}$$

Equation (3-11) is the frequency-domain equation which is used for the propagation of an ultrasonic wave, but because the thick-film algorithms operate in the time domain it is necessary to convert back into time-domain

representation as well. The time-domain equation formulation in (3-3) does not account for attenuation; as a result, the inverse Fourier transform of (3-11) will be taken to obtain an accurate time-domain representation. This inverse Fourier transform integral is shown as (3-12):

$$p(t,x) = \int_{-\infty}^{+\infty} P(\omega,x) \cdot e^{j\cdot\omega\cdot t} \cdot d\omega \tag{3-12}$$

which can be rewritten as:

$$p(t,x) = \int_{-\infty}^{+\infty} \left[P(\omega,0) \cdot e^{-j\cdot k\cdot x} \cdot e^{-\alpha_0\cdot\omega^2\cdot d} \right] \cdot e^{j\cdot\omega\cdot t} \cdot d\omega \tag{3-13}$$

or

$$p(t,x) = \int_{-\infty}^{+\infty} P(\omega,0) \cdot e^{j(\omega\cdot t - kx)} \cdot e^{-\alpha_0\cdot\omega^2\cdot d} \cdot d\omega \tag{3-14}$$

Note that in (3-14) the attenuation term is entirely real; as such, it does not impact the propagation of the wave or the waveform but rather only the amplitude. Because the amplitude of the received wave is not important for the time-domain thick-film measurement algorithm, it can be neglected and (3-3) can be used instead.

2. Propagation at an Interface Between Materials

In the majority of the situations encountered during this project, the boundaries encountered by a traveling ultrasonic wave will be normal to the propagation vector of the wave. This section assumes such normal incidence; those situations in which this is not the case are sufficiently complex to merit numerical modeling instead of analytical derivation and are discussed at the end of this chapter.

When a wave as described above traveling in the $+x$ direction interacts with a boundary between two different materials, a portion of the incident wave will be reflected back in the $-x$ direction and another portion will be transmitted into the second material and continue traveling in the second medium in the $+x$ direction. The amplitudes of both the transmitted and reflected waves, as well as the phase of the reflected wave, are determined by the reflection and transmission coefficients both of which are functions of the acoustic impedances of both materials. The acoustic impedance of a material, r, is defined as the density of the material multiplied by the speed of sound in that material. In this discussion, r_1 will be the acoustic impedance of the first material in which the incident wave is traveling and r_2 will be the acoustic impedance of the second material.

When interacting with a simple interface at normal incidence, both reflection and transmission coefficients are entirely real and as such are multiplied with the incident wave to calculate the reflected and transmitted waves. The transmission and reflection coefficients for a planar harmonic wave encountering an interface at normal incidence as described above are given as (3-15) and (3-16), respectively.

$$T = \frac{2 \cdot r_2}{r_2 + r_1} \tag{3-15}$$

$$R = \frac{r_2 - r_1}{r_2 + r_1} \tag{3-16}$$

In the transmission case, since $r_1, r_2 > 0$, T is entirely real and must always be greater than zero meaning that no phase shift occurs when a wave is transmitted through a boundary. However, as seen from (3-16), while R is likewise entirely real, it lies in the range [-1,1]; this implies that the reflected wave is a scaled and negated version of the incident wave when $R<0$. It can easily be seen from (3-16) that this inversion occurs when $r_1 > r_2$. In the situation of the condensation experiment, $r_1 > r_2$ for the copper/fluid (traveling from copper to fluid) and fluid/air interfaces, but not when traveling from the fluid into the copper at the fluid/copper interface.

The above discussion addresses only a single interface; if a thin layer of fluid is present, a more appropriate expression of the reflection and transmission

coefficients is obtained by analyzing the fluid as a layer rather than as two discrete interfaces. The pertinent physics for a fluid layer is given later in this chapter, in the section that addresses thin-film (frequency domain) measurement theory.

a. Transducer and Excitation Theory

The transducers used in this project are ¼" (6.4mm) diameter 5-MHz center-frequency wideband piston transducers. The waves they produce can be approximated as plane waves in the "near field"; the "near field" is defined by the region for which the path length from the transmitter to the receiver satisfies (3-17):

$$r < \frac{a^2}{\lambda} \tag{3-17}$$

where *r* is the path length from the transmitter to the receiver, λ is the wavelength, and *a* is the radius of the transducer. Since the transducers used are ¼"(6.4mm) diameter, i.e., their radius is roughly 3.2mm, a^2/λ can be calculated for the center frequency of 5MHz to be approximately 10mm in copper. This implies that as long as the copper block is less than 1cm in thickness, the fluid film can be treated as being in the near field. The cross-

section of the ultrasound beam is roughly constant and the same as the footprint of the transducer element over the near field; beyond the near field, the beam begins to diverge and thus its cross-section becomes significantly larger. The thickness of the fluid film is not considered, since the assumption of a plane wave is only important for the thin-film theory; thickness estimates for a thick film are not dependant on the assumption of being in the transducer's near field. This implies that for a film thick enough to give rise to far-field effects for a copper block of <1cm thickness, the far-field effects do not impact the theory.

Since the transducers used are wideband transducers, they can be modeled from a systems standpoint as bandpass filters with center frequency 5MHz and very slow rolloffs on both high- and low- frequency ends. When excited by a wideband voltage pulse, the ultrasonic pulse generated has a roughly Gaussian spectrum centered at 5 MHz with a several MHz wide passband. The effects of different excitation waveforms will be discussed further at the end of Chapter 4.

b. Characteristics of Materials Used

In any given experimental setup, there are three materials of interest. One is the solid (usually copper) of which the cooled block is made, a second is the liquid which is condensing onto the block, and the third is the vapor which has not yet condensed. The speeds of sound, density, and acoustic impedances for

all materials used in this project are given in Tables 3-1 (solids), 3-2 (liquids), and 3-3 (vapors), below.

Table 3-1: Material Properties of Solids

Material	Speed of Sound $\left[\frac{m}{s}\right]$	Density $\left[\frac{kg}{m^3}\right]$	Acoustic Impedance $\left[\frac{kg}{m^2 \cdot s}\right] = \left[\frac{Pa \cdot s}{m}\right]$
Copper	5010	8.93×10^3	44.74×10^6
Brass	4700	8.60×10^3	40.42×10^6

Table 3-2: Material Properties of Liquids

Material	Speed of Sound $\left[\frac{m}{s}\right]$	Density $\left[\frac{kg}{m^3}\right]$	Acoustic Impedance $\left[\frac{kg}{m^2 \cdot s}\right] = \left[\frac{Pa \cdot s}{m}\right]$
Water	1497	1.00×10^3	1.50×10^6
Methanol	1103	0.79×10^3	0.87×10^6
Glycerol	1904	1.26×10^3	2.34×10^6
Ethylene Glycol	1658	1.11×10^3	1.81×10^6
n-Pentane	1006	0.63×10^3	0.63×10^6

Table 3-3: Material Properties of Vapors at room temperature

Material	Speed of Sound $\left[\frac{m}{s}\right]$	Density (at 1atm) $\left[\frac{kg}{m^3}\right]$	Acoustic Impedance $\left[\frac{kg}{m^2 \cdot s}\right] = \left[\frac{Pa \cdot s}{m}\right]$
Water Vapor	405	0.6	243
Methanol Vapor	335	.48 (est.)	160.8
n-Pentane Vapor	Approximately Equal to Methanol (non-critical parameters)		

B. Theoretical Basis of Film Thickness Estimates

1. General Overview

The structures to be probed acoustically using the ultrasound pulse-echo system described in this thesis are fundamentally made up of three layers. The first layer encountered by the ultrasonic pulse is the copper layer; this is followed by the thin fluid layer formed by condensation and finally the air (or other vapor) layer. The air layer is assumed to be semi-infinite, and the time scale examined is limited to a short enough period to allow the copper layer to be modeled as semi-infinite as well. Because of these assumptions, the situation can be modeled as a finite fluid layer between semi-infinite copper and air layers.

The ultrasound pulse generated by the transducer is of finite duration, consisting of approximately three cycles due to a very short excitation voltage pulse; as a result, for fluid layers which are thicker than the spatial extent of the

pulse the behavior of the system can be modeled in the time domain as a single pulse propagating through the layered model. In this case, a simple time domain model using only transmission and reflection coefficients at the materiel interfaces may be used. However, for layers less than approximately 1.5 wavelengths thick, there will be interaction between successive echoes in the fluid layer. The effect of this interaction is most suitably observed in the frequency domain.

Section 2, below, analyzes the system for the thin-layer case and Section 3 performs an analysis on the thick-layer case. The final section in this chapter will discuss the effects of a fluid film which is not uniformly thick, and their implications on ultrasonic measurement of such films.

2. Thin Layers: Frequency Domain Analysis

Although non-uniform fluid layers are too complex to treat analytically, the case of the simple uniform fluid film is much more amenable to such a treatment. The three layers of such a structure are defined in Figure 3-1:

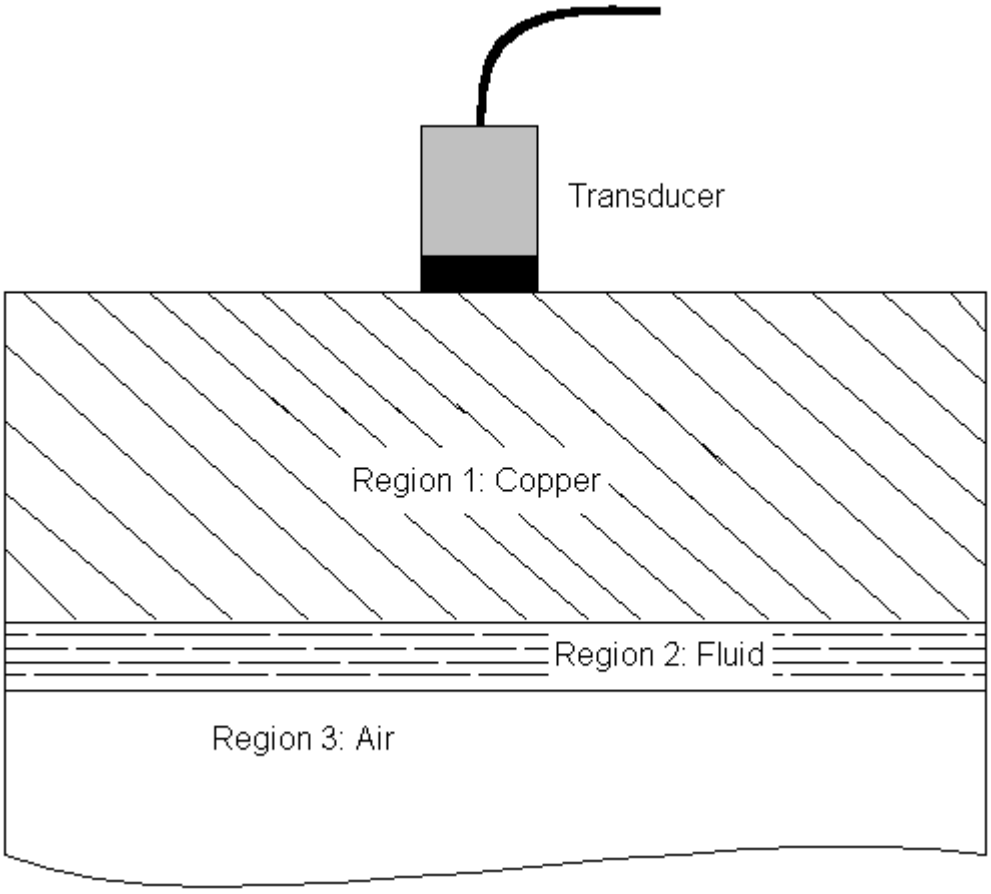

Figure 3-1: Defining the Regions of a Simple Fluid Layer

The transducer is not perfectly coupled in the sense that there is an acoustic impedance mismatch between the transducer and the copper block. The effect of the mismatch is a longer pulse, but to simplify the situation for the purposes of this discussion the transducer is assumed to be perfectly coupled into the copper block. This assumption is invalid, but acceptable, since the performance of the system does not strongly depend on the nature of the ultrasound pulse, as will be shown in Chapter 4, Signal Processing.

The system can be modeled from a systems standpoint as in Figure 3-2:

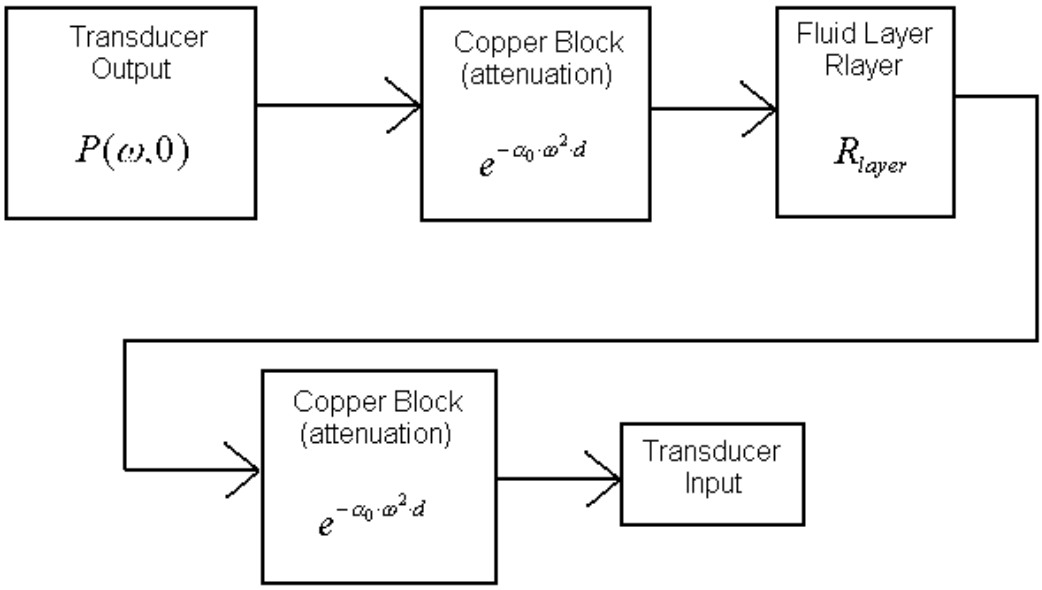

Figure 3-2: Model of thin-film (frequency domain) system behavior

In this model, the initial pulse $P(\omega,0)$ is multiplied by two attenuation terms and a fluid layer reflection coefficient before being received back at the transducer. The signal received at the transducer from this type of system can thus be described by (3-18):

$$P(\omega,x) = P(\omega,0) \cdot e^{-2 \cdot \alpha_0 \cdot \omega^2 d} \cdot R_{layer} \tag{3-18}$$

where *d* is the thickness of the copper block.

The complex, frequency-dependant reflection coefficient for a layer is given in (3-19):

$$\widetilde{R} = \frac{\left[1-\frac{r_1}{r_3}\right]\cos(k_2 \cdot L) + j\left[\frac{r_2}{r_3}-\frac{r_1}{r_2}\right]\sin(k_2 \cdot L)}{\left[1+\frac{r_1}{r_3}\right]\cos(k_2 \cdot L) + j\left[\frac{r_2}{r_3}+\frac{r_1}{r_2}\right]\sin(k_2 \cdot L)} \tag{3-19}$$

Definition of Terms:

r_1 = acoustic impedance of copper

r_2 = acoustic impedance of fluid

r_3 = acoustic impedance of air

k_2 = wave number in fluid, i.e. $\frac{\omega}{c}$ or $\frac{2 \cdot \pi \cdot f}{c}$ where ω and f are frequency terms and c is the sound speed in the fluid layer

L = thickness (in meters) of fluid layer

The expression for $\widetilde{R}$, given in (3-19), may be separated into real and imaginary parts:

$$\widetilde{R} = \frac{\left[1-\left(\frac{r_1}{r_3}\right)^2\right]\cos^2\theta + \left[\left(\frac{r_2}{r_3}\right)^2-\left(\frac{r_1}{r_2}\right)^2\right]\sin^2\theta}{\left[1+\frac{r_1}{r_3}\right]^2\cos^2\theta + \left[\frac{r_2}{r_3}+\frac{r_1}{r_2}\right]^2\sin^2\theta} + j\left[\frac{\left(\frac{2 \cdot r_1 \cdot r_2}{r_3^{\,2}}-\frac{2 \cdot r_1}{r_2}\right)\sin\theta\cos\theta}{\left[1+\frac{r_1}{r_3}\right]^2\cos^2\theta + \left[\frac{r_2}{r_3}+\frac{r_1}{r_2}\right]^2\sin^2\theta}\right] \tag{3-20}$$

where

$$\theta \equiv k_2 \cdot L = \frac{2 \cdot \pi \cdot f \cdot L}{c} \tag{3-21}$$

While (3-20) gives the response of the entire layer, the echoes from the copper-water interface are much larger in magnitude than the echoes from the fluid-air interface which have back-propagated through the fluid layer. Since the latter echoes are the portion of the signal containing thickness data, it is desired to extract them from the total echo signal. To do this, an equation for the echoes from the copper-water interface is developed by simply using the equation for the reflection coefficient from a simple boundary (3-22):

$$R_{boundry} = \frac{r_2 - r_1}{r_2 + r_1} \tag{3-22}$$

Noting that (3-22) is entirely real, it is then subtracted from the real part of (3-20) to yield the echo of interest (R_{EOI}) (3-23).

$$\widetilde{R}_{EOI} = \left\{ \frac{\left[1 - \left(\frac{r_1}{r_3}\right)^2\right]\cos^2\theta + \left[\left(\frac{r_2}{r_3}\right)^2 - \left(\frac{r_1}{r_2}\right)^2\right]\sin^2\theta}{\left[1 + \frac{r_1}{r_3}\right]^2 \cos^2\theta + \left[\frac{r_2}{r_3} + \frac{r_1}{r_2}\right]^2 \sin^2\theta} - \frac{r_2 - r_1}{r_2 + r_1} \right\} + j\left[\frac{\left(\frac{2 \cdot r_1 \cdot r_2}{r_3^2} - \frac{2 \cdot r_1}{r_2}\right)\sin\theta\cos\theta}{\left[1 + \frac{r_1}{r_3}\right]^2 \cos^2\theta + \left[\frac{r_2}{r_3} + \frac{r_1}{r_2}\right]^2 \sin^2\theta} \right] \tag{3-23}$$

The magnitude of (3-23) is plotted in Figure 3-3, using values which correspond to a 0.2mm thick water layer with the appropriate impedances for copper, water, and air.

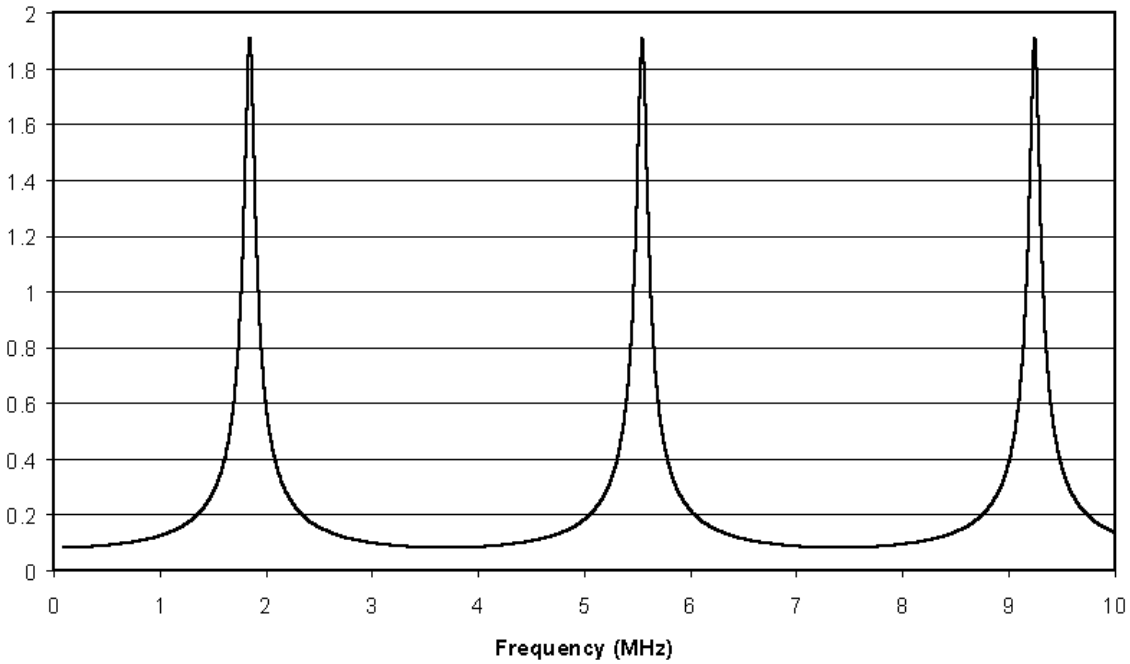

Figure 3-3: The Magnitude of the Frequency Response of a 0.2mm Water Layer. Note the peaks at f_0=1.85MHz, as well as 3 f_0=5.55 MHz and 5 f_0=9.25MHz.

The pulse incident on the layer from the transducer is the result of exciting the transducer with a ½ cycle square wave, resulting in a roughly Gaussian spectrum spanning several MHz of spectral width centered at 5MHz. The multiplication in the frequency domain of the spectrum of the incident pulse and the frequency response of the transducer results in the received spectrum shown in Fig. 3-4. The situation modeled here results in only one significant visible peak due to very little spectral energy being emitted from the transducer at low

frequencies such as the f_0 peak at1.85MHz and higher frequencies such as the $3f_0$ peak at 9.25MHz. With thicker layers, f_0 – and thus the interval between peaks – decreases resulting in multiple peaks occurring within the frequency range which has significant spectral energy. Since this will cause more peaks to be in the visible region (i.e. the region with sufficient spectral energy to be seen), this will result in multiple peaks seen in the received signal. An example of such a case is shown in Fig. 3-5, which is the same as Fig. 3-4 with a thicker fluid layer (0.5mm instead of 0.2mm).

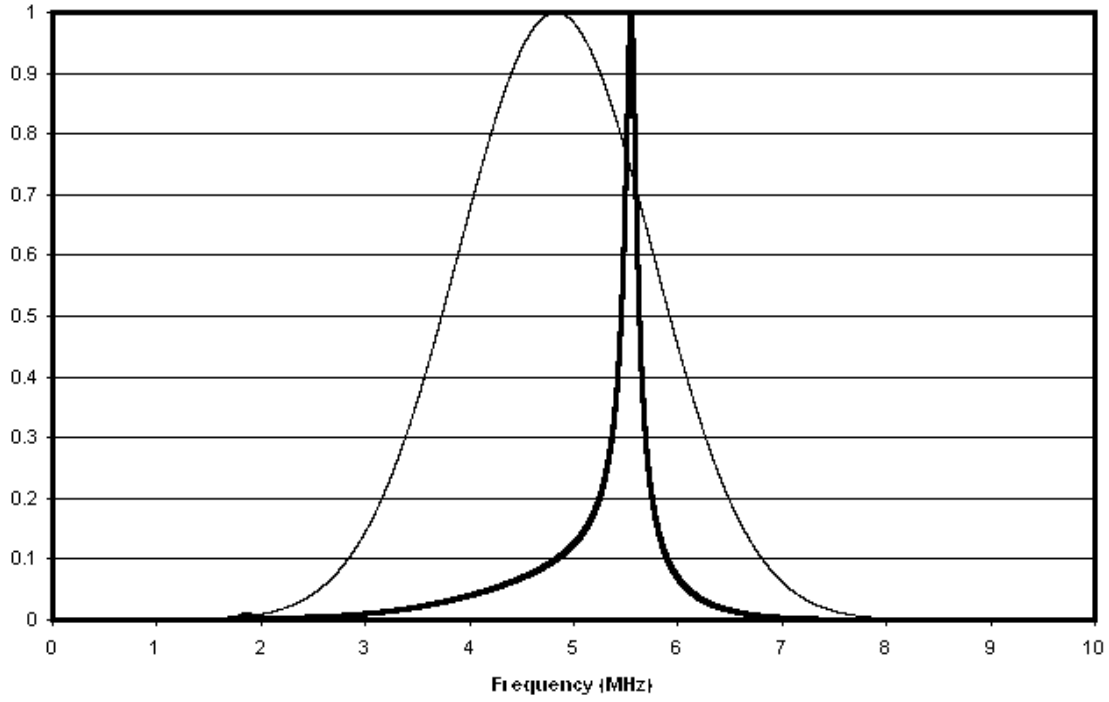

Figure 3-4: Normalized Analytically Predicted Received Signal for a 0.2mm water layer with a 5MHz center frequency transducer excited by a 5MHz ½ cycle square wave. Note only one major peak, at $3f_0$=5.55MHz. The f_0 peak at 1.85MHz is barely visible. The transmitted spectrum used (i.e. transducer output) is shown superimposed, also normalized to a maximum amplitude of 1.00.

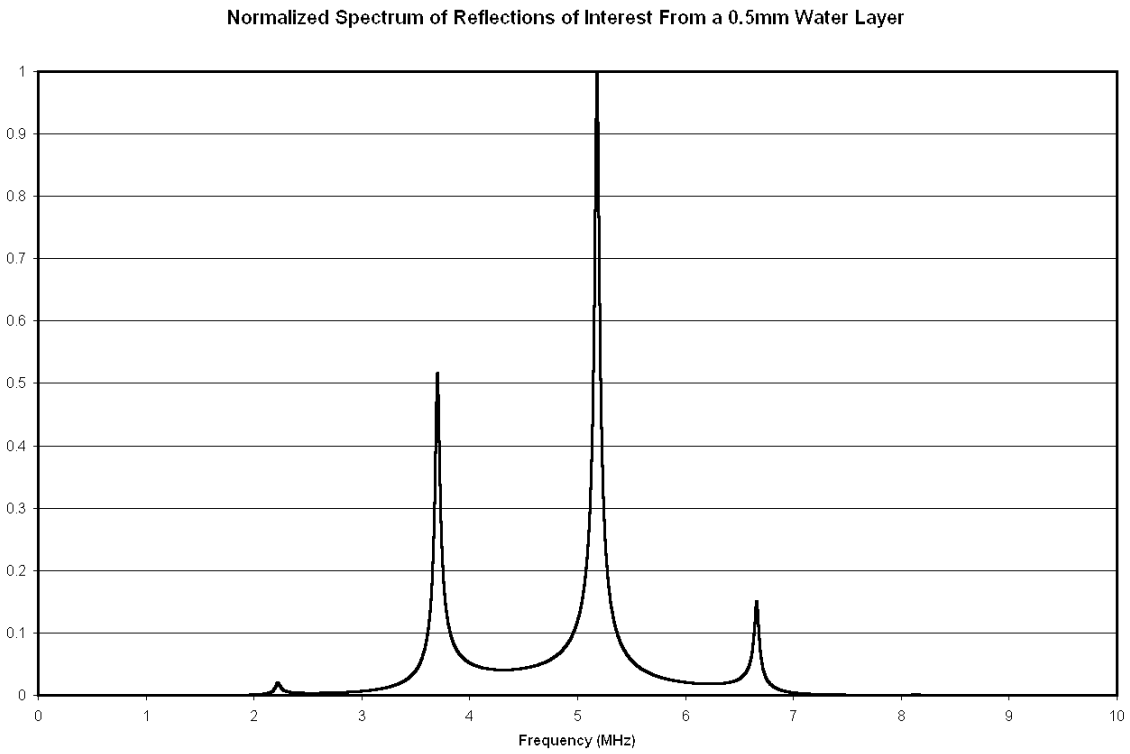

Figure 3-5: Normalized Analytically Predicted Received Signal for a 0.5mm water layer with a 5MHz center frequency transducer excited by a 5MHz ½ cycle square wave. Note obvious major peaks at $5f_0$=3.70MHz, $7f_0$=5.18MHz, and $9f_0$=6.66MHz. The f_0 peak at 0.74 MHz is not seen at all, and the $3f_0$=2.22MHz is barely visible.

Spectra such as the ones in Figures 3-4 and 3-5 can be obtained by taking the FFT of the output of the P/R unit in the system described in this thesis, and these experimental results have been in good agreement with the theoretically predicted spectra. Using a peak-detection algorithm, the f_0 frequency can be extracted from such spectra.

To calculate the relationship between f_0 and layer thickness, we note that Fig. 3-3 (as well as, of course, Figures 3-4 and 3-5) show spectral peaks when

$\theta = \frac{\pi}{2} + n\pi$ using the definition of θ given above in (3-21). Solving (3-21) for $\theta = \frac{\pi}{2}$ (i.e. f = f_0) results in (3-24):

$$\frac{\pi}{2} = \frac{2\pi \cdot f_0 L}{c} \tag{3-24}$$

which can easily be rearranged to give (3-25):

$$L = \frac{c}{4 \cdot f_0} \tag{3-25}$$

(3-25) gives a simple relationship between f_0 and the thickness of the fluid layer, L. This allows the thickness to be easily calculated via Fourier analysis as outlined above.

3. Thick Layers: Echo-Ranging

In the discussion in the previous section, the incident signal was assumed to have sufficient length that interactions occurred between subsequent echoes in the fluid layer. Clearly, if this is not the case than constructive and destructive

interference are not possible subsequent echoes will simply be seen as separate pulses. Because of this, for fluids which are greater than approximately 1.5 wavelengths thick – since the incident pulse is only approximately three cycles long – a different method must be used. This “thick layer” method is much simpler that the analysis of thin layers, as it simply measures time differences in the time domain.

If the ultrasound pulse is emitted with waveform *p(t,0)* it can be represented as in (3-14):

$$p(t,x) = \int_{-\infty}^{+\infty} P(\omega,0) \cdot e^{j(\omega \cdot t - kx)} \cdot e^{-\alpha_0 \cdot \omega^2 \cdot d} \cdot d\omega \qquad (3\text{-}14)$$

As discussed above the only advantage of (3-14) over the much simpler (3-3) is that (3-14) can account for attenuation; however, since the amplitude of the received pulse is not important in the determination of film thickness, the attenuation can be disregarded and (3-3) can be used instead:

$$p(t,x) = p(t,0) \cdot \delta\left(t - \frac{x}{c}\right) \qquad (3\text{-}3)$$

After traversing the copper block, which is a distance *b* thick and has a sound speed of c_b, the pressure pulse will be time-shifted but otherwise unchanged:

$$p(t,b) = p(t,0) \cdot \delta\left(t - \frac{b}{c_b}\right) \tag{3-26}$$

The portion of the pulse which is reflected back to the transducer without entering the fluid layer is the product of the reflection coefficient $R_{c/f}$ (indicating the reflection coefficient for a pulse traveling from copper to fluid) and the pulse in (3-26); after traversing the copper block back to the transducer, the received pulse is:

$$p(t,b) = p(t,0) \cdot \delta\left(t - \frac{2b}{c_b}\right) \cdot R_{c/f} \tag{3-27}$$

In comparison, if no fluid layer is present it can be assumed that r_2=0 since air, and the fluid vapors used, have acoustic impedances several orders of magnitude less than copper; in this case, the equation given for the reflection coefficient of an interface given as (3-16) yields R = -1. The reflection coefficient of no fluid – i.e. a copper/air interface – and the reflection coefficient of a semi-infinite layer of fluid would therefore be expected to be a factor of ($-R_{fluid}$) different in amplitude. This will be shown to be a useful fact in Chapter 4.

The pulse which does enter the fluid layer will be the product of (3-26) and the copper/fluid transmission coefficient, $T_{c/f}$:

$$p(t,b) = p(t,0)\cdot\delta\left(t-\frac{b}{c_b}\right)\cdot T_{c/f} \tag{3-28}$$

The pressure pulse described by (3-28) is time-shifted further by crossing the fluid layer, and then reflects off of the fluid/air interface. It is then again time-shifted by propagating back through the fluid layer to the fluid/copper interface. On its arrival at the fluid/copper interface, it can be represented by (3-29); in (3-29), $R_{f/a}$ is the reflection coefficient at the fluid/air interface, c_f is the speed of sound in the fluid, and f is the thickness of the fluid layer:

$$p(t,b,f) = p(t,0)\cdot\delta\left[t-\left(\frac{b}{c_b}+\frac{2f}{c_f}\right)\right]\cdot T_{c/f}\cdot R_{f/a} \tag{3-29}$$

This pulse then is transmitted through the fluid/copper interface with transmission coefficient $T_{f/c}$, and after propagating back through the copper block arrives at the transducer as:

$$p(t,b,f) = p(t,0)\cdot\delta\left[t-\left(\frac{2b}{c_b}+\frac{2f}{c_f}\right)\right]\cdot T_{c/f}\cdot R_{f/a}\cdot T_{f/c} \tag{3-30}$$

Since the first echo from the fluid layer was described by (3-27), the time delay between (3-27) and the first echo from the fluid layer (3-30) can be easily seen to be Δt, defined as:

$$\Delta t = \frac{2f}{c_f} \tag{3-31}$$

The two signals described by (3-27) and (3-30) will have the same pulse shape as long as all transmission and reflection coefficients are entirely real, since the only difference between the two equations is a lower amplitude in (3-30) due to transmission/reflection coefficients (as well as due to attenuation, which was neglected in this discussion) and a time-shift. Since both reflection coefficients are negative, while both transmission coefficients are positive, the two signals are the same polarity as well.

In other words, if an echo which appears the same as the previous echo – except with lower amplitude – arrives at the transducer a time lapse of Δt μs after the previous echo this time lapse corresponds to the round trip travel time through the fluid:

$$\Delta t = \frac{2L}{c} \tag{3-32}$$

If subsequent echoes can be observed as discrete pulses, the time lapse Δt between them is easily measured. Given Δt, (3-32) solved for L yields a simple equation to find L from Δt:

$$L = \frac{\Delta t \cdot c}{2} \tag{3-33}$$

4. Films with Non-Uniform Thickness

In earlier sections of this chapter, it was assumed that all ultrasound waves encountering interfaces were at a normal incidence. This is a valid assumption for uniform fluid films, since the ultrasonic waves are traveling in a vertical direction and all interfaces are horizontal. However, for nonuniform films the surface of the film is not exactly horizontal, and thus the waves encounter the interface at an oblique incidence.

Instead of carrying out an extensive analytical treatment of this case, it was modeled using numerical modeling software which will be discussed in Chapter 5. In general, it was found that slight nonuniformities did not significantly impact the performance of the ultrasound system; however, larger nonuniformities resulted in most of the ultrasonic energy being reflected away from the transducer and thus a significantly degraded signal-to-noise ratio and inability to measure the layer thickness. Full results of this modeling are presented in Chapter 7.

Chapter 4: Signal Processing and Algorithms

A. Overview

The basic conceptual model for the ultrasonic fluid layer thickness measurement system is shown below in Figure 4-1:

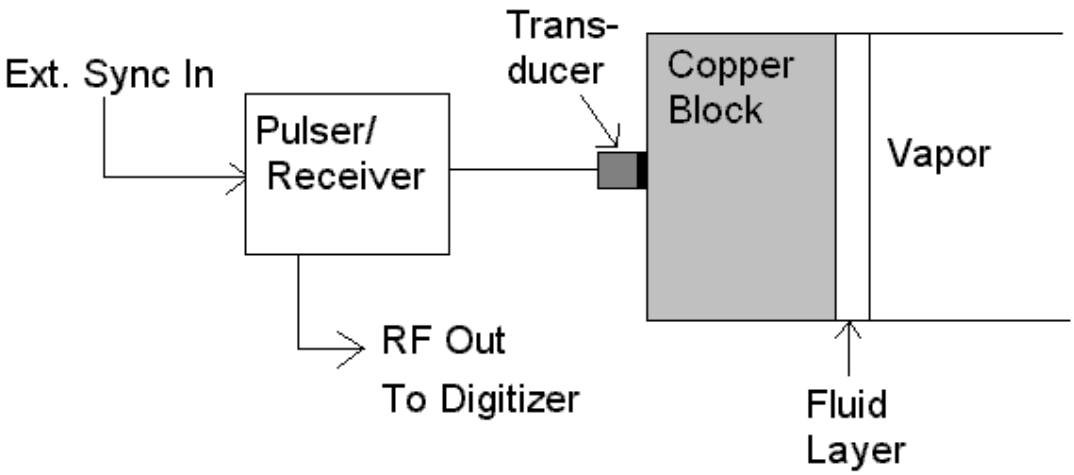

Figure 4-1: Basic Conceptual Model of Ultrasonic Fluid Layer Thickness Measurement System.

After the raw RF data has been acquired from the pulser/receiver by the digitizer, but before a thickness estimate can be made, a significant amount of signal processing must be done for a successful measurement to occur. There is some basic processing that is needed for all sets of data whether the thick-film or thin-film algorithm is to be used; once this is done, there is a large amount of additional processing specific to the thin-film algorithm if it is needed. This

chapter discusses all signal processing as well as the structure of the LabVIEW control and measurement program.

1. LabVIEW Control Program Structure and Flow Chart

The LabVIEW control program is described in detail in Appendix B, *LabVIEW Program Technical Manual*, but the general program structure and signal processing algorithms are described here.

The overall control program consists of three main modules. These are the main module, the communications module, and the baseline acquisition module. The main module is what the user interacts with when acquiring data, and it is also the program which contains the bulk of the signal processing and interpretation software. The communications module has only one function: to control and communicate with (including retrieval of raw data) all hardware in the system. Since it performs no signal processing at all, and has no user interaction, it will not be described further in this chapter. The baseline acquisition module, as the name implies, acquires the baseline sample which will be used to normalize all future data. This module performs a limited amount of signal processing, and will be addressed briefly.

The general flow chart of the LabVIEW program is shown in Figure 4-2.

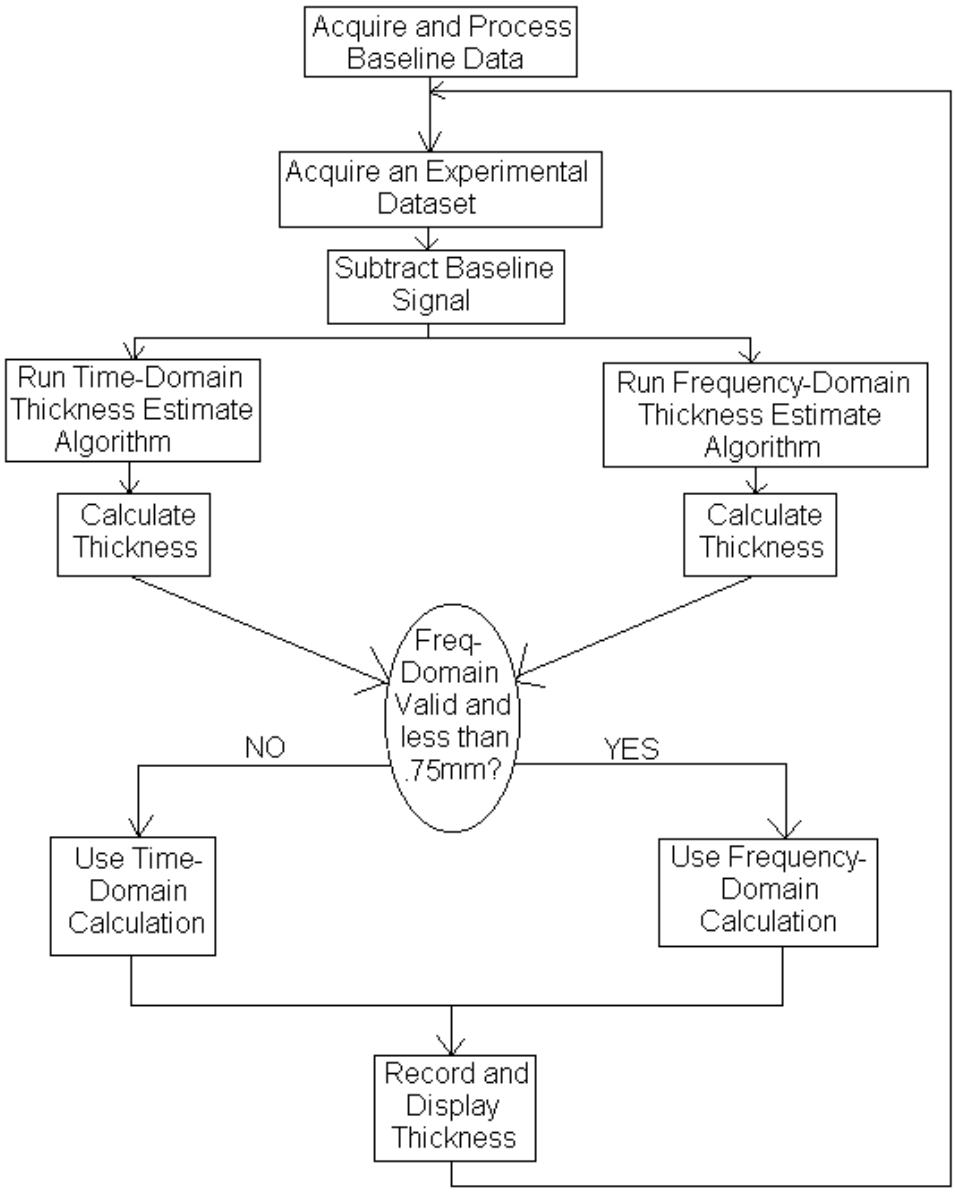

Figure 4-2: LabVIEW control program overview flow chart

As can be seen from Figure 4-2, there is a limited amount of data processing common to both time and frequency domain methods; however, the time domain method requires very little additional data processing beyond this point while the frequency-domain method requires a significant amount.

2. Signal Processing Common to both Thin and Thick Films

The RF signal received by the digitizer from the transducer via the pulser/receiver consists of the desired signal – that which contains information about layer thickness – in addition to a much larger amount of "noise". In this case, "noise" does not refer to the traditional Gaussian "white noise", but rather to artifacts in the form of unwanted portions of the signal which contain no useful data and which obscure the useful data that is present. These artifacts include the result of such phenomena as grain scattering within the copper block and the copper/fluid interface echo. The latter would appear at first glance to be part of the useful signal, but is not in fact useful since the distance from the transducer to the far side of the copper block is not the distance being monitored and this echo carries no information about the fluid layer whatsoever. This copper/fluid interface echo is in fact harmful since it can bury useful data due to its much larger amplitude.

The relative magnitudes of the desired (data-containing) signal and the artifact signal result in an extremely low effective SNR. This SNR varies with the fluid and with the thickness of the copper block, but averages roughly 0.1 (= -20dB). However, since the artifact components of the received signal can be mostly removed, a significant SNR improvement can be achieved. The reason for this nearly complete removal is that both the grain scattering from within the copper block and the copper/fluid echo are very repeatable.

The copper/fluid interface echoes are, in fact, the exact same for each pulse with a given fluid and a given transducer location. If the fluid layer can be made thick enough such that the first fluid/vapor interface echo does not arrive at the transducer until well after the first copper/fluid echo has been received, this artifact signal can be recorded. However, often the echo from the bare copper block (no fluid layer) is easily recorded but creating a thick fluid layer to record for normalization is impractical; in these situations, the copper/fluid echo can be calculated from the copper/air echo and the ratio of the reflection coefficients of copper/air and copper/fluid. The system is set up to allow the acquisition of the baseline signal with a bare copper block, after which it scales the portion of the signal which is the copper/air echo to correct it so that it can be used to cancel out the copper/fluid echo. The rest of the signal, meaning the signal segment which comes before the copper/air echo is received, is left unscaled as it is a result of scattering within the copper block and is not affected by the presence of the fluid. Theoretically, this method should be perfect; however, in practice, it is not as effective as an actual measurement of a very thick fluid layer since the artifact cancellation is not as complete. As a result, an actual “baseline” measurement of a very thick fluid layer is the desired method with the calculated method acting as a marginally acceptable backup if creating a very thick film is impractical.

Since the raw RF signal from thin fluid layers is simply a sum of the artifact signal and the data-containing signal, only the useful portion of the signal

remains once the previously recorded or calculated artifact signal is subtracted. By doing this point-by-point subtraction, which is computationally very simple and thus does not add much time to the data processing, the SNR is improved greatly. An example of pre-subtraction and post-subtraction signals is shown in Figure 4-3 using simulation data for a thick film.

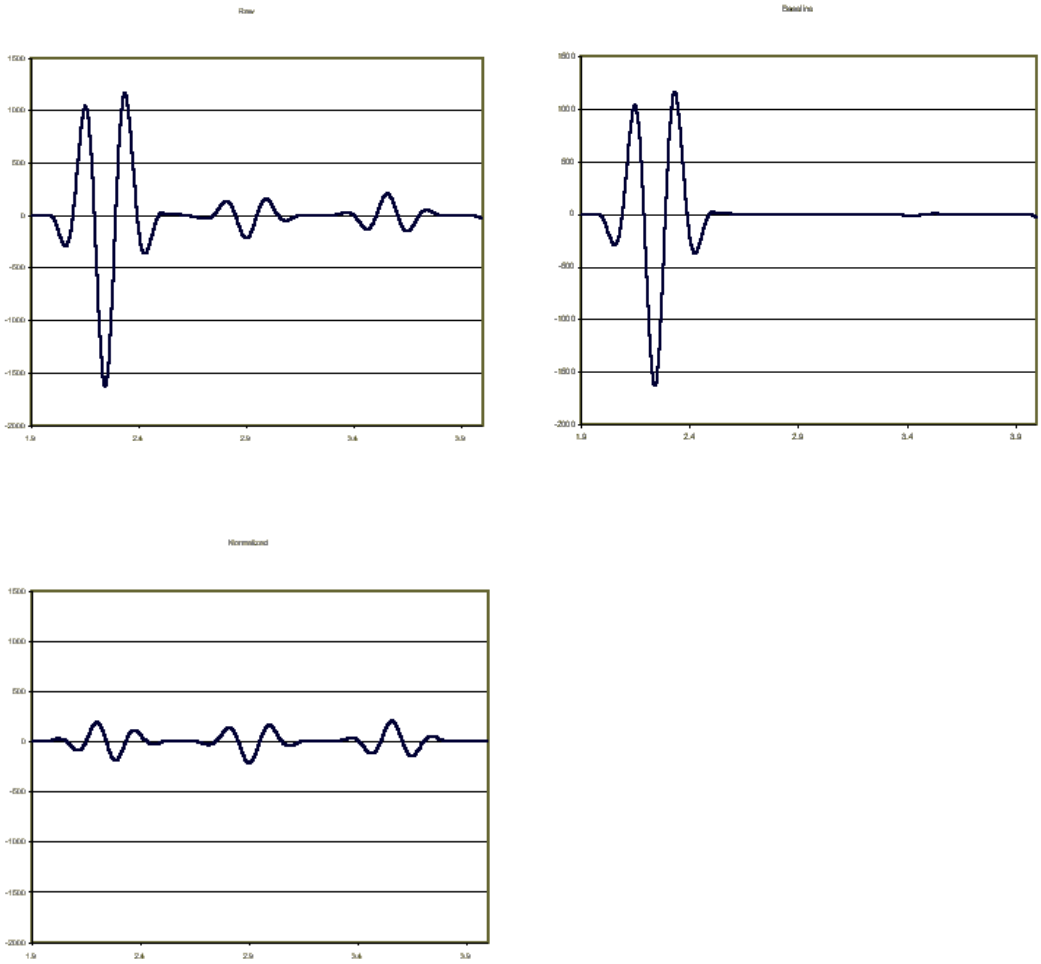

Figure 4-3: Extraction of the Desired Portion of the Signal. "Raw", upper left: the unprocessed signal, "Baseline", upper right: the previously stored "baseline" signal obtained with a bare copper block and uncorrected for reflection coefficient, and

"Normalized", bottom: the processed signal. The scales of all three frames are the same.

A problem which has been solved in the current system is the importance of trigger synchronization. If the sample clock of the digitizer is not synchronized with the trigger source for the pulser/receiver, the resulting time offset of up to plus or minus one half of a digitizer sampling period will cause the normalization to be inaccurate. This does not significantly affect the time-domain method, since it is simply looking for large peaks in the time domain, but it can cause significant distortions in the Fourier transformed data. The current system uses a built-in synchronous trigger output in the digitizer to trigger the pulser/receiver; any future system will need to incorporate such a feature as well.

The signal processing up to this point, primarily consisting of the removal of the artifact caused by the copper/fluid echo, is carried out for every sample acquired regardless of whether the time domain or frequency domain method of measurement is to be used; the processing specific to each method is described in the next sections.

B. Time Domain

1. Detection of Δt and Calculation of Layer Thickness

Conceptually, the time-domain algorithm is fairly simple. The first fluid/vapor interface echo to return to the transducer will be result in a negative voltage pulse

received at the digitizer, and will in fact be the most negative voltage seen for the entire sample period once the artifacts discussed above have been subtracted. The exact time that the first copper/fluid interface echo returns to the transducer can be easily seen from the "baseline" dataset – by simply finding the most negative point, and noting the timestamp – and the exact time that the first fluid/vapor interface echo returns to the transducer can by found by a similar method using the processed (i.e. post baseline subtraction) data set. Simply determining the difference between these two times gives the round-trip travel time within the fluid layer, which by (4-1) easily yields the layer thickness.

$$L = \frac{\Delta t \cdot c}{2} \tag{4-1}$$

One problem encountered in the calculation of the time-domain thickness algorithm is that the peak of the first fluid/air echo will sometimes not be the most negative point in the post-normalization dataset; this can be cause by noise or slight changes in transducer position resulting in an inaccurate "baseline" dataset. In either case, a system which simply looks for the most negative point in the dataset will not always successfully detect the actual thickness. In order to minimize this problem, a windowing algorithm was set up. Instead of looking for the most negative point in the entire dataset, the algorithm looks only for the most negative point within a set time before and after the previous value. The width of the window can be changed by the user while measurements are in

progress, and the width below the previous value and above the previous value can be changed independently. This allows the user to set the window to allow for the tracking of drops falling off, and thus a suddenly thinner layer, but not allow for sudden layer growth. The second-largest peak in the normalized signal, and thus the one most likely to momentarily exceed the magnitude of the desired peak, is generally either the second fluid-air echo or the second copper-fluid echo. Since both of these are after the peak of interest, setting a window which allows sudden decreases but not sudden increases will track anticipated events such as drop departure but significantly reduce the effects of noise.

2. Limitations of Time-Domain Method

This algorithm works quite well as long as the artifact cancellation by baseline subtraction performs as expected. If the “baseline” is not accurate, for example if the transducer position has shifted slightly since the “baseline” dataset was acquired, significant interference will be present in the processed dataset and this method is less reliable. However, a fairly significant change in the baseline is necessary before this occurs.

There are three main limitations to this method. The first is that the digitizer must acquire data for a sufficiently long time to capture the first fluid/vapor interface echo returning to the transducer. This only creates a problem for very thick (>5cm for the current system) layers, and if necessary can very easily be changed by simply acquiring data for a longer period. However, the sample

period to be used must be determined before the experiment commences due to the need to acquire a “baseline” of suitable length before actual experimentation starts. This means that if an unexpectedly thick layer were to be encountered during experimentation, it may not be able to be monitored if not planned for ahead of time.

The second main limitation is that the resolution is limited by the sampling rate of the digitizer. Since the algorithm simply records the time stamp of the point with the most negative amplitude, the time resolution is determined by the sampling frequency of the digitizer. This means that for the 20Msamples/s digitizer used, the time resolution is 50ns. From Equation (3), this corresponds to 35 microns (in the case of water). This means that the output of this algorithm will always be a multiple of 35 microns, creating a resolution of 35 microns for this method. If a resolution finer than this is required, it can be easily obtained by using an digitizer with a faster sampling rate. For example, a 100Msample/s digitizer would correspond to a 7 micron resolution. The 20Msample/s digitizer currently in use was selected because it was the fastest digitizer with a PCMCIA interface available; a faster digitizer would result in the need for an digitizer external to the laptop used and thus an additional piece of equipment for a theoretically easily portable system.

The third limitation is that this method is not suitable for very thin films (<500 microns). At these thicknesses, the individual echoes are not easily discernable and the frequency-domain algorithm is more appropriate.

One major advantage to this method is that it uses relatively few computational resources. When measuring using multiple transducers this is not important since the multiplexer switching time is approximately twice the computation time required for both algorithms to execute; however, when using a single transducer the computational time required for the frequency-domain algorithm is the limiting factor in the sample rate. The time-domain algorithm executes fast enough that other factors, such as the digitizer-software communication, are rate-limiting rather than the algorithm.

C. Frequency Domain

1. Additional Signal Processing

The frequency-domain algorithm is significantly more complex both conceptually and computationally than the time-domain method. It is shown in block-diagram form in Figure 4-4.

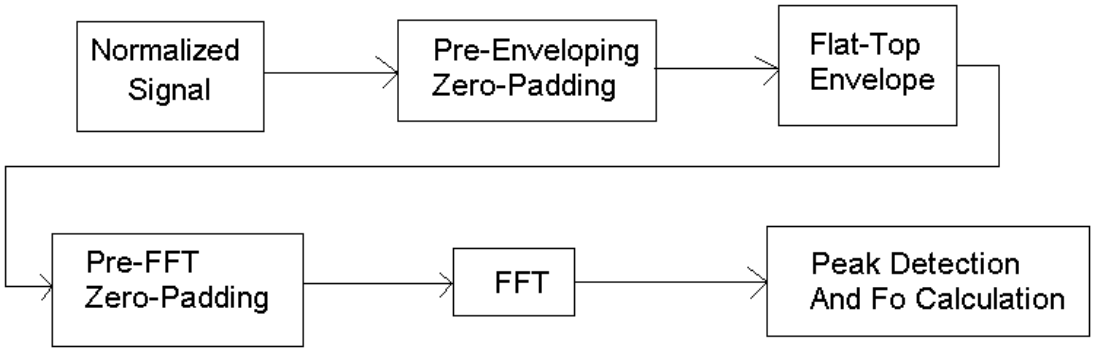

Figure 4-4: Frequency-Domain Algorithm Additional Signal Processing

After the signal is preprocessed (i.e. the “baseline” is subtracted out), the dataset appears to be a series of “ringing” signals. Each time the fluid layer is excited either by the original short pulse from the transducer or by an echo of that pulse, the reflected signal from the layer is a decaying sine wave with fundamental frequency f_0. This fundamental frequency can be used in (4-2) to find the fluid layer thickness. Isolating this frequency entirely automatically without human input can be quite challenging, however.

The first step in the process is to multiply the signal with a “flat-top” enveloping function. This has the effect of tapering the ends of the data array without affecting the center portion significantly. This filter is done by a point-by-point multiplication with the center half of the signal being multiplied by unity while both the beginning and end quarters are multiplied by coefficients which taper from unity at the center of the segments to zero at the ends. This filter is used to cut down on noise in the next step of processing due to sudden drops at the ends of the data segment. Because the rolloffs of the filter are not variable, the effect of the filter is changed by zero-padding the signal slightly at both ends before passing through the flat-top enveloping function. The user can select the amount of zero-padding; increased zero-padding results in a more accurate signal due to less of the actual signal being lost in the beginning and end portions of the sequence which are reduced by the envelope function. However, less zero-padding results in less abrupt transitions at the beginning and end of the time-domain signal which significantly reduces the noise seen after the FFT.

Approximately 50-100 zeroes are usually added to each end of the time-domain signal prior to the envelope function; with a signal of interest typically approximately 300 points long this results in a fairly low-noise FFT without too much signal loss.

As seen in Figure 4-4, the next step is to again zero-pad the signal. The signal under analysis may only be several hundred data points long; it is symmetrically padded at both ends with zeroes to create a sequence which is a power of 2 long to allow for a computationally efficient FFT. An 8192- or 4096-point total sequence (original data plus pre-enveloping and pre-FFT zero-padding) is usually used, but the exact value is user-selectable and can be changed for each measurement run. A higher value allows for higher resolution, but a lower value allows for lower computation time if faster sampling is desired.

The next step is a fast Fourier transform, resulting in a frequency spectrum. This frequency spectrum is then used to calculate the layer thickness, as described in the next section.

2. Detection of f_o and Calculation of Layer Thickness

The spectrum resulting from the processing above is analyzed with a peak-detection algorithm to identify the spectral peaks; a flow chart is shown in Figure 4-5.

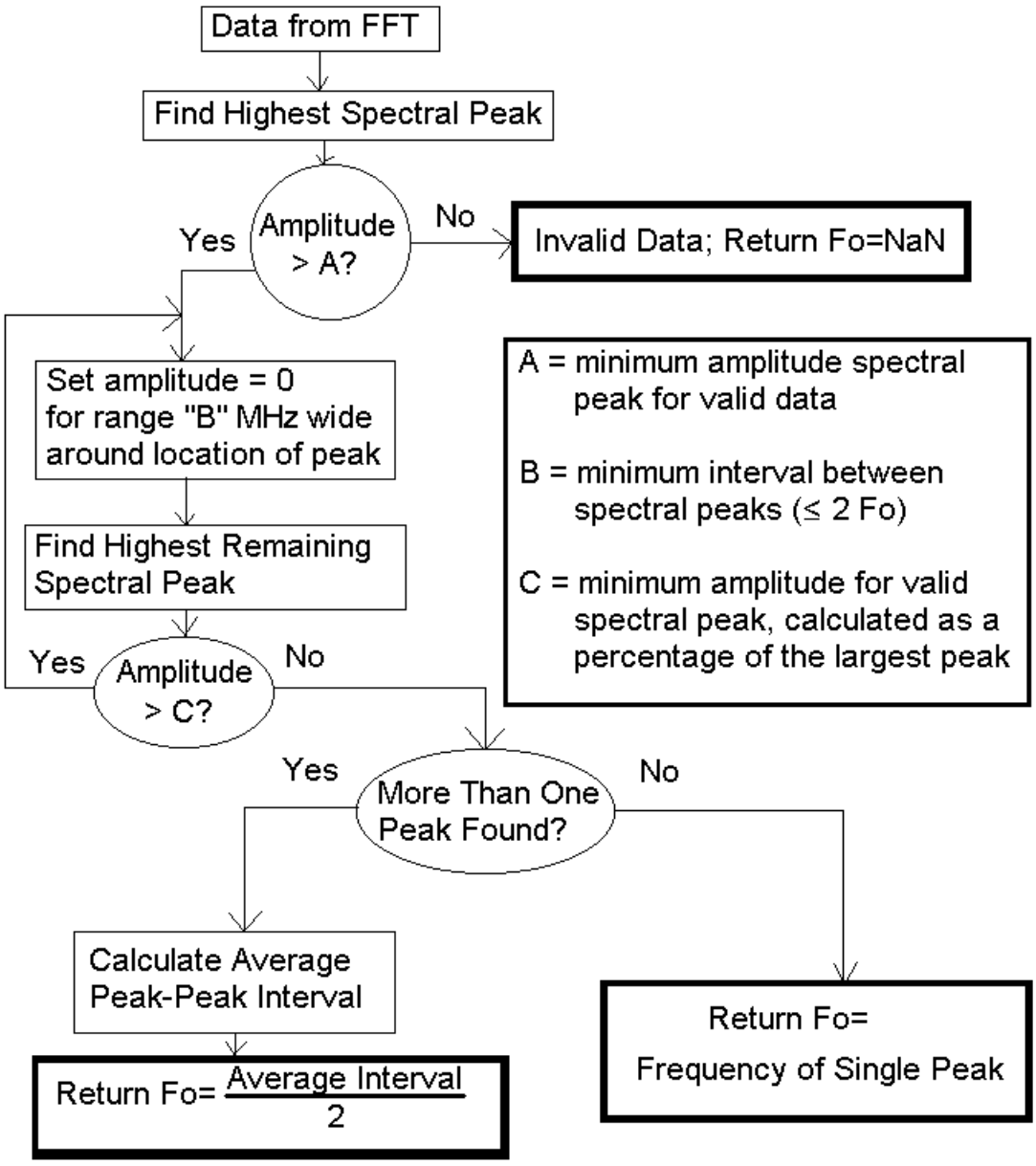

Figure 4-5: Peak-Detection Algorithm Flow Chart

This peak detection algorithm begins by identifying the highest peak in the spectrum. If there is no peak with amplitude greater than a set minimum, the data is deemed invalid and f_0 is reported as "NaN" ("Not a Number"); this is done to avoid treating noise as valid data if no actual spectral peak is present as in the

case of no fluid layer at all. Once the highest peak has been detected, the values of the array containing the FFT data are set to zero for a preset frequency interval surrounding the location of the highest peak. This interval is set based on previous layer measurements and is one of the largest challenges in this algorithm; if it is too narrow, a broad peak may be read as two peaks if while if it is too broad only every other peak will be detected. In either of these cases, erroneous data will be reported.

The algorithm then detects all other peaks in the spectrum which are greater than a set percentage of the height of the highest peak by finding the highest remaining peak, setting the surrounding portion of the array to zero, and repeating until the highest remaining peak is less than the set percentage of the original highest amplitude peak.

Spectral peaks occur at odd multiples of f_0, i.e. f_0, $3f_0$, $5f_0$, and so forth. Since for thicker fluid films the f_0 – and sometimes $3f_0$ and $5f_0$ – peaks are not visible, the interval between each pair of adjacent spectral peaks is calculated and all intervals in a given spectrum are averaged. The average interval is divided by 2 to yield f_0, which is then used in (4-2) to calculate the layer thickness.

$$L = \frac{c}{4 \cdot f_0} \tag{4-2}$$

If only one identifiable peak is detected, as happens with very thin fluid layers, the peak-detection algorithm cannot perform in this manner as no intervals exist in the spectrum; in this case, the frequency of the sole peak is deemed f_o.

3. Limitations of Frequency-Domain Method

The frequency-domain method works well for films which exceed a minimum detectable thickness of approximately 50 microns but are thin enough that the echoes from the fluid/vapor interface create a signal with enough of a resonant character to analyze. At fluid layers thicker than approximately 1mm (1000 μm) in water, the fluid/vapor interface echoes become too discrete to analyze using this method. The critical thickness in other fluids scales linearly with the speed of sound, with slower sound speeds resulting in thinner critical thicknesses. Because the time domain method works at layers as thin as 500 microns, this creates a sufficiently large overlap zone in which both work, from thicknesses of 500 to 1000 μm. The current system switches over at 750 μm; below this level the frequency domain algorithm is used while at above this level the time-domain system is used. It is desired to use the frequency-domain method for as long as possible, since its resolution is on the order of five μm compared to the time domain method's 35 μm resolution, but it becomes

increasingly unreliable as the layer grows thicker so 750 μm was chosen as an optimal changeover point.

As with the time-domain algorithm, the frequency-domain method has several drawbacks. The first is that if the fluid layer is too thin, not enough of an echo is generated to be detectable. In tests with water, a layer as thin as 50 μm has been monitored; however, it is unknown at present how thin a layer is actually detectable as no water layer thinner than 50 μm was stable enough to be measured. It is anticipated that this method will work at thinner layers than are stable with many fluids, and in any case down to at least 50 μm as seen in the lab, so this limitation is not expected to be a factor with the current research.

For thicker layers, specifically layers thicker than approximately a millimeter in water, f_0 becomes very low and is increasingly difficult to detect. Because f_0 becomes low, the adjacent peaks in the frequency spectrum become more closely packed together and less distinct. Since f_0 is calculated based on the spacing of adjacent peaks, if the peaks are indistinct f_0 can not be calculated so this algorithm fails. In lab experiments, fluid layers as thick as 2mm in water have been measured with this method; however, at thicknesses over 1mm this method is increasingly unreliable. In the few cases that the frequency-domain algorithm has successfully measured films as thick as 2mm, several attempts were required to produce a valid thickness estimate.

Finally, for fluid layers with variable thickness, for example if the peak of a wave is visible over half of the beam and the trough the other half, the spectrum

will have peaks from both thicknesses. This is usually not a problem with a 6mm transducer and a copper block thin enough that the fluid film is located in the near field since most fluid phenomena which could cause this are no smaller than the beamwidth. However, in trials with thicker copper and brass blocks where beam spreading phenomena result in an effective beamwidth of 10-15mm this is a commonly encountered problem which makes automated peak-detection unreliable. This is also a problem with dropwise condensation before a layer forms, since bare copper over part of the beamwidth and a thin layer over another part can cause the same effect. For a continuously varying thickness, as in the case of a slanted film, numerical models have shown that a 45% difference from the center of the beam to the edge can cause sufficient perturbation to the resonance to make it impossible to generate a thickness estimate even under ideal conditions. Under actual experimental conditions, a considerably smaller degree of difference will make measurements difficult.

D. Additional Topics

1. Transducer Excitation

The pulser-receiver currently used in this system excites the transducer with a single half-square-wave of selectable duration. The original pulser-receiver used a more conventional delta-function excitation. Theoretically, the new P/R will couple more energy into the transducer since it is an excitation near

the natural resonant frequency of the transducer rather than an extremely broadband signal. When the tuneable P/R became available, it was evaluated at several different frequency settings to determine whether it had any advantage over the conventional P/R; the results of this test with a 0.75mm water layer are shown below as Figure 4-3.

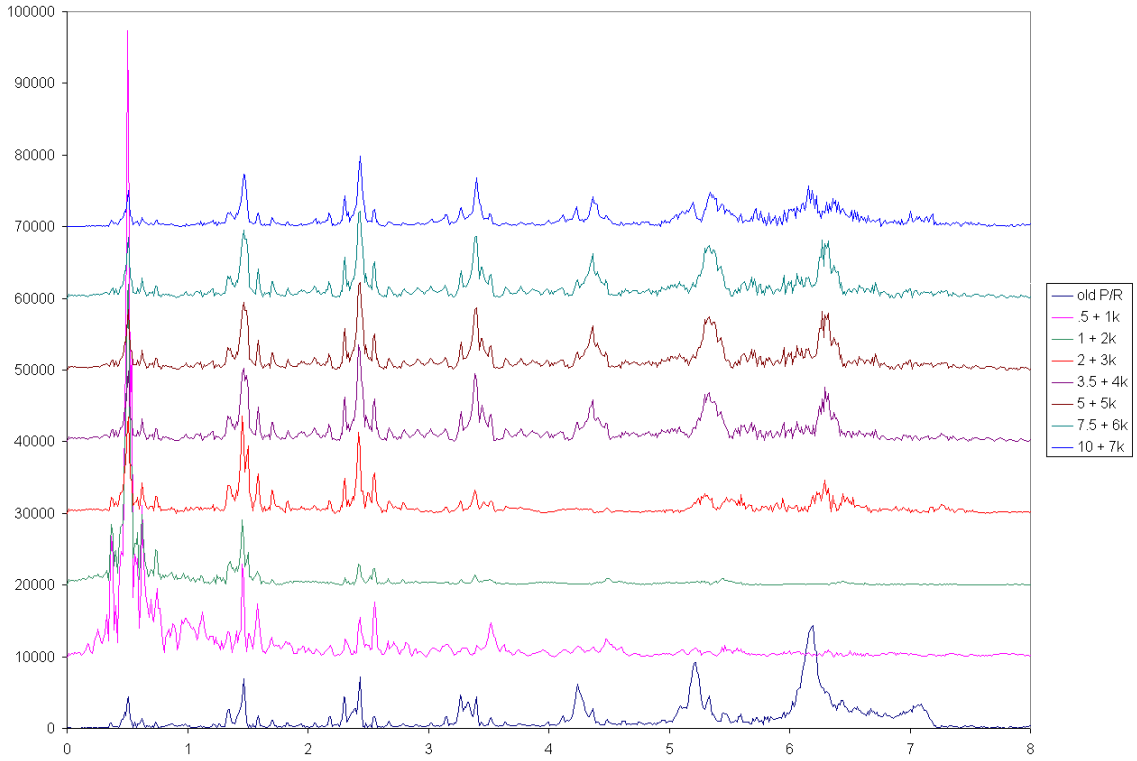

Figure 4-6: An Evaluation of an Untuned Pulser-Receiver vs Different Tuneable Pulser-Receiver Settings for a 0.75mm Water Film. The horizontal axis is a frequency axis, calibrated in MHz; the vertical axis is amplitude. Each successive dataset is offset on the amplitude axis by 1,000. The bottom trace is from the old (untuned) pulser-receiver; the seven above it are the tuneable P/R unit with the highest frequency settings at the top.

From Figure 4-6, it is clear that the tuneable pulser-receiver had better performance than the untuned unit for very low frequencies (below 2 MHz) with any setting; with settings such as the 3.5 MHz center frequency (the purple trace

which is offset by 4,000) the tuneable pulser-receiver had better performance than the untuned unit for all frequencies below 5MHz.

2. Signal Averaging

When acquiring the baseline signal, acquisition time is not particularly important but noise minimization is very important; if the baseline signal is noisy then all measurements made using that baseline for normalization will be noisy as well. Because of this, the baseline acquisition is done by averaging together 1,000 separate acquisitions for each transducer. This takes several seconds, so clearly is not practical when acquiring thickness data; however, with particularly noisy data which is the result of a stationary or slow-moving fluid layer it is possible to average together a small number of acquisitions (usually two to five) to reduce noise. The more datasets used for averaging, the less noisy the data will be; however, the longer acquisition time means a lower sampling rate. In addition, if the conditions in the fluid film are rapidly changing signal averaging can be counterproductive. This can occur when, for example, five signals are acquired for averaging over the course of perhaps 50 ms; if the layer thickness over the transducer is changing while this occurs, the five samples will be different which will act to create more noise. However, in the case of low SNR due to high noise when the fluid film is not rapidly changing, signal averaging can help significantly. Signal averaging is user-selectable, and can be changed during the experiment.

Chapter 5: Acoustic Numerical Modeling

A. Introduction

1. Goals for Modeling Experiments

Due to the complexity of the ultrasonic measurements undertaken in the course of this research, analytical modeling beyond the most basic conceptual models discussed in Chapter 3 is not a realistic option. However, some method of predicting the experimental behavior – and thus helping to verify that it was indeed what was expected rather than some unforeseen effect – was deemed important. Numerical finite time difference modeling was the clear choice as an alternative to analytical methods, and this was in fact the modeling method used. The goals of these numerical modeling experiments were to predict the acoustic behavior of the actual physical experiment and then, once the physical experimental setup was assembled, to verify that the results of the physical setup could be reproduced using modeling thus showing that the experiment was behaving in a predictable manner.

Once the initial simple numerical models had been shown to correlate with the results of the initial simple physical experiments, namely static non-condensing films, numerical modeling was used to predict the behavior of hard-to-create physical states. For example, numerical modeling was used to determine the sensitivity of the frequency-domain thin-film measurement method

to local thickness variation in the fluid layer. Acoustic modeling of a fluid layer with well-characterized variations in thickness is an easy task; however, actually carrying that experiment out in a physical model would be much more inexact. Another example of the usefulness of modeling is determining the response of the measurement system to droplet formation in the fluid layer. Numerical modeling of the received signal from a droplet of known dimensions is again relatively straightforward, while creating a physical drop of known and repeatable dimension and location is nearly impossible. The closest approach to this in the physical model would be to create actual droplets during condensation, but because of the gravity field they would be a different shape and size than the droplets expected in reduced gravity as well as being much less well characterized than those in the numerical models.

In sum, the goals of numerical modeling were first to verify that the physical experimental setup was functioning correctly and second to predict the outcome of measurements in conditions which would be difficult to create in the lab, but are expected to be seen in low-gravity operation.

2. Acoustic Modeling Software – Wave2000

The software used for acoustic numerical modeling was “Wave2000”, created by CyberLogic Inc. Wave2000 is a two-dimensional ultrasonic modeling software package written primarily for the non-destructive testing market, but it is well suited for this project as well. A two-dimensional cross-section is defined,

and the algorithm used by the software assumes that the two-dimensional cross-section in the plane of the screen extends into and out of the screen infinitely far with a constant cross-section of the object as defined on the screen. This results in a slightly unrealistic model in a number of small ways; for example, the transducer is modeled as being an infinitely long (in the direction normal to the screen) rectangle instead of a circle. However, the results from Wave2000 agree fairly well with actual experimental results so it is concluded that the effect of using a 2-D model rather than a more realistic 3-D model are relatively insignificant.

B. Modeling Theory used in Wave2000

1. Equation Used

Wave2000 represents the modeled objects as a series of grid elements, and it solves the acoustic wave equation for each grid element for each time step. The equation used is given below as (5-1). The equation and the explanation of terms are from the User's Manual to Wave2000.

$$\rho \cdot \left(\frac{\partial^2 \overline{w}}{\partial t^2} \right) = \left(\mu + \varepsilon \frac{\partial}{\partial t} \right) del^2 \overline{w} + \left(\lambda + \mu + \phi \frac{\partial}{\partial t} + \frac{1}{3} \varepsilon \frac{\partial}{\partial t} \right) grad\left(del \bullet \overline{w} \right) \qquad (5\text{-}1)$$

Where ρ = material density $\left[\frac{kg}{m^3} \right]$; λ = first Lame constant $\left[\frac{N}{m^2} \right]$; μ = second Lame constant $\left[\frac{N}{m^2} \right]$; ε = shear viscosity $\left[\frac{N \cdot s}{m^2} \right]$; ϕ = bulk viscosity $\left[\frac{N \cdot s}{m^2} \right]$; "grad" denotes the gradient operator; "del" denotes the divergence operator; $\bullet$ denotes the vector "dot" product; ∂ denotes the partial difference operator; t = time [s]; $\overline{w}$ is a two-dimensional column vector whose components are the x and y components of displacement of the medium at location (x,y), that is, $\overline{w} = [Wx(x,y,t), Wy(x,y,t)]^T$ where ^{T} indicates matrix transpose.

2. Explanation of Modeling Parameters

In addition to the geometry of the objects being modeled, there are several parameters that control the performance of the Wave2000 software package and which must be set appropriately. These parameters fall into the three major categories of temporal, spatial, and material. The temporal parameters control the size of the Δt used between steps of the simulation, the spatial parameters

control the size of the grid used, and the material parameters determine the materials being simulated.

a. Temporal Parameters

Based on the grid size as defined by the spatial parameters and the velocity of sound in the materials being simulated, Wave2000 internally calculates a suitable Δt. This internally calculated value can be modified by the user by setting the "time step" parameter; the actual time step used is the internally calculated value, multiplied by the value entered by the user as the "time step". For example, with an internally calculated value of 0.1μs per step and a user-entered value of 0.5 the actual time step used by the simulation would be 0.05μs. For most modeling runs for this project, the user-entered time step was set to 0.5 since at the default internally calculated time step (i.e. user-entered time of 1.0) the simulation exhibited slightly unrealistic behavior. Superficially the output looked correct, but after signal processing was performed the resulting data was different enough from the experimental data to be unusable. With a user-set factor of 0.5, the processed data nearly exactly matches the experimental data.

The other two temporal parameters do not directly affect the simulation processing itself. The first, simulation duration, simply determines the duration of time for which the simulation is run. Simulation durations of approximately 5-10μs were common during this project depending on the thickness of the modeled copper block; these durations were chosen to allow sufficient time for

the first echo from the fluid layer to return to the transducer while being short enough to minimize computation time. The second parameter, display frequency, controls how often the computer display was updated during the execution of a simulation run. The default setting is 1, i.e. the display is updated after every time step, but updating the display is a computationally intensive process; it is unnecessary to monitor the progress that closely, and the decrease in computation time by reducing the display frequency was significant. A display frequency of 100 was usually used, meaning that after every 100 steps the display would be updated. This value was chosen since it was infrequently enough that it would not significantly slow computation time, yet it was often enough to be able to see the progress of the simulation. In a few cases, the images displayed were also saved as images to a file resulting in a “movie” of the simulation; one “frame” every 100 steps was an appropriate rate for this.

b. Spatial Parameters

The first spatial parameters which must be set are those that control the fundamental geometry of the model; these are the model size and the model resolution in pixels per millimeter. Both of these are defined when the geometry of the model is initially created, and cannot be modified subsequently. The model size must be set large enough to contain all reflecting structures of interest, and large enough that echoes off of the borders of the modeled area do not reflect back and affect the simulation; however, the larger the modeled area is, the more computer memory is required and the longer model execution takes.

The models used for this project typically took approximately three to eight hours to execute on an 800-MHz AMD Athlon computer with 512MB of RAM, and many were as large as could be accommodated without adding more RAM. The largest models modeled were 32mmx30mm, taking approximately 30 hours to simulate; more commonly used models were 12mmx20mm, requiring six to eight hours. Some models testing only very specific ideas were smaller still, about 6mmx10mm, requiring only about an hour to simulate. Almost all models were defined in 100pixel/mm resolution. The resolution, in pixels/mm, does not control the grid size for the computation of the simulation; instead, it controls the feature size of objects which can be included in the simulation. The 100 pixels/mm value was selected to allow for very shallow slopes when investigating non-uniform films.

Boundary conditions on all edges were set to “air”; meaning that at each boundary of the model the software simulated what would happen if anything outside the modeled area was simply air. It was desired to set the boundary conditions such that the layers would be modeled as indefinitely wide (i.e. echoless absorbing boundary conditions) but this was not possible due to constraints of the software. This echoless absorbing boundary condition was advertised to be an option for an update to Wave2000, “Wave2000 Pro”, but it was decided not to invest in this software in favor of waiting for the next generation software. The next generation software, “Wave2500”, is said to model in “2.5 dimensions”. This means that it can model 3-D simulations

provided that they are axisymmetric, creating a cylinder by sweeping one plane about a central axis at one edge of the replicated plane. As of the time this writing (Spring, 2002), Wave2500 has been delayed multiple times and has still not been released. A third generation of software, “Wave3000”, which would model true three-dimensional models, will be the next step beyong Wave2500 but also has not yet been released.

Once the geometry has been defined, and the simulation is ready to run, there are two run-time spatial parameters which must be set along with the run-time temporal parameters. These are the resolving wavelength and the “points/cycle” parameter. The resolving wavelength, as the name implies, tells Wave2000 the value of the smallest wavelength of interest; this is then used along with the fastest speed of sound in any material in the model to calculate the internally-generated time step. Unlike the time step, however, the program does not internally generate a spatial step for grid spacing. The grid spacing is directly determined by the user, using the “points/cycle” parameter. The grid spacing used by the program is the resolving wavelength divided by the “points/cycle” value. This means that theoretically a “points/cycle” of 2.0 should satisfy the Nyquist criterion, but in practice a value of at least 4.0 is needed for acceptable performance.

c. Material Parameters

When defining the initial model, the user selects a “gray level” (color) for each different “material” in the model. Once the model is fully defined geometrically, material properties are associated with each “gray level”. When initially defining the geometry for a copper block with a fluid layer, three rectangles are defined. One is made the correct thickness for the copper block, and assigned “gray level 0”. The center rectangle is set to the thickness of the fluid layer, and assigned “gray level 100”. The final rectangle is created on the opposite side of the fluid layer from the copper block, and is assigned “gray level 255”. Gray level 255 is a reserved color which automatically indicates “void”, or acoustically impenetrable vacuum. The other two gray levels are defined once the geometry is complete to be copper for gray level 0 and water (or other fluid) for gray level 100.

For each gray level used in the model except gray level 255, the user can either select material properties from a library included in the Wave2000 software package or input custom parameters. For all modeling done in the course of this research, only library entries were used; specifically, those for copper, water, methanol, and brass were used during the course of this research.

C. Model Setup

1. Time Domain (Thick Film)

The modeling done for the time-domain, uniform-thickness film, case was relatively simple, as it was a case easy to test experimentally and as such the modeling served simply as a means of verification that the modeling was accurate. As with all models used for this project, the "condensing block" model used was a solid copper block 20mm wide by 10mm thick. The transducer, which was 6mm across, was on the "top" of the block while there was a fluid layer of variable thickness on the "bottom". Between the far side of the fluid layer and the edge of the simulation space was a layer of void (acoustically impenetrable vacuum). The overall size of the modeled area was 20mm wide by 20mm high, allowing for up to a 10mm fluid layer. For the initialization run of the software, which created a baseline dataset with which to process all subsequent datasets, a fluid layer of the full 10mm thickness was used. For the experimental runs, layers between 0.5mm and 9mm were used (results from these experiments are given in Chapter 7, "Results").

An example of such a setup is shown below in Figure 5-1.

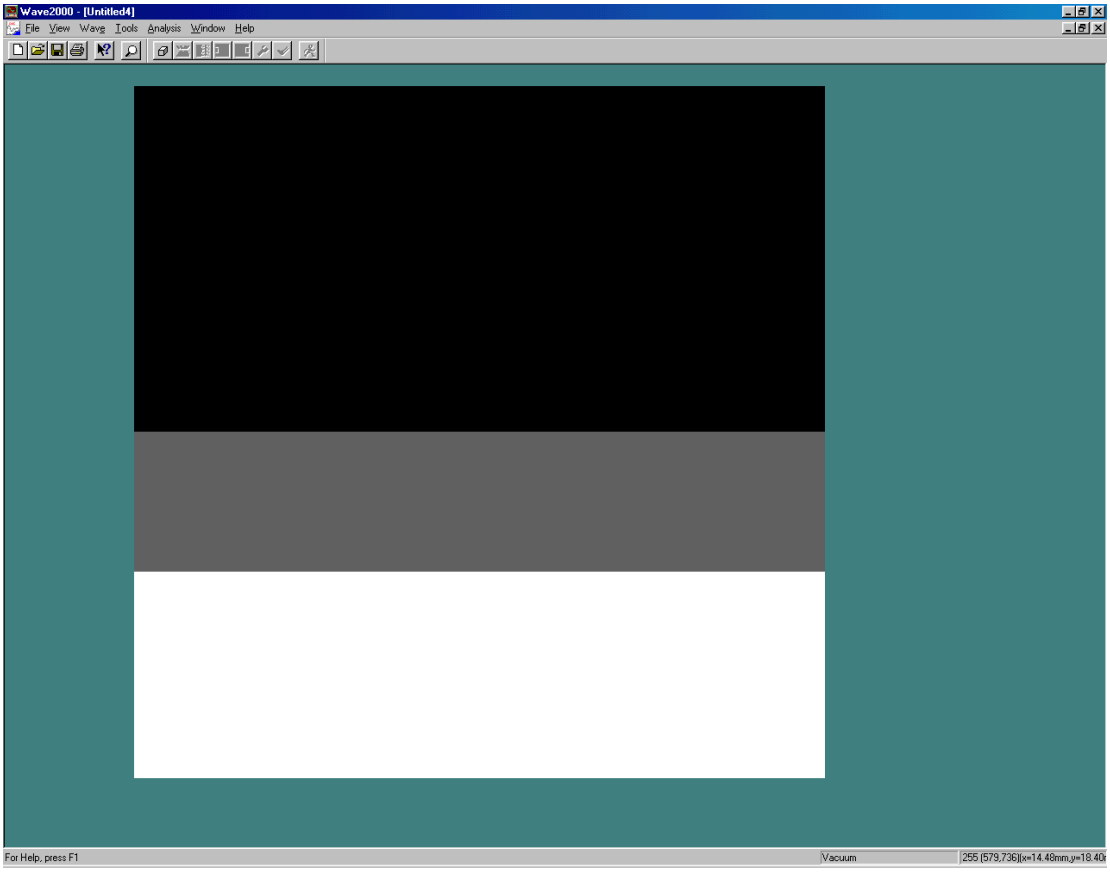

Figure 5-1. An image of a typical time-domain simulation geometry. The upper black block is the copper condensing block, and the middle gray block is the fluid layer. The bottom white block is "void", which approximates air. The transducer is not visible in this view, but is 6mm wide and is centered on the top of the "copper" block. The block itself is 20mm wide by 10mm high, with a 4mm deep water layer and a 6mm "void" layer to fill the 20mmx20mm simulation field.

The transducer was set to pulse-echo mode, with an excitation pulse of a "sine Gaussian pulse" waveform, meaning that the pulse was a sine wave with Gaussian envelope. This pulse was used for all modeling experiments, as it was desired to model them all with the same transducer and excitation just as the actual physical experiments used the same transducer and excitation. The sine Gaussian pulse was chosen to be a signal with moderate bandwidth and a center

frequency (sine wave frequency) of 5MHz, which we believed to fairly closely model the actual physical transducer characteristics. The specific excitation wave is shown in Figure 5-2, below.

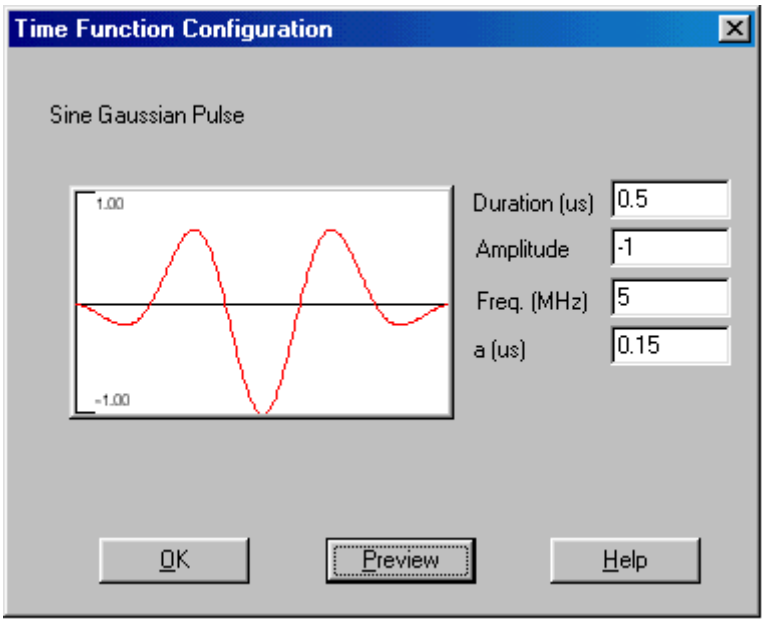

Figure 5-2. The excitation signal sent by the transducer in the Wave2000 model. This is a "sine Gaussian pulse", with amplitude enveloped by a Gaussian curve. The parameters are set as shown, resulting in the largest amplitude being negative. The actual physical transducer is excited by a negative-going square wave, but the characteristics of the transducer result in a signal similar to that shown to be actually injected into the copper block.

The run-time spatial and temporal parameters discussed above were set as shown in Figure 5-3. These parameters were used for all models, not only time-domain runs, as they were found to be the set which produced an accurate simulation while using sufficiently little memory to be practical. Settings which used less memory and computation time, for example a time step scale of 1.0, produced anomalous results which did not match physically observed results.

Settings which would theoretically be more precise, such as setting the resolving wavelength to 0.01mm, would require much more RAM than was available and so were impractical. The settings shown below produced data which matched physical data so far as was measurable while requiring only as much RAM as was available; however, simulation time was in excess of eight hours for a single run.

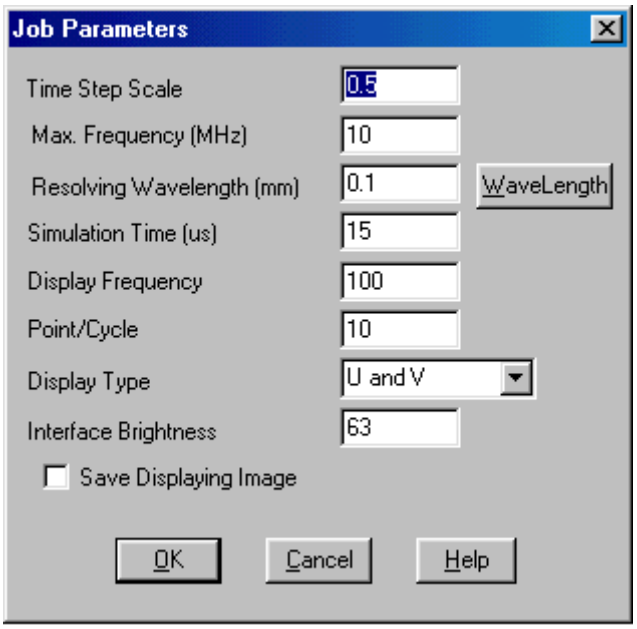

Figure 5-3. Run-time parameters used for Time-Domain models. These parameters were used for all models, not only time-domain runs, as they were found to be the set which produced an accurate simulation while using little enough memory to be practical.

2. Frequency Domain (Thin Film)

The only difference between models designed for time-domain (thick film) use and frequency-domain (thin film) use is simply the fluid film thickness. While numerical modeling experiments to test the time-domain algorithm use 0.5mm-9mm thick films, frequency-domain tests used 0.05mm (50 micron) – 1mm thick films. Aside from this geometric change, all other settings were kept exactly the same. As can be seen from the overlapping thickness ranges, films from 0.5mm to 1.0mm thick could be, and in fact were, used to test both thin and thick film algorithms since they modeled the transition region where both algorithms work acceptably. An example of a thin-film geometry is shown in Figure 5-4.

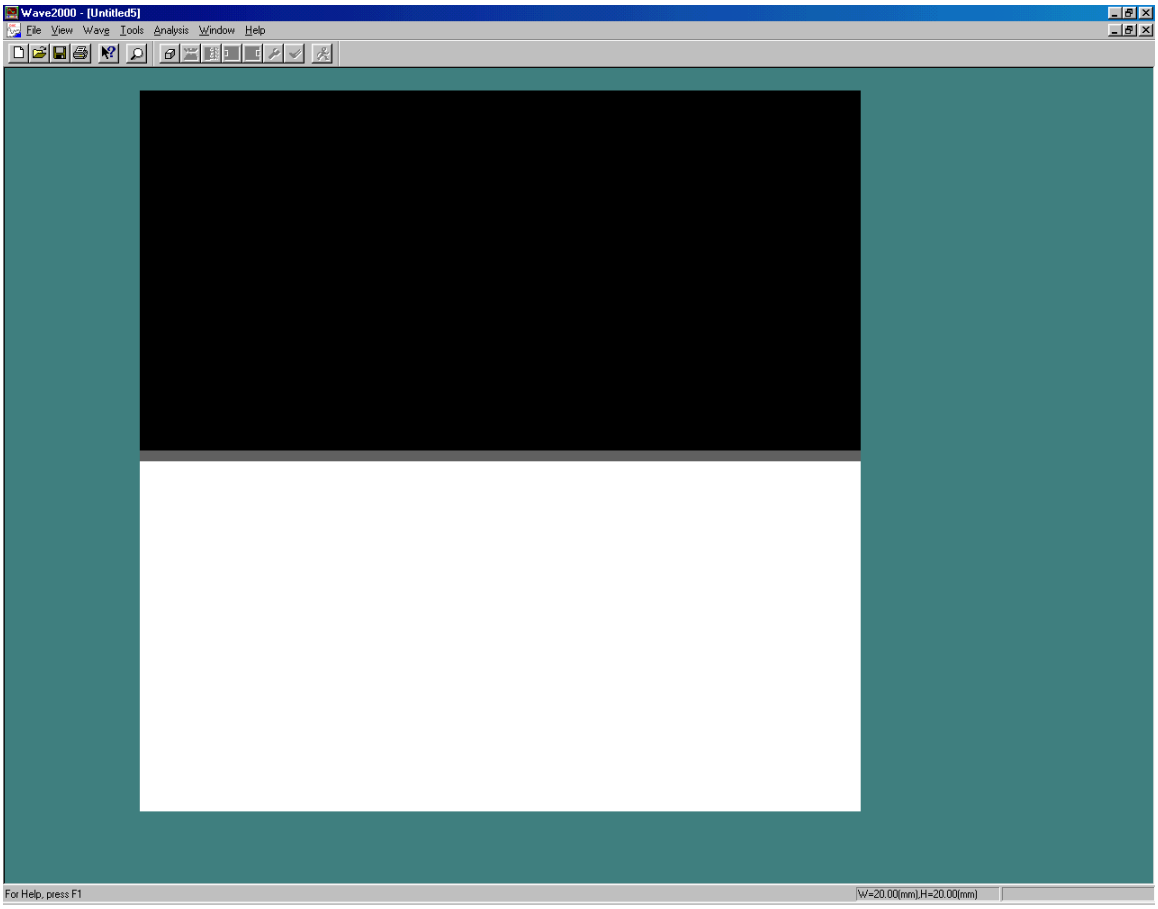

Figure 5-4. An image of a typical frequency-domain simulation geometry. The upper black block is the copper condensing block, and the very thin middle gray block is the fluid layer. The bottom white block is "void", which approximates air. The transducer is not visible in this view, but is 6mm wide and is centered on the top of the "copper" block. The block itself is 20mm wide by 10mm high, with a 0.25mm deep water layer and a 9.75mm "void" layer to fill the 20mmx20mm simulation field.

3. Non-Uniform-Thickness Film

While the utility of the uniform-thickness film models was mostly in verifying that the physical model was performing as expected, and even more so to verify that the modeling was accurately representing physical reality, the non-uniform-thickness film models were intended more to explore phenomena which was not easily created in a physical experiment. An example of this was the

exploration of wedge-shaped films, to determine how much nonuniformity can be tolerated by the frequency-domain and time-domain algorithms. This was done by creating a geometry with a slanted bottom edge to the fluid film, at an angle and thickness calculated to produce a set variance in thickness across the beamwidth. Figure 5-5 is a fairly extreme example, showing a 50% difference between the left and right edges of the beam.

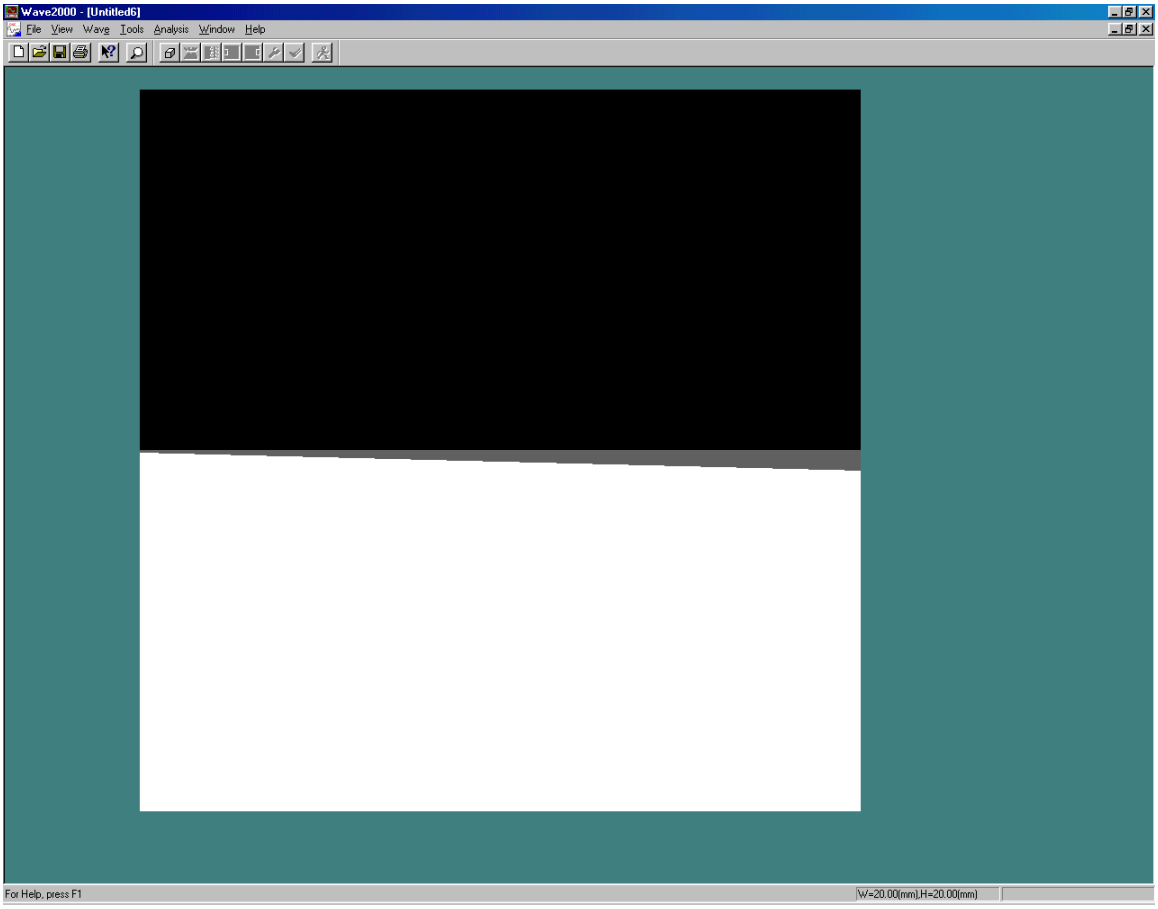

Figure 5-5. An image of a non-uniform film geometry. In this model, the thickness of the fluid film varies from 225 microns on the left edge of the nominal beamwidth to 375 microns on the right edge of the nominal beamwidth; this creates a difference of 150 microns which is 50% of the 300 micron center thickness. The angle used for the bottom surface of the water to achieve this is 1.43°, with a water layer thickness on the extreme left edge of the 20mm model width of 0.05mm.

Another example was the simulation of films with droplets; droplets of varying radial sizes, depths, and horizontal offsets from the transducer were measured. Most of these droplets were modeled as semi-ellipsoids in the 2-D plane of the screen, resulting in the numerical model of semi-cylinders since the equations used in Wave2000 model a 3-D object with a constant cross section as shown on the screen. However, some models using a series of small drops to simulate the first phase of condensation before a film forms were modeled as a series of semi-circles in the plane of the screen (resulting in the numerical model of cylinders with semi-circular cross section). Two examples of these models, one an offset single drop and the other a series of small drops, are shown as Figure 5-6.

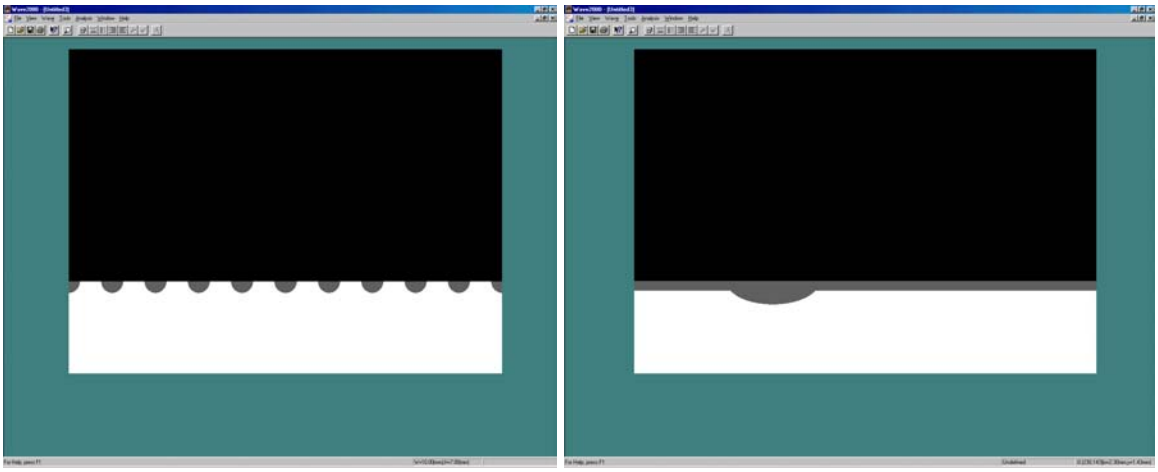

Figure 5-6. Two droplet models. On the left, a 5mm thick block is shown with multiple 0.25mm radius droplets on its otherwise bare surface; the droplets are spaced 1mm center-to-center. On the right, a droplet consisting of a semi-ellipse with 2.0mm horizontal diameter and 0.5mm vertical radius with a 0.2mm layer on the rest of the block.

Aside from the geometry, all other parameters used in the non-uniform-film models were exactly the same as in all of the other uniform-film models.

Chapter 6: Experimental Work

A. Experimental System

1. Overall System Description

The system developed by this project to carry out the ultrasonic measurement of thin fluid film layers is contained in four physical parts, shown in block diagram form below in Fig. 6-1.

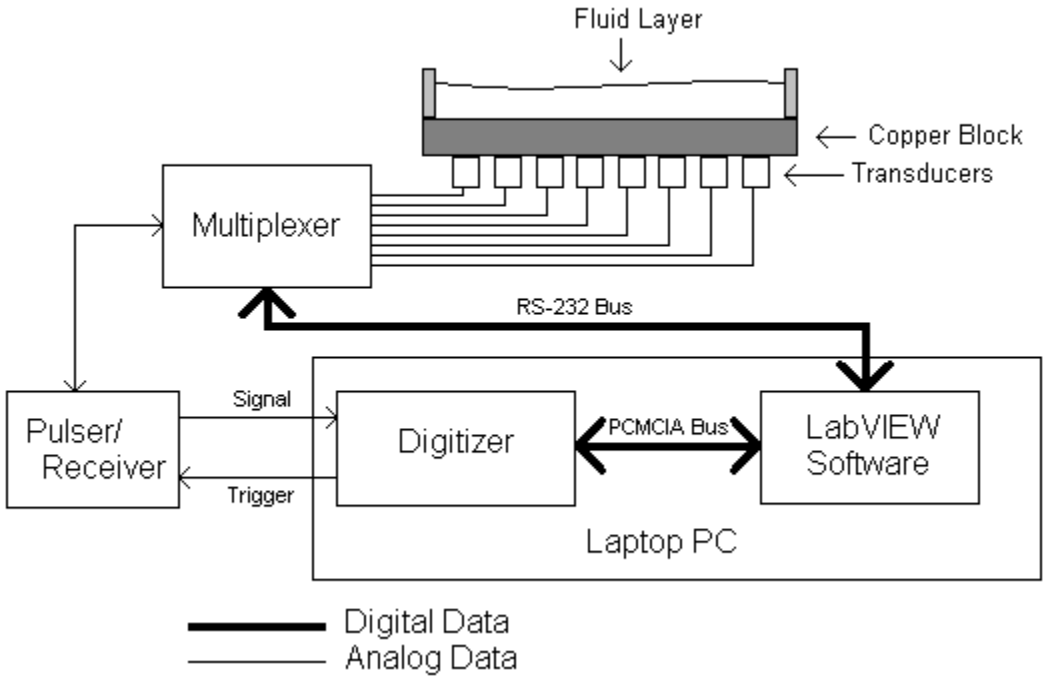

Figure 6-1: A block diagram of the ultrasonic thickness measurement system.

The large box in the lower right is a Dell laptop, which contains a PCMCIA digitizer in one of its expansion slots. The system is controlled by LabVIEW software running on this laptop, and the PCMCIA digitizer is used to acquire the

ultrasonic data. The second major element to the system is a Panametrics model 5077PR Pulser/Receiver unit. This unit generates the excitation pulses to be sent to the transducers, and receives their detected echo signal which is amplified and sent to the laptop/digitizer as the so-called RF signal. The multiplexer is an Agilent 34970A multi-function device chassis with an Agilent 34903A general purpose switching card. This device is used to allow the single P/R unit to be used with eight different transducers. The transducers themselves, mounted on the copper block with their cabling attached, are the final element in the system.

In operation, the LabVIEW software running on the laptop initiates a data acquisition cycle by first setting the multiplexer to the correct channel via an RS-232 serial communications bus and then sending a software trigger to the digitizer. The digitizer has the capability to send a synchronous external trigger pulse when it receives a software trigger, and so begins acquisition at the same time it sends the external trigger pulse. This pulse is used to trigger the P/R unit to generate a pulse to send to a transducer, via the multiplexer. The echoes received by the transducer produce the RF signal which travels back to the P/R unit, again via the multiplexer, and is amplified and passed on to the digitizer which then acquires and digitizes the data. This echo data is then processed by the LabVIEW software, and a thickness estimate is generated and displayed on the front panel. This process can be repeated as often as 40-50 times per second when using a single transducer, or as often as 20-30 times per second

when using multiple transducers since the multiplexer takes a significant amount of time to change channels.

2. Hardware

a. Laptop

i. System Description

The laptop used for this research is a Dell Inspiron 8000 series laptop with an 800 MHz Intel Pentium III CPU and 128 MB of RAM running Microsoft Windows ME. This laptop was chosen to ensure enough processor speed and RAM to support the needs of the analysis program. Since the program performs several computationally intensive tasks such as FFT's, it requires a fast processor to run at a high enough speed to allow for real-time data analysis instead of storing the data and then post-processing it after the experimental run. When designing the system, it was decided that it was worth a slight additional expenditure for a faster laptop to allow this real-time processing. Even in single-channel mode, in which only one transducer is used and the multiplexer does not change channels after the initial channel selection, the CPU speed is not the limiting factor in sample rate in most cases. However, if a large value for FFT size is selected to allow for more precision in the frequency-domain calculations, the CPU speed does become the limiting factor.

ii. Operating System

Microsoft Windows was chosen as the operating system for the laptop to allow easy interoperability with other lab computers. Specifically, the Microsoft Windows ME ("Millennium Edition") version was used. A more secure system, such as Windows 2000 Professional, was not deemed necessary since the laptop is never used on any network other than in the lab which is behind WPI's firewall. In addition, in the author's past experience LabVIEW has occasionally had interface problems with hardware similar to the PCMCIA digitizer used in this project when used on a computer with a Windows NT system. Since Windows 2000 Professional is a Windows NT derivative, Windows ME was chosen instead.

iii. LabVIEW software

"LabVIEW", or "Laboratory Virtual Instrument Engineering Workbench", from National Instruments Corp. is a graphical programming environment specifically designed for data acquisition and control use. Most instruments suitable for data acquisition use – for example, digitizers – have LabVIEW drivers available, and those that do not are generally used over a GPIB, RS-232, or other general purpose bus so do not require special drivers. The LabVIEW driver for the NI5102 PCMCIA digitizer card used in this project was supplied with the card, and the HP34970A used as a multiplexer was controlled over an RS232 bus. LabVIEW has built-in drivers to control a standard RS232 serial port so no

special drivers were required. The P/R unit was not directly controlled by the computer, so of course no special drivers were required for it either.

iv. Digitizer Card

The digitizer card used was an NI5102 PCMCIA “High Speed Digitizer” card. This card is a fully functional 20MS/s 8-bit 2-channel digitizer with standard PCMCIA card dimensions: approximately 3.4”x2.2”x0.2” (11.5cmx5.4cmx0.5cm). Power consumption is rated at 260mA when active, 60mA when inactive (both at 5VDC). The card has an external connecter cable which allows for cable connection, seen below in Figure 6-2.

Figure 6-2: Digitizer card connector cable. The card itself is in the computer’s expansion bay at the left of the photo, with the cable plugged into it. At the right of the photo is the terminal block holding all of the connecters which lead to the digitizer.

The external connector cable allows standard BNC and SMB connectors to be used with this digitizer, instead of requiring special miniature connections which would otherwise be necessary. In figure 6-2, the bottom three connectors on the right of the photo are the external trigger (top BNC connector), channel 0 input (bottom connector), and channel 1 input (middle BNC connector, unused for this

project as only one channel is needed). The top two connectors, of which only one is visible in this photo due to the angle (the two are vertically stacked), are SMB connectors and are both special function connections. These can be set at run time to be either inputs (for example, digital triggers) or outputs. In this project, one was unused and the other was configured to be an output; when the software trigger is received by the digitizer card it outputs a synchronous trigger through this port which is used to trigger the pulser-receiver. This was done to provide synchronization between the digitizer and the P/R unit. Without this synchronization, a random offset of up to plus or minus half of one sample period, or 0.05μs, would exist in data sets relative to the normalization dataset. Since data sets are subtracted from each other in the normalization process, this random offset causes an unacceptably high level of noise. By synchronizing the P/R unit and the digitizer, this problem is completely avoided.

b. Pulser-Receiver

The pulser-receiver unit used for this project is a Panametrics, Inc. Model 5077PR pulser-receiver. This P/R unit is similar to a standard lab pulser/receiver unit, except that instead of a large, impulse-like function it excites the transducer with a square wave of selectable width. This results in a much more narrowband transducer excitation, which increases the amount of spectral energy available in the frequencies of interest.

A control on the front panel, labeled “transducer frequency”, actually controls the width of the square-wave excitation pulse. The intended purpose is to match the frequency of the excitation with the resonance frequency of the transducer to allow for more efficient excitation, but for this project it was instead used with a relatively wideband transducer and set to the frequency range corresponding to the anticipated resonant frequency of the fluid layer. The frequency control can be used either in a preset mode, where each setting on the “frequency range” control corresponds to one preset frequency near the center of the range, or in a variable mode in which the actual frequency can be freely varied over the range 0.1MHz to 20MHz. In this project, the fixed mode with the frequency range of 2.5-3 MHz was used.

c. Multiplexer

The purpose of the multiplexer is to connect multiple transducers to a single P/R unit and digitizer. However, the best actual implementation of a multiplexer proved relatively difficult because of the combination of two things. The first is that switching speed is desired to be as fast as possible, which allows for a high-speed system. The second is that both the excitation pulse from the P/R to the transducers, which is on the order of 100-200 volts, and the return signal, which is on the order of several millivolts, have to travel through the same connection in a very short period of time in opposite directions. A solid-state system was investigated to allow for high switching speed, but no implementation

meeting the requirements for high voltage tolerance and very low noise for low voltages was found. Relatively old-fashioned physical relay switches had the required voltage tolerance and low noise combination, but tended to have unacceptably long switching times. The best available solution was the Hewlett-Packard / Agilent Technologies 34970A multi-function device with a 34903A 20-channel actuator/general-purpose switching module.

This device consists of a 34970A mainframe which communicates with the laptop via an RS-232 interface with a plug-in 34903A card which is simply a set of 20 independent reed relays. Each of the relays is a single-pole, double-throw relay rated for up to 1A at 300V, which exceeds the requirements for this project. Since they are physical relays, low voltages are transmitted without a problem as well. Each of the 20 relays is independently controlled, and thus more than one can be closed at a time, but the system is configured such that a single command from the laptop will close the desired relay and open all others. The system has a rated switching speed of 120 actuations/second, resulting in a 60 channel/second theoretical rate (60 channel openings and 60 channel closings). However, because of the low speed of the RS-232 bus the highest speed actually achieved is roughly 30 channels/second since the time consumed in sending the RS-232 commands is roughly comparable to the time required for the actual switching event.

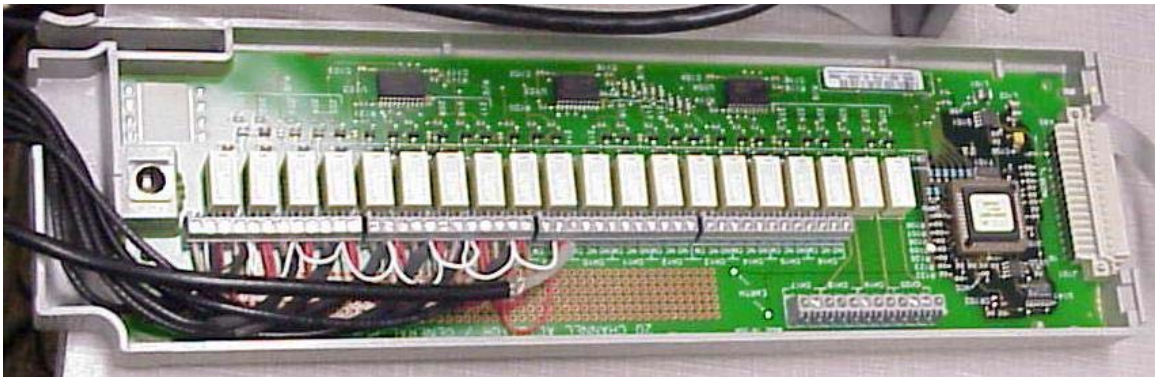

Figure 6-3: 34903A Actuator/General Purpose Switching card. This is a view of the plug-in card with its cover removed to reveal the relays and their terminal blocks. Actual size of this card is approximately 12.5" long by 3.6" wide by 1.5" thick.

All channels use a common ground, connecting the shields of the coaxial cables of all of the transducers and the shield of the coaxial cable leading to the P/R unit. This ground is also connected to the normally closed terminal of each relay. The transducer lead (the "hot" lead, or the center conductor of the cable leading to each transducer) is connected to the "common" contact of its relay, while the lead connected to the P/R unit is connected to the normally open terminal of all relays. This configuration results in the selected transducer connecting directly to the P/R unit, while all other transducers are grounded.

d. Transducers

Eight Panametrics Model # M110 5MHz ¼" (6mm) diameter contact transducers were used. The transducers were attached to the P/R unit via a coaxial cable which connected to the transducers at an SMB jack on the side of each transducer near the rear end. Several ways of mounting them to the copper block were tried, and the chosen method was to simply glue them on.

This was decided upon due to good acoustic coupling efficiency along with simplicity and ease of mounting. A common silicone sealant, DAP Auto/Marine 100% Silicone Clear Sealant, was used. A small amount of the sealant was applied to the face of the transducer, and it was then placed in the desired location on the block. It was plugged into the P/R unit, and the echo signal was monitored using either the laptop or a standalone digitizer while the transducer was pressed against the block until the echo signal reached an acceptable level. During this process, the sealant was being squeezed out of the interface between the transducer and the block leaving behind only a very thin layer which acted as an acoustic coupling layer. During testing, it was discovered that it was very important to ensure the absolute cleanliness of the transducers and block prior to mounting. In one trial, transducers which appeared clean were mounted and found to have poor coupling; they were removed, polished using very fine sandpaper, and remounted resulting in a 45dB improvement in signal.

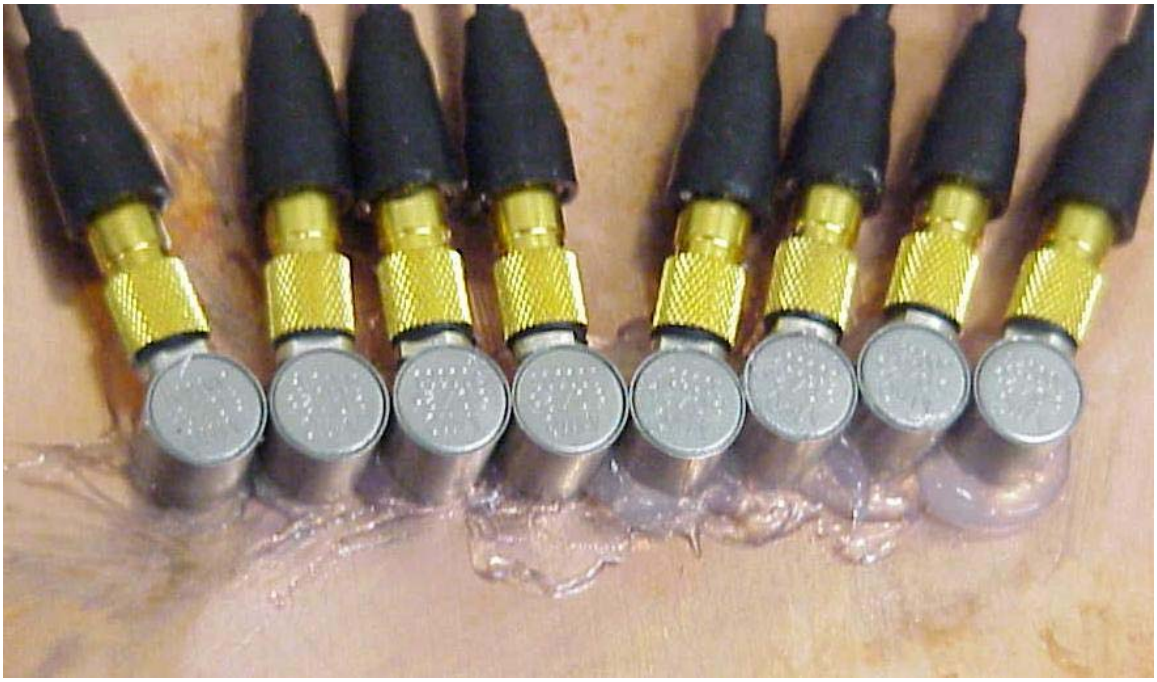

Figure 6-4: Eight transducers mounted to the copper block. In this experimental setup, the eight transducers were placed in a linear array as closely spaced as possible for maximum spatial resolution. Each transducer is ½" in diameter.

3. Software

A detailed technical description may be found in Appendix 1: *Measurement Software User's Manual*, and Appendix 2: *Measurement Software Technical Manual*. This section gives an overview of the construction and function of the software written for this project, but does not go into detail. The details of the signal-processing algorithms used, including a flow chart, are in Chapter 4: Signal Processing.

National Instrument's "LabVIEW" software package allows programs to be written in the "G" language. The "G" language is a **G**raphical programming language, in which one uses graphical symbols instead of text code. An example

of a simple G program is shown below in Figure 6-5. In this example, the user inputs two numbers on the “front panel” (left); the program then calculates the product of the two numbers using code seen in the “diagram” (right) and displays the result back on the front panel. The actual source code in this program is what is seen in the picture; there is no text code needed. To create this program, first the inputs and outputs were selected and placed on the front panel. By doing this, their “terminals” automatically appeared on the diagram. The terminals of the inputs were then connected with “wires” to a “multiply” function; the output of the “multiply” function was then “wired” to the terminal for the output.

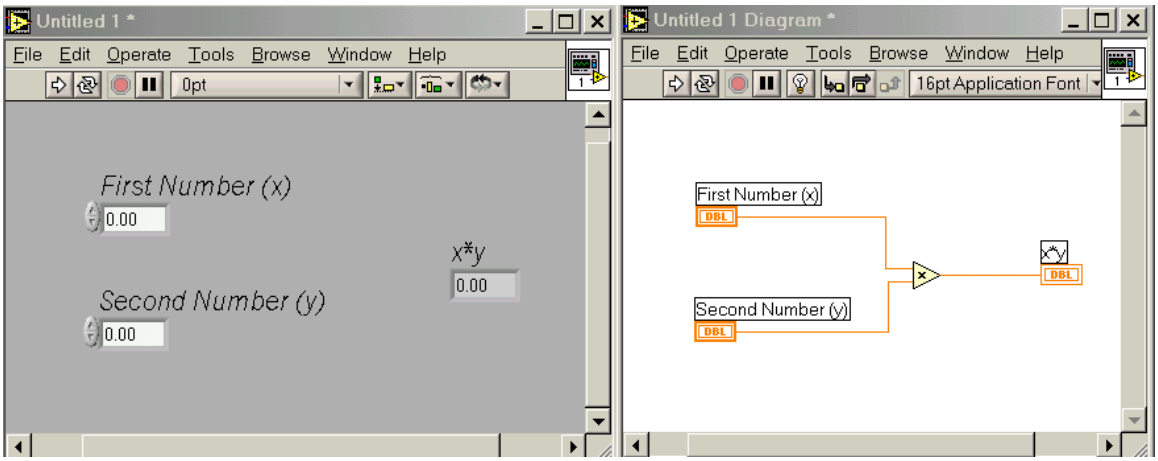

Figure 6-5: A simple example “G” program. Left: “Front panel”, containing inputs and outputs. Right: “Diagram” containing source code.

This is an example of an extremely simple LabVIEW program; the measurement program written for this project is of course much more complex. However, it uses the same approach as the simple program shown above. This means that it is much easier to understand and modify than a program written in

a traditional text programming language, as well as being faster to write initially and much easier to debug.

The measurement program written for this project is a looped program; upon startup it reads in the previously acquired baseline data and sets several parameters, such as which transducers will be active and what the speed of sound in the fluid will be, and then it enters a loop. In this loop, the data is read from another subroutine (which will be addressed below), normalized by subtracting the baseline data, and then analyzed by both the time-domain method and the frequency-domain method. The result is then displayed on the front panel in the form of a strip chart as well as numerically. A screen shot of the main front panel is shown below in figure 6-6. The stack of charts (blank in this view) on the left are the graphical depictions of thickness-vs-time for each transducer while the buttons immediately to the right of the graphs control which transducers are active for a given run. To the right of the transducer selection buttons is the numerical readout for layer thicknesses at each active transducer. All of the other controls seen are to control various other parameters, discussed in Appendices 1 and 2.

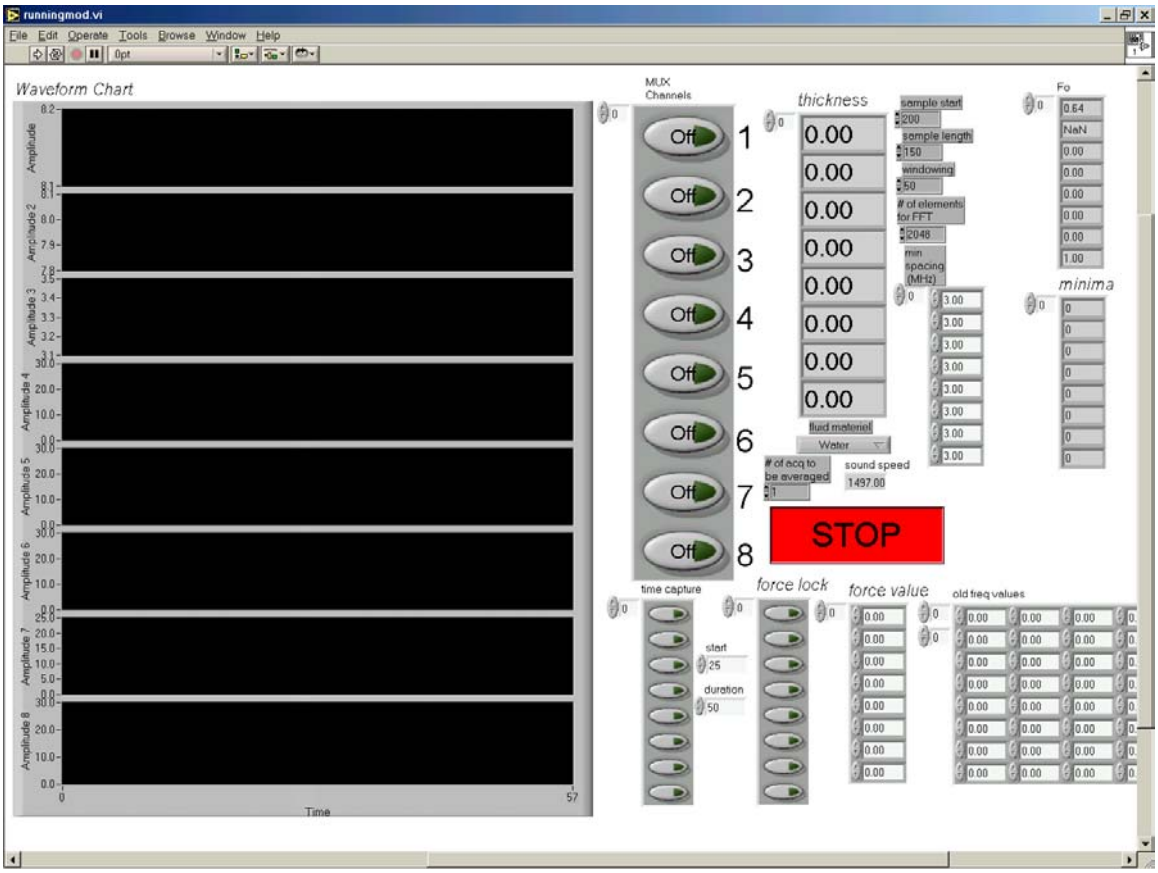

Figure 6-6: The front panel of the main measurement program.

In addition to this main program, a second program was written to perform the actual data acquisition. By executing these two separate programs simultaneously, the data acquisition program can be acquiring the next round of data while the main program is analyzing the current round. This significantly speeds up the sample rate at the cost of only slightly increased complexity. All parameters that the data acquisition program needs are sent to it by the main program. As far as the user is concerned, the data acquisition program runs entirely out of sight in the background. Since the user never directly interacts

with the data acquisition program, it will not be discussed further here or in Appendix 1; however, it is covered in detail in Appendix 2.

B. Experimental Setup

1. Stationary (non-excited)

The initial experiments were conducted with a non-excited static fluid layer. These were done using an earlier copper condensing block which was available after use in previous measurements, with a ring fashioned from a Tupperware container glued to one side to create a “swimming pool” type of effect as seen in figure 6-7.

With this setup, the transducers were affixed to the bottom of the block, being careful to avoid the cooling channels bored through the block, and used to measure the thickness of the fluid film in the Tupperware “swimming pool” on top. Due to the approximately 2” height of the Tupperware ring, fluid “films” as thick as 2” (~5cm) could be measured. Thickness verification was performed by measuring with a ruler held up against the Tupperware or dipped into the fluid.

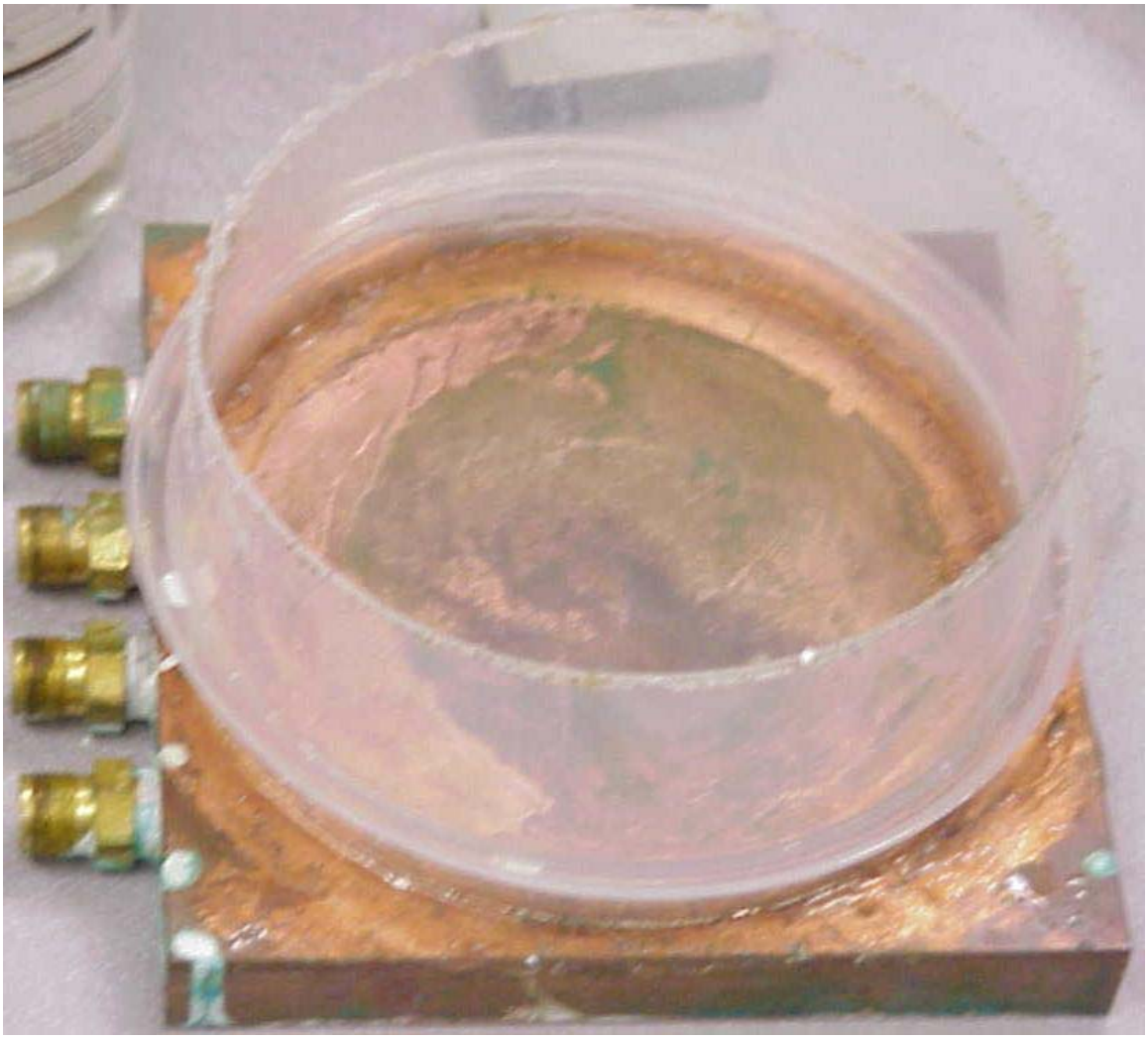

Figure 6-7: Initial experimental test block with Tupperware "swimming pool". The brass fittings at the left of the block are for cooling water; these were in place from the condensation experiment that the block was originally used for but were not used for these experiments.

With the aid of a small amount of surfactant, films as thin as 50 microns were measured; however, films less than approximately 100 microns thick were not stable enough to be reliably repeatable even with the aid of surfactant. The thickness of these thin films was not measurable in the same manner as the thick

films; the only verification available was to divide the volume of fluid in the pool by the surface area of the pool. Since this was not a very accurate method due to irregularities in the Tupperware-copper interface (i.e. glue irregularities) and surface tension effects (i.e. a meniscus), the results of these static trials were not directly verifiable. This shortcoming was addressed by the dynamic tests addressed in the next section.

2. Slow constant layer growth

Once the system had been shown to measure static layers reliably, the next challenge was to measure a fluid layer of changing thickness. This was done by starting off with a very thin static layer, and adding fluid at a very slow and constant rate. To accomplish this, a standard medical macrodrip intravenous administration set was acquired. The IV set allowed fluid to flow at a rate set by an adjustable clamp, and the flow rate was determined by counting the number of drops per second in the drip chamber where one milliliter consisted of 10 drops. The drip rate would be set to a rate allowing for layer growth over several minutes (3-5 minutes) from a very thin (<.3mm) layer to a thick (~1cm) layer. This was typically approximately one drop per second, resulting in a 1cm increase in thickness in approximately 7 minutes. For several trials where thicker layers were desired, a faster drip rate was used (for instance, 3 drops/second resulted in a 5 cm layer growth over 12 minutes). The rate of delivery of fluid was constant, and thus the performance of the system could be

measured by determining the linearity of the graph of measured layer thicknesses versus time. This also allowed for verification of thin-layer performance, since the thicknesses of the layers too thin to measure accurately could be extrapolated from the thicker layers and the growth rate.

3. Excited Layers

In the final benchtop experimental series, a second copper block was used. This block had a polyethylene rim around it, as seen in figure 6-8, creating a square “pool”. The corners of the rim were cut as square as possible, to try to reduce edge effects on waves in the fluid.

Several different methods of exciting the fluid and creating waves were tried; these included a “wiper” which was moved up to 4cm back and forth near one end of the pool, droplet excitation by letting droplets of the test fluid fall into a preexisting layer, and shaking the entire block several cm each way. The wiper and block-shaking methods created a large-amplitude wave, but the resulting wave in both cases was more of a sloshing of fluid than a true gravity wave and thus was not predictable. Since part of the goal of this portion of the experiment was to be able to show that the measured waves were the same as the predicted waves, thus validating the measurement system, this was not acceptable. Droplet excitation worked and produced quite nice waves, but they were typically of very low amplitude. In addition, they were of course point-source waves; since

the droplet itself was in many cases a significant portion of a wavelength in size, this created a non-optimal situation for theoretical predictions. Droplet excitation was used for several experimental runs, but was eventually discontinued due to difficulty seeing the low-amplitude waves with the optical measurement system.

The excitation eventually adopted for use was a modification of the wiper excitation. The wiper was connected to a solenoid which was attached to a function generator, and was originally used at full amplitude in order to drive it back and forth. However, it was noticed that if only a very small amplitude driving voltage was used the wiper would stay stationary while imparting a small wave to the fluid. This wave was small enough that it did not have any of the "sloshing" characteristics that made the original wiper excitation unusable, while it was still big enough that it was visible with the optical measurement system. A square wave at approximately 0.5Hz was used, resulting in one wave per second (one when the wiper was excited in the forward direction, another one second later when it was excited in the rearward direction).

Initially problems were encountered when using water as the working fluid, because the waves would reflect off of the far side of the pool and instead of simple waves an interference pattern would result. This problem was resolved by adding a runout area to the pool; the side of the polyethylene wall opposite the wiper was removed and an extension of the block was built out of polyethylene approximately 2' long. At the far end, a wedge was placed to help dissipate

waves. After these modifications, the waves produced by the low-amplitude wiper excitation were acceptable for use in this experiment.

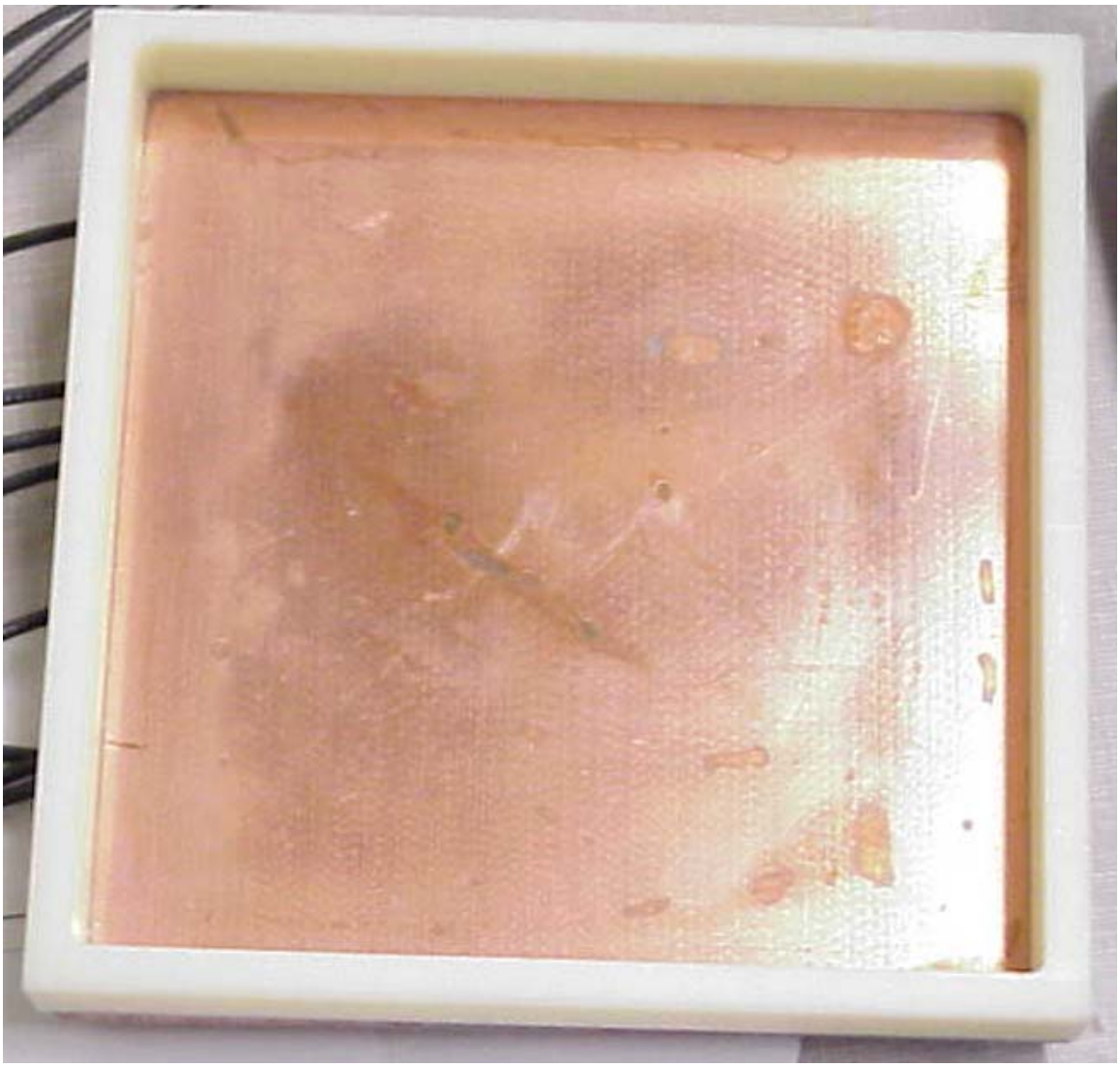

Figure 6-8: Second experimental test block with polyethylene rim. Unlike the first block, this was simply a solid block of copper with no cooling channels.

The block was highly polished, and the mechanical engineering group developed an optical system to measure waves in the fluid simultaneously with

the ultrasonic measurements. This system used an arc lamp to generate a point source of light, which was then reflected onto the block from directly above. The reflected light was deflected by a partially silvered mirror through a lens onto a screen. A video camera focused on this screen allowed the acquisition of data which were used to determine wave velocity and wavelength. The velocity and wavelength data from the optical system were compared to the velocity and wavelength determined from the ultrasonic system in order to verify the ultrasonic system. Although the ultrasonic system only measured thicknesses directly, and not velocity or wavelength, those values could be derived from the thickness-vs-time graphs of two or more transducers taken together. For instance, if the peak of a wave (maximum thickness) is seen at Transducer #1 at time 0, and the peak of the same wave is seen at Transducer #2 a distance *d* away in the direction of wave propagation at time *t*, the velocity *V* of the wave is easily seen to be:

$$V = \frac{d}{t} \tag{4-1}$$

Similarly, if the peak of a wave is seen at a transducer at time 0 and the trough is seen at time τ, or the next peak seen at time 2τ, the wavelength can be calculated to be:

$$\lambda = 2V\tau \tag{4-2}$$

Using these two equations, the wave velocity and wavelength are easily measured as long as two conditions are met. The first condition is that the waves be linear waves traveling at a known direction; the velocity and wavelength found by this method are always in the direction between the two

transducers. If the wave propagation direction is not exactly the same as the line between the two transducers, but the angle between the propagation direction and the transducer-transducer line is known, vector algebra can be used to determine the actual wave velocity and speed. The second condition is that at least two transducers must be used with a high enough sampling rate to be able to resolve the peaks and troughs of the waves. Since in this lab test the wave velocity is very high compared to what it is anticipated to be in condensation experiments, only two transducers are used in order to get a high enough sample rate. Typically these will be the transducers located reasonably far apart to increase the resolution of the velocity determination. If transducers too close together are used, one sampling period may be a significant fraction of the time *t* thus resulting in very low precision in velocity determination; if more distant transducers are used *t* will become longer, meaning that one sampling period is a less significant fraction of *t*.

4. Condensation

Due to time constraints and equipment problems, only a limited amount of actual condensation testing was carried out. However, useful data was obtained for several cases. The first experiments involved stable films, or +1G experiments, with the film condensing onto the bottom of the test cell described in Chapter 2. Two fluids, methanol and *n*-pentane, were used as the working

fluids. Once the ultrasonic system had been shown to measure these stable films, several experimental runs with unstable films were performed. In these –1G runs, in which the film condensed onto the top of the test cell and then fell off in droplets, the same two working fluids were used. In all condensation experiments to date, only two transducers were used in order to achieve a high sample rate while maintaining the ability to measure spatial variations.

Chapter 7: Results

A. Physical Experiment Results

This section gives an overview of the results obtained from physical benchtop experiments. The types of experiments described in this section include:

1) Static experiments, in which a stationary layer was measured
2) Constant layer growth experiments, in which a layer with a constant growth rate was measured over time
3) Excited layer experiments, in which the behavior of a fluid film with external stimulus such as a moving paddle was measured over time
4) Measurements of actual condensation tests

1. Static Fluid Layer Experiments

The initial tests of the system were very simple in nature; a fluid film was created on the opposite surface of the copper block from the transducer and its thickness was measured both with the ultrasonic system and with a ruler. At the time these tests were run, the ultrasound system was a single transducer, single shot system meaning that it would only acquire one thickness estimate and stop. For relatively thick films – those greater than approximately 2mm – the ruler was adequate to measure the film thickness and confirm the ultrasonic measurement. However, this did not work well for thin layers since the ruler was not a very precise measurement modality. Indeed, when taking multiple ultrasonic measurements over the space of several tens of seconds it was found that the initial fluid film wicked towards the sides of its containment ring and became very thin in the center. For many of the trials using very thin films the center of the copper inside the fluid containment ring would lose its fluid coating entirely over the course of tens of seconds.

Using this testing modality, the ultrasound system was verified to be able to measure thick (>0.5mm) films (using the time domain, or “thick film”, algorithm) accurately with a resolution of approximately 35 microns. Thin films, those less than 1.0mm and processed using the frequency domain (“thin film”) algorithm, were measured by the ultrasound system with much higher precision; however,

due to the lack of a reliable independent measurement of fluid thickness, the accuracy of this algorithm could not be established in these tests.

2. Constant Layer Growth Experiments

The main problem noted in the previous experiments was the lack of ability to confirm the ultrasound system's measurements at low fluid film thicknesses. In an attempt to address this issue, the ultrasound system was modified to be a single-transducer constant-sampling system. In this configuration, the system still only had one transducer but it took measurements constantly for an indefinite period of time. This capability allowed for the performance of rate-of-change measurements, which were the subject of this series of tests.

A nearly constant fluid addition mechanism, in the form of a medical IV bag and dripset, was procured and mounted so as to add fluid at a slow rate into the fluid retaining ring on the copper block. A thin film of fluid, made as thin as possible with the aid of a small amount of surfactant, was applied to the copper surface. The ultrasound system's acquisition was started, and the flow of water through the IV tubing was initiated. Data was then taken for several minutes, as the water film thickness changed from under 100 microns to several centimeters. The results from one such test are shown in Figure 7-1.

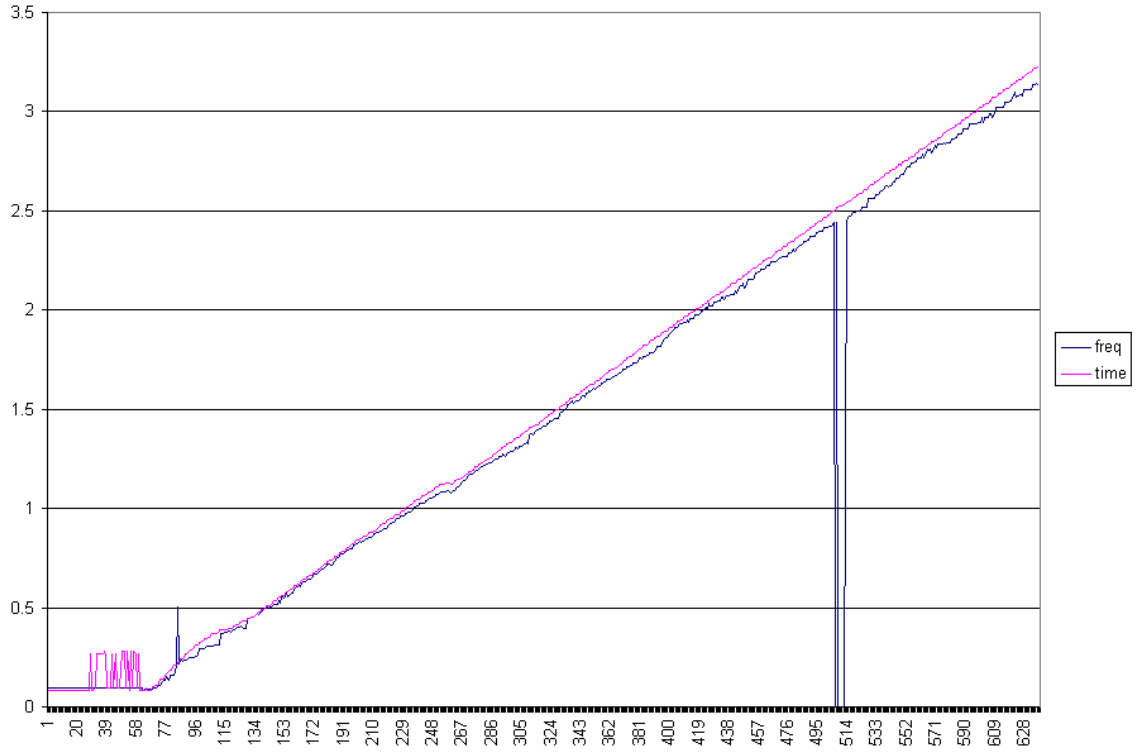

Figure 7-1: Data from a constant-layer-growth trial. The pink trace (the one which is higher for most of the graph) is from the time-domain ("thick film") algorithm, and the blue trace is from the frequency-domain ("thin film") algorithm from the same test run.

In Fig. 7-1, the outputs of both the time-domain and frequency-domain algorithms for the same test run are shown. They show good agreement with each other, with the exception of several glitches in the time-domain algorithm at significantly less than 500 microns of thickness and in the frequency-domain algorithm at over 2mm of thickness; these glitches are a result of high noise not well handled by the measurement algorithms. The algorithms used for the data in Fig. 7-1 were early versions, which have been improved upon, but further improvements of the algorithms are suggested for future work. It should be

noted that to achieve the high-thickness results from the frequency domain algorithm shown above, several parameters were adjusted manually during the test run; without operator intervention, the frequency-domain algorithm has been found to cease reliable operation at approximately 1-2 mm of layer thickness. Also significant is that the algorithms used to generate the measurements which are shown in Fig. 7-1 were early versions; current algorithms are significantly less noisy. A second graph of the same test run is shown in Fig. 7-2; this shows the time-domain algorithm's output superimposed with a "true" linear growth rate (a linear best-fit curve) and the percentage difference between the two. Since the fluid addition was at a constant rate, and the walls of the fluid containment ring were vertical, the growth rate of the fluid should be constant. The measurement of the difference between the measured thickness and the "calculated" (assuming linear growth) thickness over the range of 0.05 mm to approximately 8.7 mm shows that the difference is less than 1.5% over most of the range; even at relatively low thicknesses where the time-domain algorithm is expected to perform poorly a <3% difference is shown.

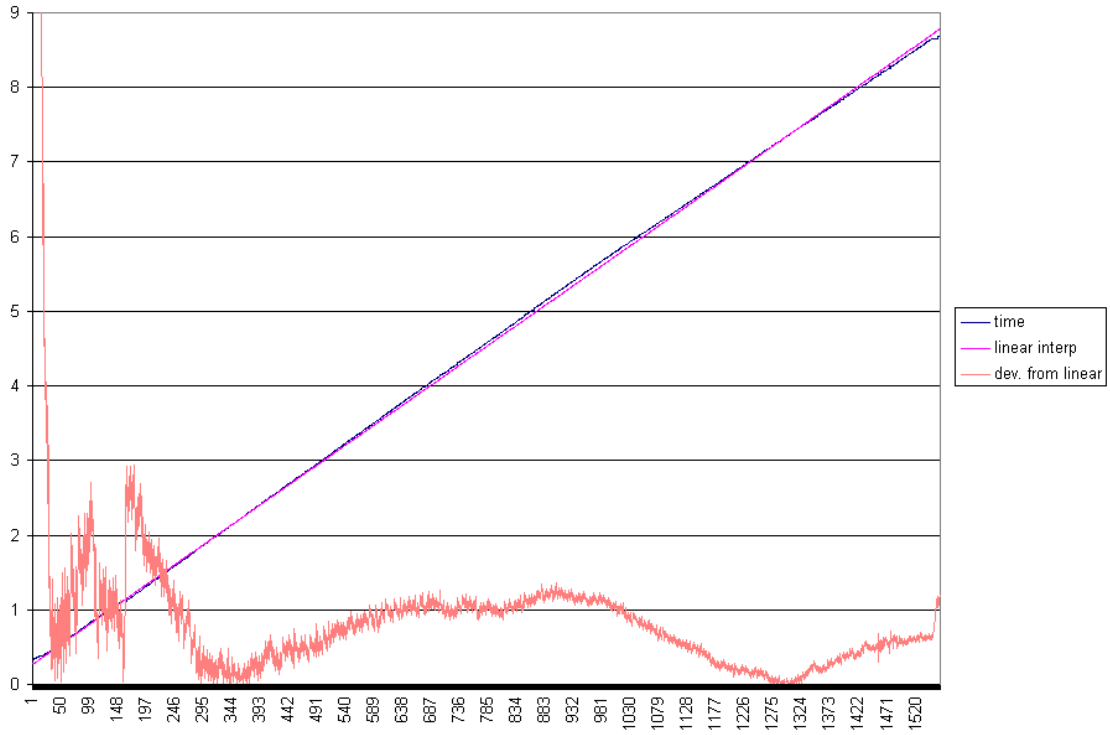

Fig. 7-2: Linearly growing fluid thickness. The y-scale is in mm of water thickness and % error.

3. Excited Layer Experiments

Since it is anticipated that the condensate layer will be dynamic, with phenomena such as waves and traveling droplets, it was desired to test the ultrasound system with a layer which included these types of non-stationary perturbations of layer thickness. This was done by starting with a flat layer of fluid and then perturbing it with such things as droplets of the same fluid impacting the layer after falling from a height of several feet or a paddle driven by a signal generator. The resulting surface perturbations were recorded using an optical imaging system as well as the ultrasound system, and the results were to be compared;

however, the optical system did not perform as well as anticipated and the optical data was never successfully interpreted.

The droplet experiments, as measured with the ultrasound system, were found to behave as expected. Waves were seen which traveled away from the impact point, and waves close to the impact point were seen to have shorter wavelength than the waves monitored farther away from the impact point. This phenomenon was expected due to the dispersive effects of wave propagation through water. However, this made an accurate measurement of wave speed very difficult.

In the paddle experiments, on the other hand, a constant wave speed and only slowly varying wavelength were observed. A table of the observed wave velocities and wavelengths for experiments with ethylene glycol is shown as Table 7-1. In this table, the wave velocity can be seen to decrease as the layer became thinner as expected; the wavelength at a given transducer location shortened as the layer thinned also as expected. Finally, for a given layer thickness the wavelength can be seen to lengthen as it is sampled at locations farther away from the paddle; this is due to the dispersive effect of propagation through water. Similar results were obtained for water.

The data in Table 7-1 was obtained by first establishing the fluid thickness, and then setting the excitation to a level which produced visible waves. Data was first acquired with two transducers spaced approximately 3cm apart, and the time delay between the wave crest passing each transducer was used to

calculate the wave velocity. The system was then reconfigured to sample with a single transducer at a high sampling rate, and for each transducer the time between the peak and trough of each passing wave was measured, doubled, and multiplied by the velocity to yield the wavelength. Because the velocity and wavelength measurements were not done until after the experiments were run, it was not discovered until post-processing was performed that in two cases (5.4mm layer and 3.9mm layer) the data was not adequate to determine a wavelength. This was due to too small a wave amplitude; the amplitude of the waves was set separately for each layer thickness, with the goal of using as small an amplitude as would be usable. A small excitation was used because the paddle used to create the waves was noted to not behave consistently at higher amplitudes; the smallest excitation possible to create visible waves was used in an attempt to avoid variability.

Layer Thickness [mm]	Velocity [cm/sec]	Wavelength At 3cm [mm]	Wavelength At 4cm [mm]	Wavelength At 5cm [mm]	Wavelength At 6cm [mm]
10.3	19.4	9.5	13.9	15.6	16.3
8.5	16.9	8.3	8.6	10.5	12.4
7.1	16.6	8.6	8.7	9.7	9.8
5.4	14.7	Unable To Measure At these Thicknesses			
3.9	14.5				
2.8	10.2	5.8	7.1	7.9	9.3

Table 7-1: Results from Ethylene Glycol experiments with paddle excitation. Wavelengths at 5.4mm and 3.9mm layer thicknesses were not possible to determine due to low wave amplitude probably due to low excitation amplitude.

An example of the data used to generate Table 7-1 is shown below as Figure 7-3, consisting of two layer thickness vs. time graphs. On the left is a two-transducer sample run used to determine velocity; on the right is a single-transducer run used to determine wavelength. In the two-transducer run, the baseline (between waves) thicknesses sensed by the two transducers differ by approximately 0.15mm; this is because the test block was not perfectly level and thus the several-centimeter spacing between the transducers resulted in slightly different film thicknesses.

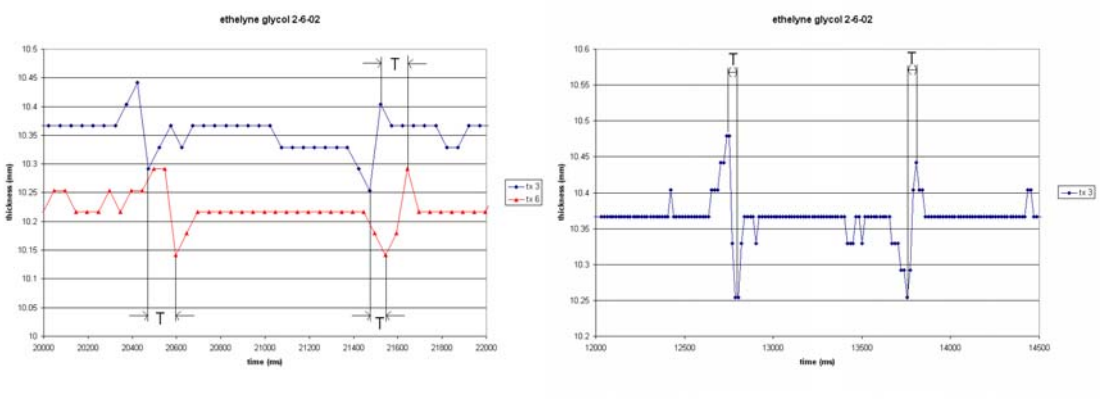

Figure 7-3: Data used to generate velocity(left) and wavelength (right) measurements for paddle-excited layers of ethylene glycol. Note that several time intervals are denoted for each graph; in practice, at least ten to twenty time intervals were measured and averaged together for each graph. This was done to correct for the low sampling rate; however, mostly due to the low sampling rate the uncertainty of the velocity and wavelength measurements was high.

4. Condensation Experiments

In early condensation experiments to date, a useable growth rate was not able to be ascertained. Possible sources of this problem were too large a beamwidth, too low a SNR, and a nonuniform condensing film. All analysis for this research project assumed that the condensing film would be in the near field of the transducer; while this was the case with the copper blocks used for noncondensing tests, the copper block originally used in the condensation test cell was approximately 30mm thick. The near field of the transducers used was calculated to be approximately 10mm, after which the beam – which had a constant circular cross-section in the near field – would begin to approach an approximately 37° wide cone. At 30mm in copper, the beam width was calculated

to be approximately twice the 6mm width in the near field. This results in four times as much analysis area, which implies a much greater chance of significant inhomogeneities over the area sensed. In the case of a drop over part of the beamwidth and a thin film over another part, the spectral contributions of both are superimposed which significantly degrades the ability of the peak-detection algorithm to correctly identify an f_0.

Additionally, the thicker copper block results in a significantly greater attenuation of the ultrasound pulse before it returns to the transducer. While this is not an insurmountable problem in the time-domain method, it significantly interferes with the frequency domain method since it makes the spectral peaks less distinct; the combination of less distinct peaks with multiple sets of peaks as described above makes the frequency-domain method very unreliable with a 30mm copper block.

Finally, the condensing film has been determined by direct visual observation to be very nonuniform. Early trials included methanol and n-pentane condensing onto a clean, polished surface; in both cases, droplets form on a bare copper surface first and then a film develops later. The portion of condensation which it is desired to measure is the initial portion during which there is a growth rate; growth has slowed significantly by the time a film formed in both methanol and n-pentane. All previous experiments done for this research project had been with uniform films, and the system was in fact designed specifically to monitor film growth rather than droplets; previous condensation

trials run during the feasibility study phase were run with water using a surfactant to ensure a wetted surface and thus a fairly uniform film. The nonuniformity of the films, in combination with the enlarged beam width as discussed above, prevented useful data from being acquired in the original runs.

A copper block with a channel cut into it to allow measurements through a 10mm thick portion of copper was fabricated to address this problem. Due to time constraints, only limited experimentation was done with this block; however, several condensation runs were successfully observed. Methanol was observed to condense in both +1G and –1G orientations; n-Pentane was also observed in the unstable (-1G) orientation. The results from these three runs are shown in Figures 7-4, 7-5, and 7-6 respectively.

In Figure 7-4, the methanol can be seen only erratically until a film approximately 0.1mm thick formed; from this point on, a fairly steady growth rate was seen for several tens of seconds. Near the end of the run, the film thickness at each of the two transducers shown is seen to decrease slightly and then continue a slower growth; this can be interpreted as film redistribution to cover non-wetted areas of the block. The slower growth rate once the entire block is covered is expected due to poor thermal conductivity through the liquid film.

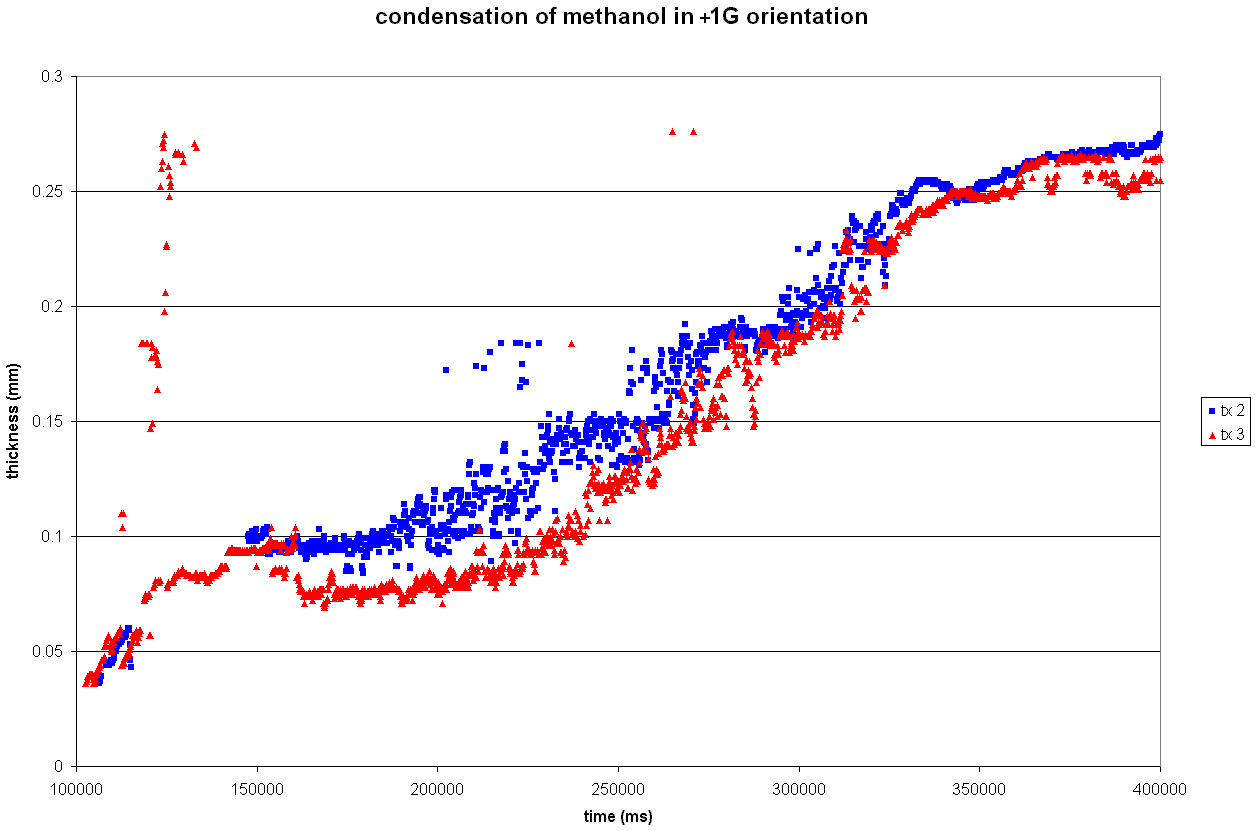

Figure 7-4: Condensation of Methanol in Stable (+1G) orientation

In Figure 7-5, a similar growth curve can be seen for n-Pentane in the stable (+1G) configuration. n-Pentane forms a film much more readily than methanol, which explains the visibility of the film at a much thinner initial thickness. The phenomena of film thinning due to redistribution and growth rate slowing which were seen with methanol are also seen in Figure 7-5 with n-pentane.

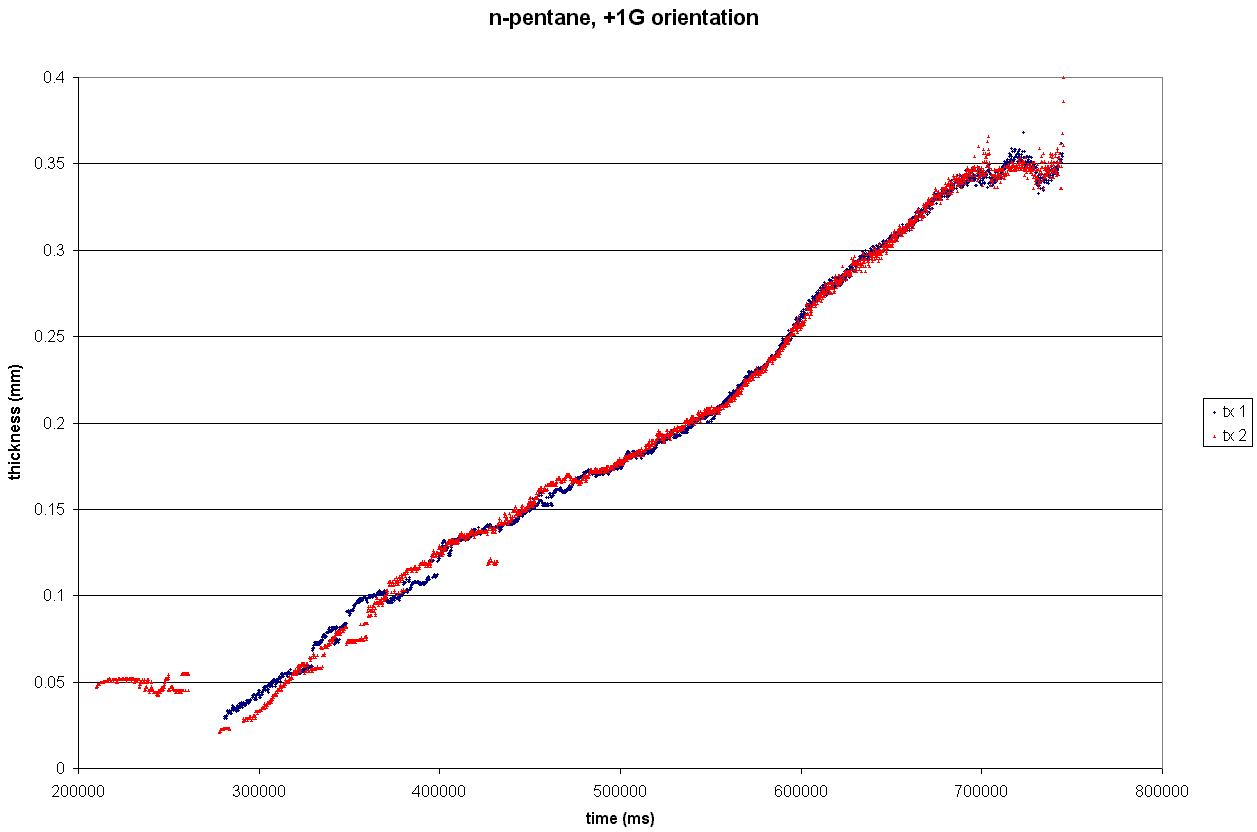

Figure 7-5: Condensation of n-pentane in the stable (+1G) orientation.

Figure 7-6 is the sole dataset acquired from an unstable (-1G) film; specifically, an n-pentane film. The data shown in Fig. 7-6 is particularly interesting in that it appears to show some sort of wave action, or possibly droplet growth and release. It should be noted that the data shown in Fig. 7-6 has not been repeated, as only one trial was done due to lack of time; as a result, it is possible that this is due to some form of artifact although it is unknown what form of artifact this may be.

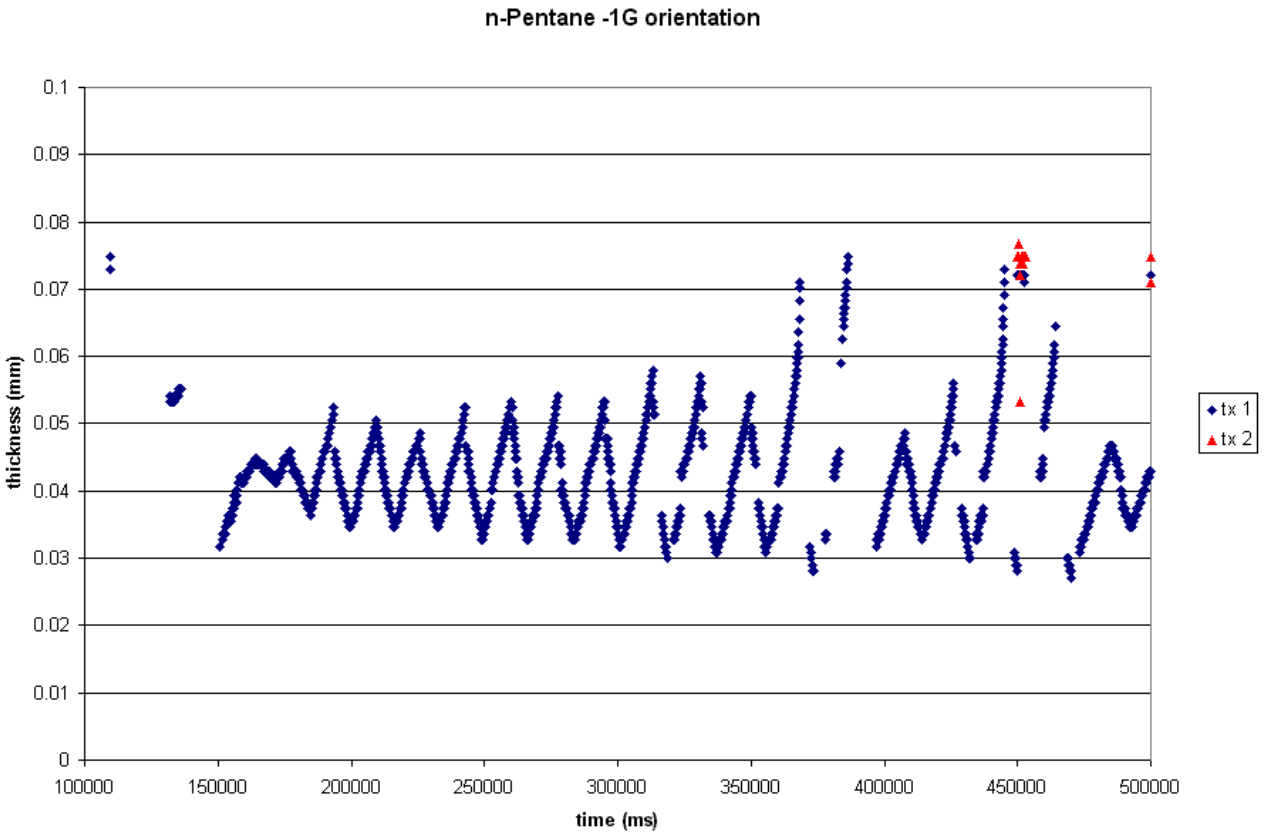

Figure 7-6: Condensation of n-pentane in the unstable (-1G) orientation

B. Numerical Modeling Results

Numerical modeling of simple layers was successfully accomplished after the initial physical tests, and as such was mostly done to validate the modeling program rather than to predict physical results. However, the numerical models were of great use in determining the structure of the received signal for more complex situations.

1. Model Verification

The first model verification was carried out with a model of a 0.1mm water layer. The raw model output is shown as Figure 7-7; the frequency spectrum from this model is shown as Figure 7-8. Note the single peak at f_0=4.15 MHz. The result of the frequency-domain algorithm for this sample is 0.090mm, which correctly corresponds to f_0=4.15 MHz. The sample was processed with a variety of different filter settings, with consistent results; from this it is concluded that the filtering built into the measurement program is not the source of the errors.

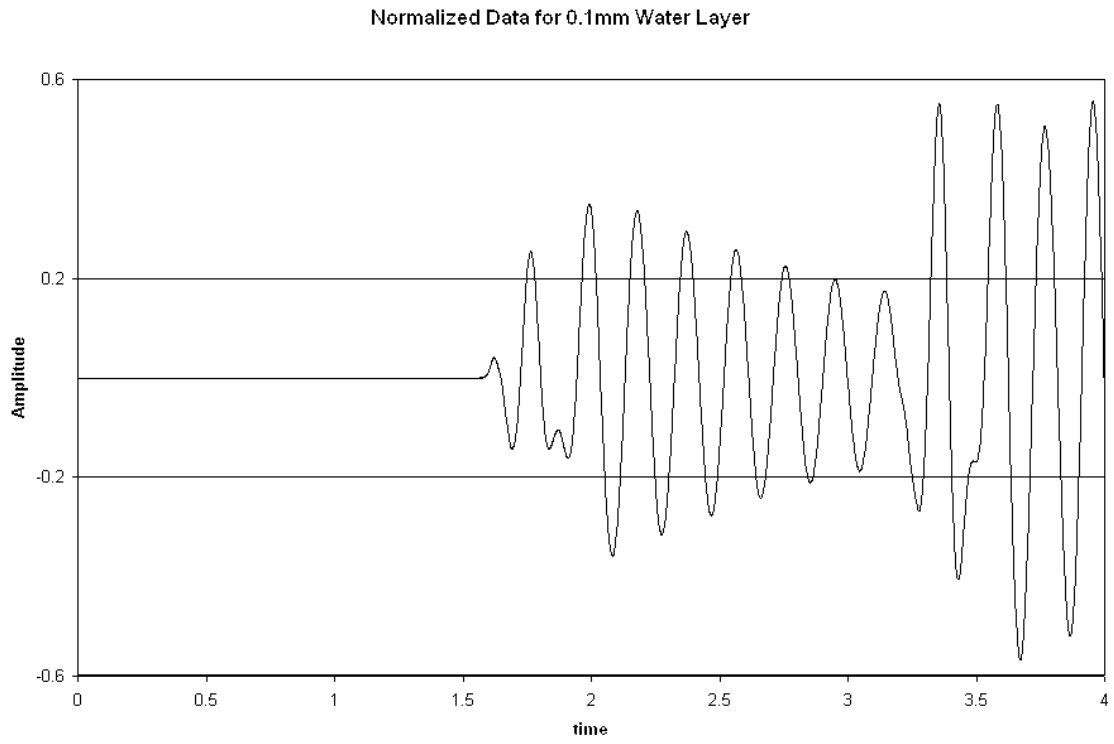

Figure 7-7: Normalized Model output for a simulated 0.1mm water layer.

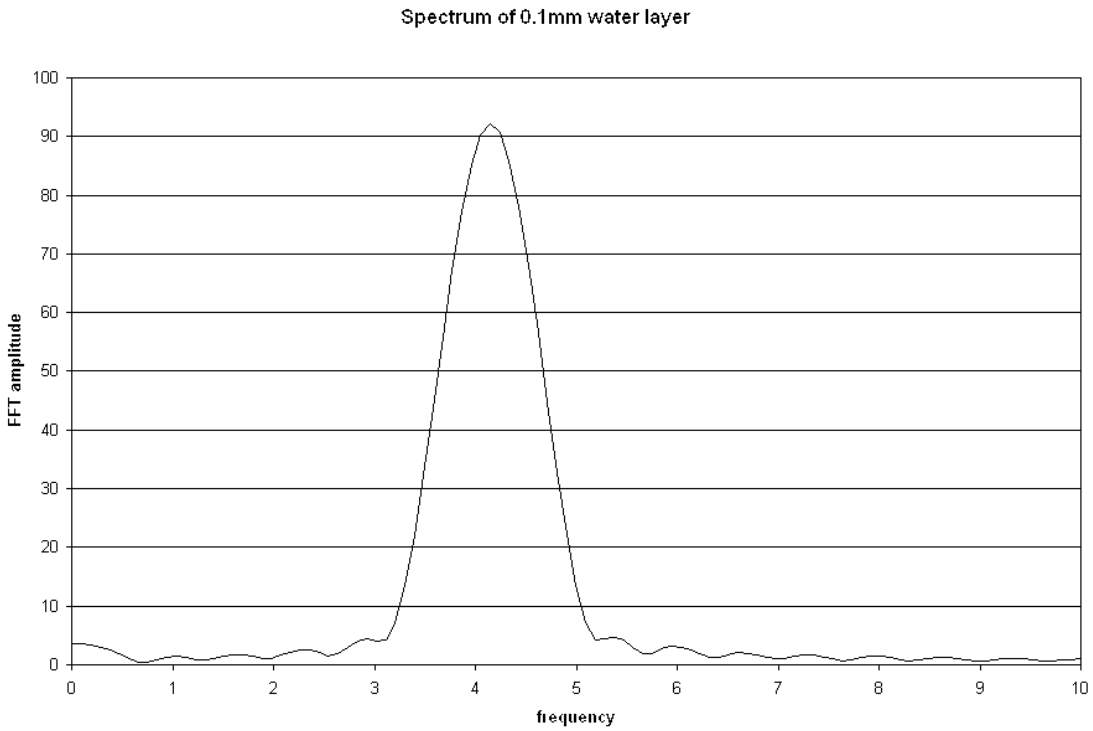

Figure 7-8: Spectrum of 0.1mm Water Layer Model Output

Similar models were run for different simple fluid layers, with thicknesses 0.05mm, 0.1mm, 0.2mm, 0.3mm, 0.4mm, and 0.5mm. The results of these trials are tabulated in Table 7-2. All of the trials referenced in Table 7-2 were run with a simulated 5mm thick copper block; this was done in the interest of saving computational time. Modeling an accurate 30mm copper block multiplied the time required by an order of magnitude: the 5mm-block models required approximately 3 hours to simulate, while the one 30mm-block model attempted using identical parameters required approximately 30 hours.

Actual Thickness Modeled [mm]	**Measured** Thickness [mm]	Absolute Error [mm]	% Error [%]
0.05	0.060	+0.010	+20%
0.10	0.090	-0.010	-10%
0.20	0.189	-0.011	-5.5%
0.30	0.305	+0.005	+1.7%
0.40	0.418	+0.018	+4.5%
0.50	0.529	+0.029	+5.8%

Table 7-2: Results of thin simple layer simulations

From the results shown in Table 7-2, it is concluded that the combination of modeling errors and interpretation errors did not exceed 11 microns absolute error for thinner layers or 6% error for thicker layers. The source of these errors remains unidentified, as no pattern was seen to indicate a correctable cause.

Models of simple thick films were also run; the model output of an example is shown as Figure 7-9. This example was a model of a 0.5mm thick fluid layer, which is near the lower limit of the usefulness of the time-domain method. The “T” noted on the graph is the time difference which is measured to determine the layer thickness; Figure 7-9 has not had the baseline subtracted in order to provide the fires copper/fluid echo as a reference to the reader.

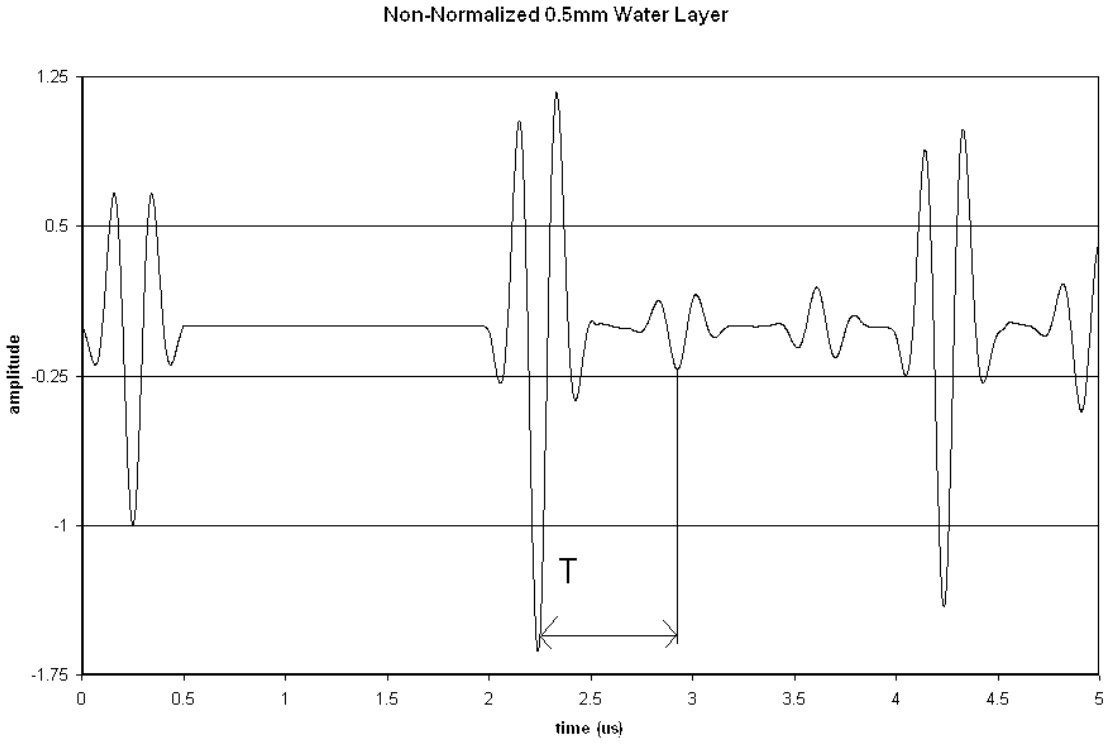

Figure 7-9: Model Output for a Simulated 0.5mm water layer. Note the ΔT shown in the figure between the first copper/fluid echo and the first fluid/air echo.

Only a limited number of thick-film models were run, as they invariably had less than 20 microns error for thicknesses greater than 0.5mm; for thicknesses less than 0.5mm, the time-domain method was unreliable as was expected.

2. Numerical Modeling of Complex Layer Geometries

Numerical modeling was used to determine the tolerance of the ultrasound system for layers which had non-parallel copper/fluid and fluid/air interfaces (i.e. a non-flat layer). The two types of layers investigated were 1) layers with a

planar fluid/air interface that was not parallel to the planar copper/fluid interface and 2) layers containing one or more droplets of fluid projecting into the air space.

The modeling showed that for flat-surfaced films in the thin-film regime, specifically in a model with a center thickness of 300 microns, a center-edge difference of 40% in the film thickness (corresponding to a 2.6° angle between the copper/fluid interface and the fluid/air interface) would be sufficient to cause the ultrasound system to be unable to generate a thickness estimate. The spectrum of the limiting case, which was the model with the largest difference to be successfully measured, is shown as Figure 7-10. The width of the spectral peaks steadily degraded until, by 45% center-edge difference, the spectral peaks were too wide and had too little amplitude for the peak-detection algorithm to function. This modeling also showed that the thickness estimate generated for layers with a <45% difference would be the thickness in the center of the ultrasound beam, or directly centered below the transducer. The amplitude of the FFTs from such slanted layers were also significantly decreased; this is significant because the signals are normalized to a maximum amplitude of 1.00 before the FFT is taken. As a result, a low amplitude in the FFT corresponds directly to a low SNR.

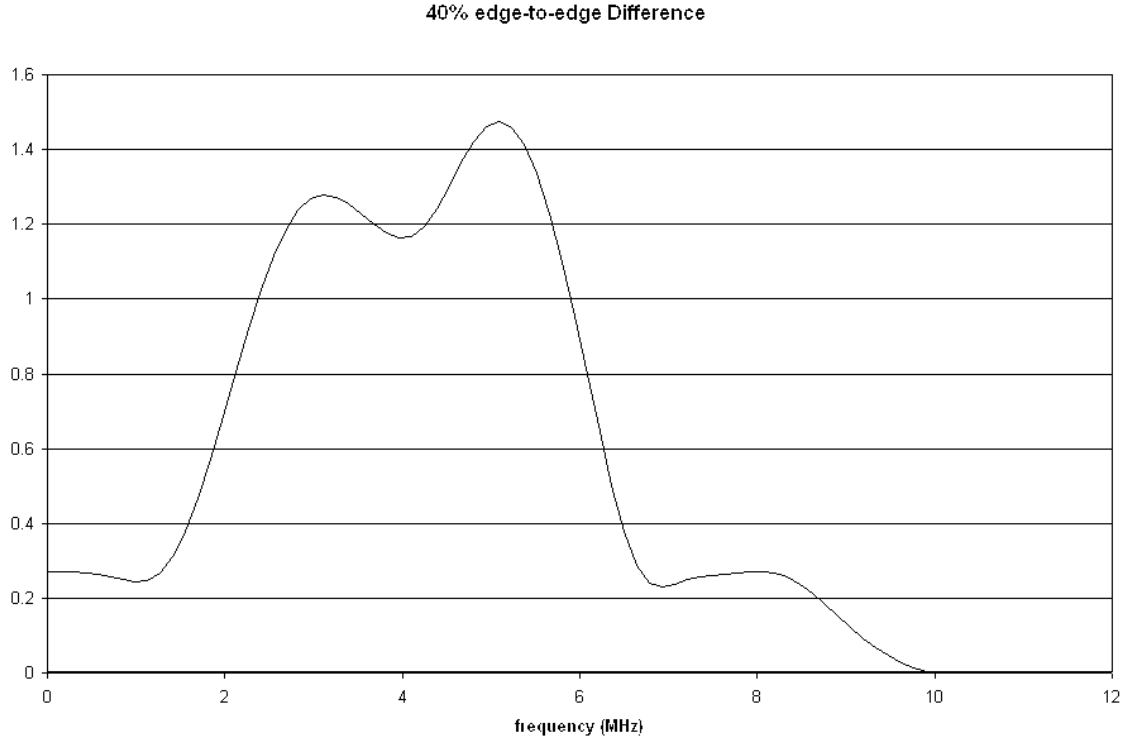

Figure 7-10: The spectrum of a 0.3mm (center thickness) water layer, with 40% center-of-beam to edge-of-beam (3mm radius) thickness difference. Note that in this case there are just sufficiently large peaks to perceive. At a 45% difference center-to-edge difference, the peaks are too blended to detect. Note also the amplitude of ~1.5, compared to ~92 in Figure 7-5.

For thicker films, in the time-domain region, the amplitude of the signal of interest reduced with increasing angle between the two faces of the film resulting in a decreased SNR. However, at angles of up to 5° (the largest angle simulated to date) in a 1mm base thickness film the system was still able to extract thickness data reliably.

Despite these results, performance by the actual system is expected to be considerably poorer and less tolerant of non-uniform films. This is because the effect of nonuniformities in the film is a combination of decreased SNR and slight

temporal or spectral shifts; the models, because of their relative noise-free ideal nature, have a very high SNR to start with and can thus tolerate more SNR degradation before becoming unusable.

Numerical modeling was also used to investigate the behavior of the ultrasound system when presented with droplet formation. These models showed that there was a very strong positional dependence, in that droplets on the same order of size as the beam width would only be seen by the system if they were almost exactly centered in the beam. A strong size dependence was also shown; drops significantly smaller than the beam width were not seen regardless of position although if centered they noticeably degraded SNR.

With a 6mm diameter beam and 6mm diameter droplet which was 0.5mm thick on top of a 1.0mm base fluid layer, as little as a 1.0mm offset would result in the ultrasound system reporting only the 1.0mm fluid layer. When the droplet was exactly centered, the system would report the thickness at the center of the droplet (in that particular case, 1.5mm). When the droplet was offset by only 0.5mm, the ultrasound system reported the thickness at the center of the drop; however, examination of the raw signal showed a very low SNR which would be expected to result in unreliable results in that situation.

In the case shown in Figure 7-11, a 1.5mm thick drop with 1.5mm diameter was superimposed onto a 1mm water layer, resulting in a drop protruding 0.5mm beyond the rest of the water layer. However, the droplet's

1.5mm diameter was significantly smaller than the ~6mm beam size; as a result, the drop was not detected. The only influence of the drop was the lower the signal strength noticeably.

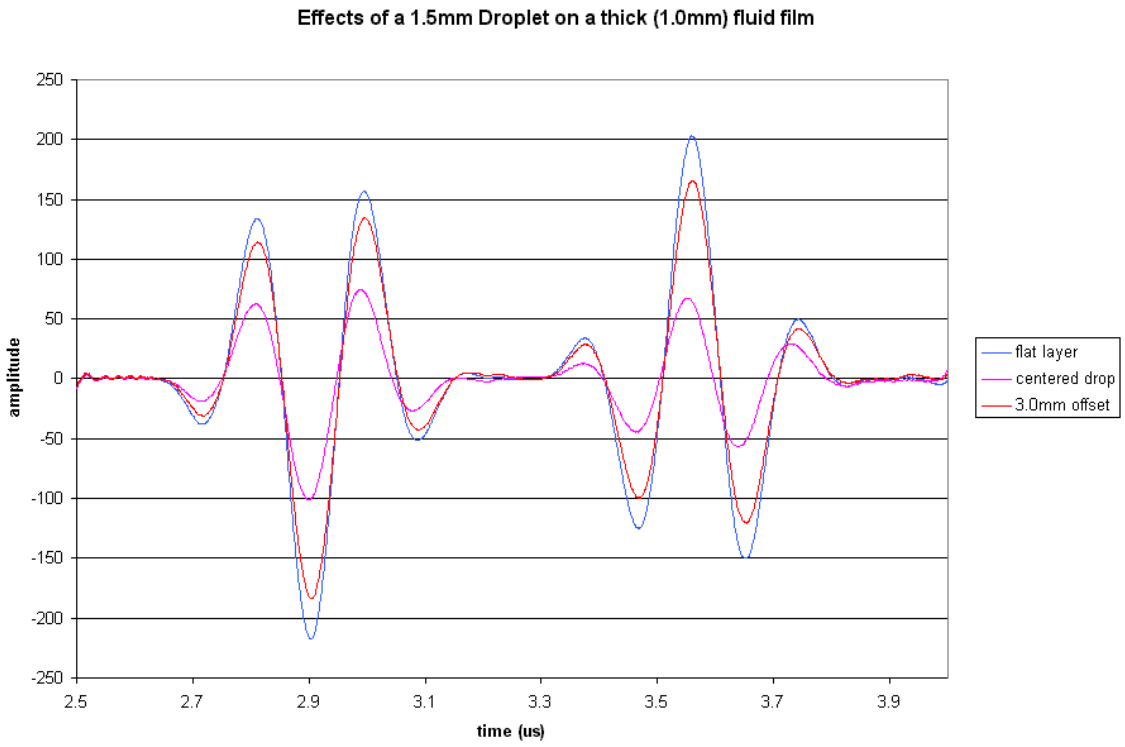

Figure 7-11: Effect of a 1.5mm diameter droplet on the measurement of a 1.0mm water layer. The temporal positions of the peaks are barely affected, but the amplitudes are noticeably decreased.

Another situation modeled was the case of multiple small droplets on an otherwise bare copper block. Results of these trials were very interesting; in one particular model series, which modeled 0.1mm radius hemispherical droplets at different spacings, the measurement system produced the same thickness reading regardless of drop spacing. 0.1mm radius drops, creating 0.2mm

diameter footprints on the copper block, were modeled with spacing ranging from 0.25mm center-to-center (resulting in only 0.05mm dry area between drops) to 2.00mm center-to-center spacing. In both cases, as well as intermediate cases (center-to-center spacing of 0.25mm, 0.50mm, 0.75mm, 1.00mm, and 2.00mm), the system output was a thickness of 0.067mm. However, the amplitude of the spectral peaks used to generate this thickness measurement fell by approximately an order of magnitude between the 0.25mm pitch and 2.00mm pitch simulations. The 2.00mm pitch simulation had barely enough amplitude to be successfully measured. Spectra of the extreme pitches are shown in Figure 7-12.

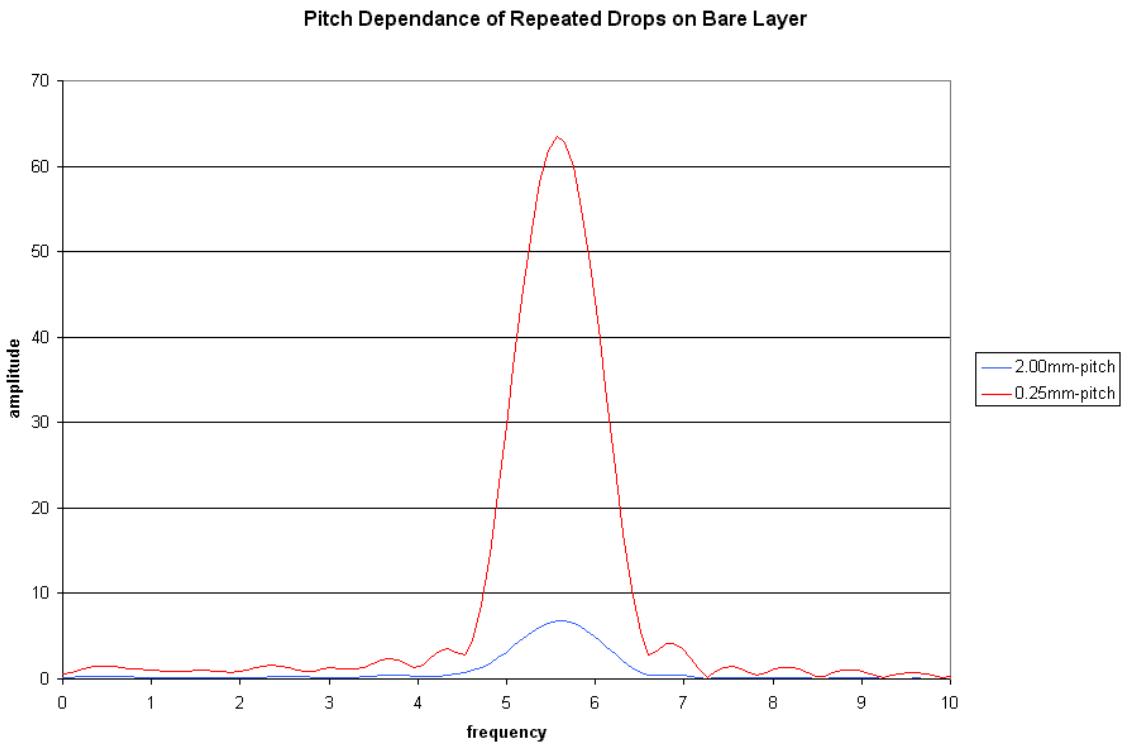

Figure 7-12: Spectra of repeated 0.1mm radius droplets on bare copper. Note that the more widely-spaced series has an FFT amplitude almost an order of magnitude less than the more closely-spaced series, but both have the same f_0 and thus both have the same reported thickness.

Chapter 8: Conclusions

1. Evaluation of the Ultrasonic Thickness Measurement System

The ultrasonic thin-fluid-film thickness measurement system designed and built for this research project is generally successful, but not in all cases. For thick (>0.5mm) homogeneous fluid films, the system is highly reliable and accurate to within its 35 micron resolution limit. In the case of thick films which are nonhomogeneous over the beam width, the absolute thickness measurement is not as reliable but an accurate relative thickness measurement (i.e. rate-of-change, wave detection, drop break-off detection, etc.) is successfully obtained. Thinner film layers (<0.5mm) which are homogeneous over the beam width are successfully measured with <5 micron resolution down to a lower thickness limit of approximately 50 microns. The main failing of the current system is its inability to reliably measure thin films which have significant thickness variations over the beam width.

The system has been developed with the capability to take up to 60 measurements per second using a single transducer, or up to 30 measurements per second using multiple transducers. The transducers to be used for a given experimental run are chosen in software, allowing consecutive runs to use the multi-transducer capability and the high-speed single transducer capability without hardware changes. All data are displayed on-screen in real time in the

form of a numerical readout and thickness-vs-time strip chart for each transducer; additionally, time stamped data is saved to a text file readable by a spreadsheet program allowing for post-analysis.

Tests with the actual condensation conditions were successful, although limited due to time constraints. These initial tests served to validate the system, and future tests using the same equipment will be suitable for the intended condensation research.

2. Suggested Directions for Further Research

- The condensation measurement system in its present physical form is suitable for benchtop experimentation, but not for flight experiments. Accordingly, the system should be physically modified (perhaps by rack-mounting all components) to be able to operate under flight-testing conditions.

- The peak-detection algorithm is the weakest point in the frequency-domain measurement algorithm; a better peak-detection algorithm would significantly improve the performance of the system for thin fluid layers.

- Although the time-domain algorithm incorporates a “time-windowing” function which reduces errors, a similar function has not been successfully implemented in the frequency-domain algorithm. Implemented as part of a better peak-detection system, this could reduce the problem caused by inhomogeneous layers.

- Further investigation into the sources of errors in the measurement of simulated thin films could determine whether the errors are in the simulation program or in the analysis; if the latter, these errors could hopefully be reduced.

References

[1]Hermanson, J.C.; Pedersen, P.C. A Proposal to NASA entitled: "Stability and Heat Transfer Characteristics of Condensate Fluid Layers in Reduced Gravity". Contract Number NRA-98-HEDS-03; March, 1999.

[2]Hermanson, J.C.; Pedersen, P.C.; Durgin, W.W. Final Report to NASA entitled "A Study of the Behavior of Condensing Films in Simulated Reduced Gravity Using Ultrasound". Submitted to the NCMR under Cooperative Agreement No. NCC3-554; July, 1999.

[3]Faghri, A.; Khrusalev, D. Evaporation on/in capillary structures of high heat flux two-phase devices. Third Microgravity Fluid Physics Conference, Cleveland, OH, 189-194; July 1996.

[4]Ostrach, S. Low Gravity Fluid Flows, Ann. Rev. Fluid Mech. 1982:313-345.

[5]Westbye, C.J.; Kawaji, M. Boiling Heat Transfer in the Quenching of a Hot Tube Under Microgravity. J. Thermophysics and Heat Transfer 9:302-307; 1995.

[6]Peyayopanakul, W.; Westwater, J.W. Evaluation of the Unsteady-State Quenching Method for Determining Boiling Curves. Int. J. Heat Mass Transfer 21:1437-1445; 1978.

[7]Kinsler, L.E.; Frey, A.R.; Coppens, A.B.; Sanders, J.V. Fundamentals of Acoustics, Fourth Edition. New York: John Wiley and Sons; 2000.

[8]Mills, A.F. Heat and Mass Transfer. Chicago: Irwin; 1995.

Appendix 1:

Ultrasound Film Thickness Measurement System

User's Manual

1. Hardware

A. Equipment

The four major items of equipment used in this system are shown below in Figure A-1:

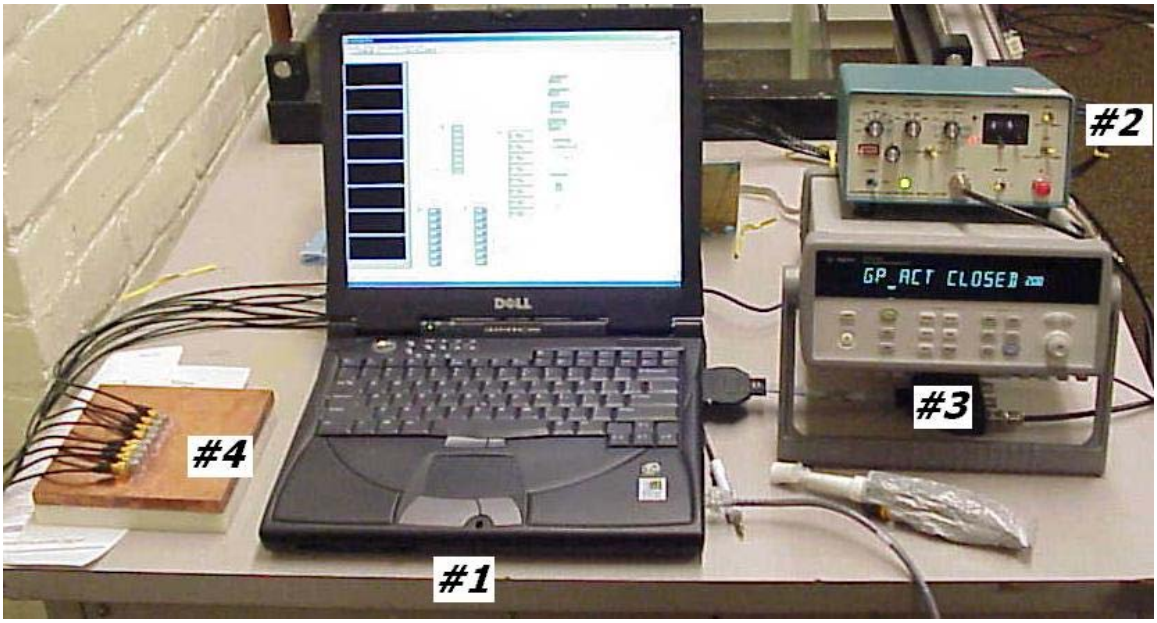

Figure A-1: The ultrasonic thickness measurement system. #1: laptop, #2: P/R unit, #3: multiplexer, #4: transducers mounted to copper plate

#1 is a Dell laptop, which contains a PCMCIA oscilloscope in one of its expansion slots. The system is controlled by LabVIEW software running on this

laptop, and the PCMCIA oscilloscope is used to acquire the ultrasonic data. The second major element to the system, #2 in the figure, is a Panametrics 5077PR model Pulser/Receiver unit. This unit generates the excitation pulses to send to the transducers, and receives their return signal and amplifies it before sending it to the laptop/oscilloscope. #3 is an Agilent 34970A multi-function device chassis with an Agilent 34903A general purpose switching card. This device is used as a multiplexer, to allow the single P/R unit to be used with eight different transducers. The transducers themselves, mounted on the copper block with their cabling attached, are shown as #4.

B. Electrical Connections

There are two major electrical connections which must be made when setting the system up. The first is connecting the transducers to the multiplexer. The internal wiring in the multiplexer card is pre-wired, and the system when disassembled has a terminal block permanently attached to the multiplexer card. The terminal block has eight BNC male plugs, to which the transducer cables must be attached. The eight plugs are labeled, and it is important to plug each transducer into its corresponding plug; the “transducer one” in the measurements corresponds to the transducer plugged into terminal one on this block. The block, with all eight transducer cables attached, is shown in Figure A-2.

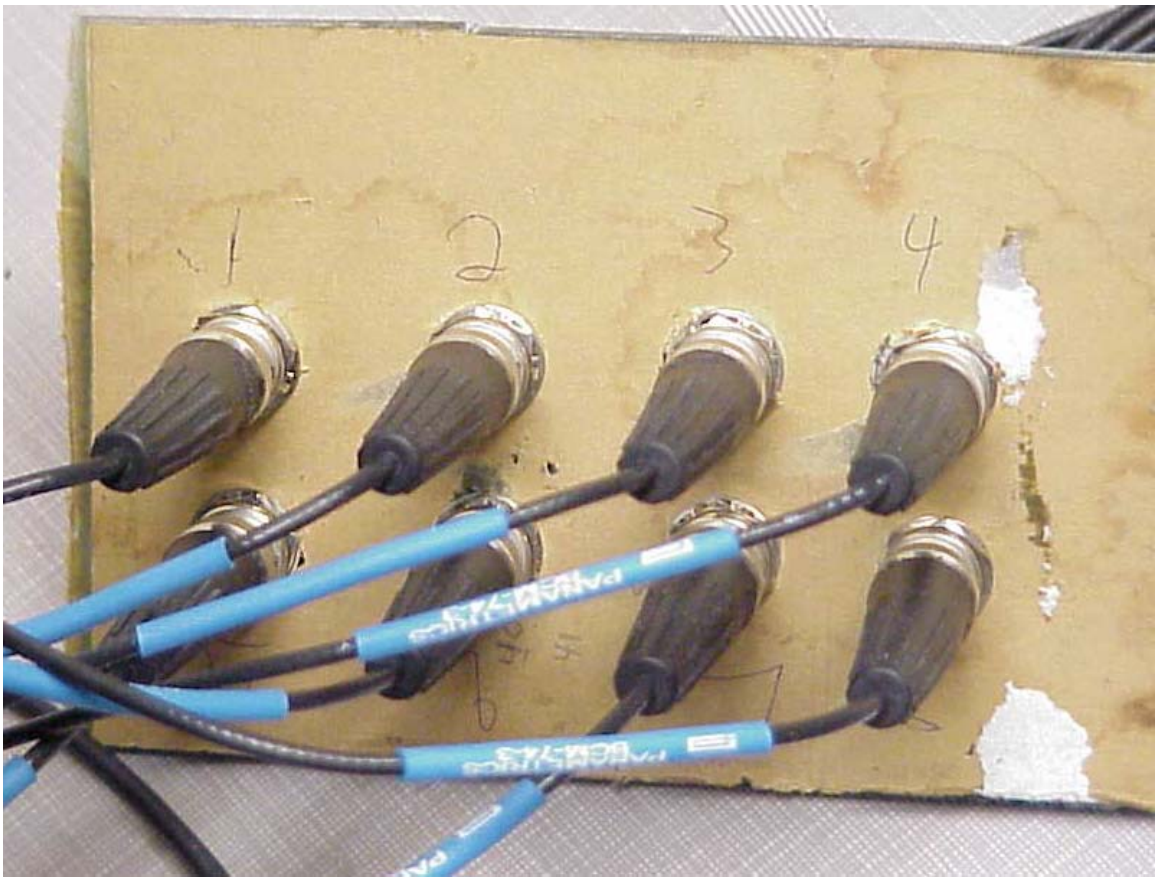

Figure A-2: Interface block for transducer cables to be attached to multiplexer cable harness.

The other major electrical attachment necessary is to attach the puler/receiver module to the oscilloscope. This is done by first attaching the oscilloscope's breakout cable to the PCMCIA card 'scope, and second attaching the cables from the P/R module to the breakout cable. This breakout cable is shown in figure A-3; it simply plugs into the exposed edge of the PCMCIA card as shown with all writing facing up. The output from the P/R is attached to the BNC jack labeled "CH0", and the BNC-SMB adapter cable is used to attach the BNC "synch in" terminal on the P/R to the "PR1" SMB terminal on the breakout cable.

Figure A-3: Oscilloscope Breakout Cable

Several other miscellaneous simple connections must be made, as well. These include:

1) The P/R "T/R" terminal (on the front panel) must be connected to the single BNC cable which comes out of the multiplexer card.
2) A standard serial cable must be used to connect the serial port on the laptop to the serial port on the rear of the multiplexer.
3) All equipment must be plugged into wall power.

   IMPORTANT NOTE: When actually acquiring data, whether it be a baseline or an actual measurement, the laptop's power supply should be unplugged at the back of the laptop. If it is left connected, a significant amount of electronic noise will leak into the signal and seriously degrade the quality of data gathered. The power supply should, however, remain attached when not acquiring data to maintain battery charge.

C. Mechanical Connections

The only significant mechanical connection required is to attach the transducers to the copper (or other metal) block. During development, this was best accomplished by gluing the transducers to the block using a commercial "auto/marine" clear silicone sealant. It is important to ensure that the transducers are mounted such that the ultrasound beams will avoid any cooling passages in the metal block. Additionally, when the transducers are attached to the block a minimum of silicone should be necessary (an amount large enough to cover the active face of the transducer to a depth of approximately 2mm is sufficient); once the transducers are placed in their desired locations, a significant amount of downward force should be applied for several minutes to squeeze as much silicone out from between the transducer and the block as possible. In the prototype, the transducers were pressed against the block using the operator's thumb with as much force as possible for approximately two minutes; this procedure yielded good attachment. Once mounted, if undisturbed the transducers will stay attached for at least several months before the attachment begins to degrade. The mounted transducers from the prototype system are shown in Figure A-4.

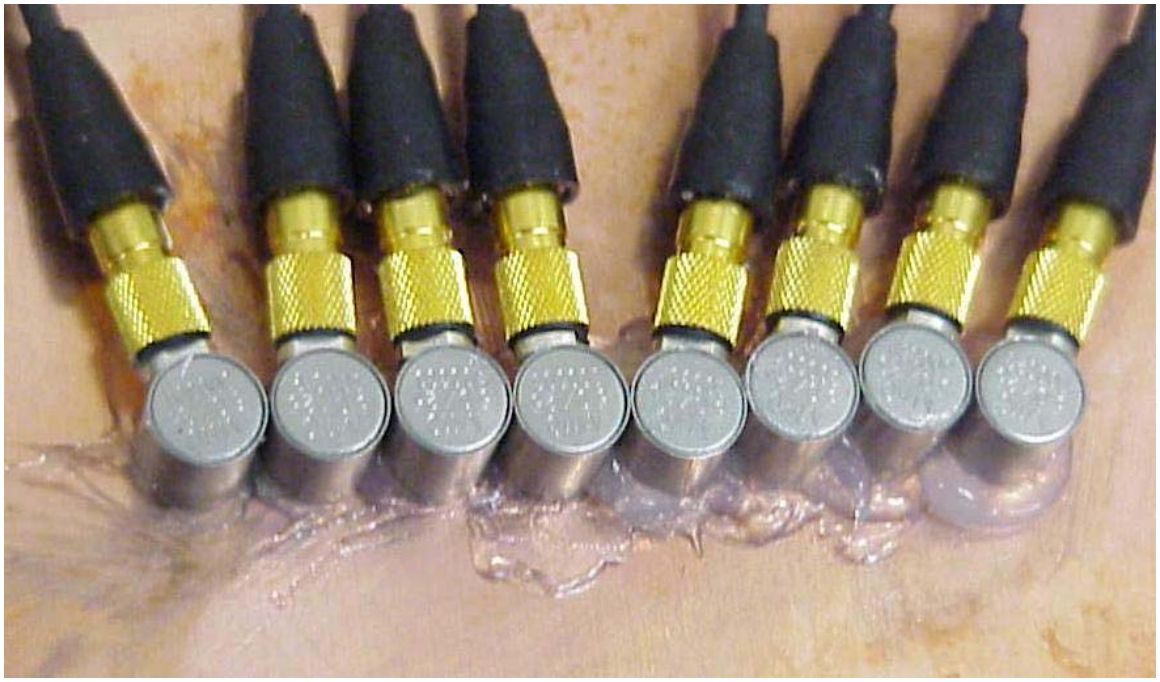

Figure A-4: A close-up view of the mounted transducers; excess silicone sealant was wiped away before it dried.

2. Software

A. Measurement Process Overview

In order to measure a fluid film, the first step is to start the master program. Once this is done, a "baseline" acquisition must be performed with a very thick fluid layer following which actual data may be acquired. The steps to do this are detailed below.

B. Starting the Measurement Program

Before starting the software, ensure that all equipment is powered on and connected. In the laptop's "LVProgs" folder on the desktop, there is an icon

labeled “measurement_X-YY.llb” where “X-YY” will be the last date on which the program was modified. This nomenclature is used to provide version control, and allow regression to an earlier version if the “current” version is changed for the worse during development. Double-clicking on the icon with the most recent date (4-03-02 as of the writing of this manual) will start two programs: the “communications module” and the main program which is entitled “runningmod.vi”. The communications module does not require any user intervention and should be allowed to run undisturbed in the background while the user interacts solely with the “runningmod.vi” program. If a baseline measurement has already been obtained, the system is now ready to acquire measurements; if a baseline is needed, the next section describes how to acquire one.

C. Acquiring Baseline Measurement

The “runningmod.vi” should be on the screen at this point. Go to file→open, and select the “measurementXX-YY.llb” icon again; a listing of the programs contained in that library file will open. Double-click on “basemod.vi” to start the baseline acquisition program. Once the “basemod.vi” program opens, select the transducers which are currently installed. Select **all** currently installed transducers, even if only some will be used for measurements; this allows the ability to acquire measurements with any installed transducer at a later time but does not **require** all transducers to be used.

By default, the program will signal-average 1000 samples for each channel. If either more or less signal-averaging is desired, this can be done by changing the value in the appropriate box at this time.

Click the “Run” button, located near the left end of the toolbar at the top of the “basemod.vi” window (it appears as a right-pointing arrow). Wait approximately eight to ten seconds per transducer selected (for 1000 signals averaged per point); you should hear the multiplexer switching channels every eight to ten seconds. Once all data is acquired, manipulate the two sliders below the data window to window in on the region from just after the first echo to just before the second. The top slider controls the location of the beginning of the window; the bottom slider controls the length of the window. Next, click the “Done” button directly under the top set of sliders.

Next, set the adjustment factor if applicable. Then use the second set of sliders to find the most negative location on the first echo; the top slider controls the location of the window while the bottom slider controls the width of the window. Once the most negative value is exactly centered in the window (it is suggested that window be alternately centered and narrowed, until it is no more than five points wide, to ensure accurate centering) and the adjustment factor is set (set to 1.00 for “wet”, very-thick-film, baselines), press the second “done” button.

Repeat for each transducer. Once all transducers are done, the program will prompt for a filename to save the baseline data in. Select an appropriate filename, and close the basemod.vi program.

D. Beginning Film Measurements

With the “runningmod.vi” program on the screen, select the transducers which you desire to measure with and the desired liquid and then press the “run” button. The program will prompt you for the name of the file containing baseline data. Double-click on the appropriate file. The program will then begin acquiring data, and displaying it both numerically and graphically. Several controls may be modified during execution, including the “# of samples to be acquired” (signal-averaging), “# of samples for FFT”, “windowing” (pre-flattop filter zero-padding; a larger value creates less filtering and thus more signal – but also more noise), and the “min spacing” which is used by the peak-detection algorithm to find the spacing between peaks in the FFT (this value should be constantly adjusted to be approximately 1.75 f_o, never exceeding 1.9 f_o or falling below .75f_o).

When data acquisition is complete, press the large red “STOP” button. Nothing will happen for several seconds; this is normal. Eventually, a file dialog will pop up; select the name of the file you wish to save the data as.

Appendix 2:

Ultrasound Film Thickness Measurement System

Technical Notes

LabVIEW is a very intuitive language, but the code does not lend itself well to being printed out. The purpose of this appendix is not to go over the code in great detail, but rather to explain certain aspects of the code which are not immediately obvious from a brief study of the code itself. Each of the three major modules (the “Runningmod.vi”, “Comm-mod.vi”, and “Basemod.vi” modules) will be addressed.

1. Communications Module

The communications module has only one control on the front panel; this control is “milliseconds to wait” and controls the wait phase between the multiplexer being commanded to change channels and the next acquisition of data. One flaw in the code which should be addressed in future versions is that this wait state occurs both when a channel change occurs and when no channel change occurs; in the latter case, as when only one transducer is being used,

this value is manually set to “zero”. In the future, a case loop should be used to determine if a need exists to enter this wait state at all.

The first frame of the main sequence loop is simply serial port initialization, and also sets the “data ready/read” flag to “ready”.

The second frame initializes the digitizer; if a faster digitizer is used in the future, this frame will have to be totally replaced as it is specific to the device used. It also sends a serial command to the multiplexer to close channel 1 on card 2 (the location of the mux card in the present system; slots 1 and 3 are empty) exclusively (i.e. open all other channels), which is basically initializing the multiplexer.

The third frame contains the “while” loop which in turn contains the “guts” of the program. Once entered, this “While” loop never stops.

Within the while loop is another sequence loop. The first frame waits until the data ready/read flag is set to “Read”.

The next frame contains a “For” loop; this loop is executed for each of the active transducers. Within this loop, the multiplexer is commanded to select the appropriate channel; the wait state, controlled on the front panel as discussed above, is carried out; and data is acquired from the digitizer and timestamped. The data, once it is acquired from all active transducers, is placed in the “data” global variable (the timestamps are placed in the “timestamp” global variable).

The program then sets the “data ready” flag, and returns to the beginning of the sequence loop (waiting for the “Data read” flag to be set).

2. Running Module (Main Measurement Program)

The “running module” is structured similarly to the communications module; the outermost loop is a sequence loop with several frames of initialization before a final loop containing a while loop which contains the guts of the program.

The first initialization frame reads several front-panel controls, including the “Transducer active” controls (which are then disabled for the rest of run-time) and the fluid material. Neither of these parameters can then be changed during run-time.

The second frame cycles the “Data read” flag from “read” to “Ready” to “read”; this passes all acquisition parameters which were set in the globals in the first frame to the communications module (which, every time it cycles, updates its parameters from the globals).

The third frame calculates the scaling for the FFT, and reads in and normalizes the baseline datasets. The first three entries in each baseline dataset are acquisition parameters (the sample start and length as well as location of minima as set by the user in the execution of basemod.vi), so they are stripped off for later use before the normalization.

The last frame in the outermost sequence loop contains the while loop which contains the rest of the program. Inside the while loop, there is another sequence loop; the first frame simply waits for the “data rady” flag. The next frame reads the “Data” and “Timestamp” values from the globals, and the third

sets the “data read” flag. The final frame contains a “for” loop, which executes once for each active transducer, which in turn contains yet another sequence loop.

The first frame of this innermost sequence loop performs two tasks. The actual subtraction of the baseline from the experimental data is carried out, and the frequency scale for the FFT output is regenerated (since the number of values for the FFT can change from cycle to cycle – this is another area for improvement and saved computational time). The next frame normalizes the (experimental minus baseline) signal to zero-mean.

The third and fourth frames contain the algorithms to determine layer thickness, which were discussed at length earlier in this document.

The other pertinent aspect of this VI worth special mention is that there is a for loop which executes the inner for loop (which in turn executes the inner sequence loop for each transducer) twelve times, following which the data from those twelve cycles is sent to the front panel for display. Also, when the VI is ended by pressing the “stop” button on the front panel, at the end of the next twelve-cycle period, the program will end acquiring data and save all acquired data in a spreadsheet file along with the corresponding timestamps. This data is saved in a format appropriate for direct import into Excel or other spreadsheet.

3. Baseline Acquisition Module

The baseline module is structured similarly to the other two, in that it starts out with several frames of initialization. Once initialized (and worth noting here is that the "# of acquisitions" is set by default to 1000 for signal averaging), the user is walked through setting the three parameters which are added to the header of the baseline file (signal start, signal length, and location of minima) for each transducer. The resulting data is then saved to a spreadsheet file for later use in the "runningmod". Note that for troubleshooting, this data **is** saved in a spreadsheet format suitable for direct import into Excel.